BRAIN TISSUE RESPONSE IN NEUROCHEMICAL SAMPLING: MICRODIALYSIS AND LOW-FLOW PUSH-PULL PERFUSION

By

David E. Cepeda

A dissertation submitted in partial fulfillment
of the requirements for the degree of
Doctor of Philosophy
(Biomedical Engineering)
in The University of Michigan
2013

Doctoral Committee:

Professor Robert T. Kennedy, Chair
Professor Joseph Bull
Assistant Professor Cynthia Chestek
Research Assistant Professor Stephen I. Lentz
Professor Jon-Kar Zubieta

DEDICATION

A mis padres, Dr. Abel F. Cepeda & Sra. Martha L. López de Cepeda
Not a word in this dissertation could have been written without their eternal love, sacrifice, and guidance

ACKNOWLEDGEMENTS

First, I would like to thank my Dissertation Committee members —Dr. Joseph Bull, Dr. Cindy Chestek, Dr. Stephen Lentz, and Dr. Jon-Kar Zubieta— for their time, assistance, and dedication. Special thanks are given to my advisor, Dr. Robert T. Kennedy, for his continuous leadership, counsel, and encouragement.

I would like to express my appreciation to Dr. Daryl Kipke for providing his laboratory space to conduct animal studies. I am also indebted to our collaborator Dr. William Shain from the Wadsworth Center in the New York State Department of Health for his help and generosity. Special thanks are also given to Dr. Leah Hains and Karen Smith for their training and willingness to help me in my academic pursuits.

I would like to express my gratitude to all current and former Kennedy, Kipke, and Bull lab members for their constant help and friendship. Special thanks go to Dr. Robert Dodde, Dr. Hernan Fuentes, Neil Hershey, David Li, Rachel Miriani, Paras Patel, John Pitre, Robinson Seda, and Dr. Thomas Slaney for their facilitation and contribution of data. I would also like to acknowledge the instrumental mentorship of Dr. Samesha Barnes, Dr. Stephen Tedeschi, and Dr. Jonathan F. K. Earle during my undergraduate years at the University of Florida.

My deepest appreciation goes to the faculty, staff, and mentors from the Department of Biomedical Engineering, Department of Chemistry, College of Engineering, Rackham Graduate School, and the University of Michigan at large;

particularly Mary Jo Desprez, Dr. Debby Mitchell, Dr. Susan Montgomery, Mike Nazareth, and Ilona Phillips for their extracurricular support. Further, I would like to thank all the student organizations I participated in; namely, the Society of Hispanic Professional Engineers (SHPE), Students for Recovery, and the Alliance for Graduate Education and the Professoriate (AGEP).

Last but not least, I would like to express my deepest gratitude to all my family and friends who helped keep me positive and determined throughout my graduate school career. Special thanks go to my parents, Abel Fernando and Martha Lucía, my brother and sister, Miguel Darío and Sandra Lorena, my extended family in Colombia, and my close friends in Michigan, Florida, and abroad.

TABLE OF CONTENTS

LIST OF FIGURES

ABSTRACT

Neurochemical sensing via sampling probes is essential for deciphering neuronal communication and enabling technologies to alleviate brain disorders such as mental illness and Parkinson's. The brain tissue response associated with neural probes is one of the major barriers to sustained, accurate measurements of neurotransmitters *in vivo*. Ultrastructural tissue damage studies following microdialysis (MD), the most established method of neurochemical sampling, have shown intercellular disruption up to 1.4 mm from the probe. However, information on whole-cell populations has not been collected. Push-pull perfusion (PPP) is a less popular sampling method that offers up to a 500-fold increase in spatial resolution. Yet, macroscopic tissue lesions in its initial high-flow stages have deterred its widespread use. The current low-flow PPP method has reduced the potential for tissue damage significantly, but has not been investigated thoroughly.

To quantitatively characterize the brain tissue response in low-flow PPP versus MD, cell viability (CV) measurements and immunohistochemical (IHC) labeling of specific neural cell types were conducted in rat specimens, as well as computational modeling of fluid flow. To calculate CV in terms of dead/total cell ratio, Sytox Orange and Hoechst 33342 nuclear stains were infused in situ to label damaged and all cells, respectively, within reach of the dye cocktail. By labeling cell nuclei, neurons, microglia, and vasculature with IHC stains, changes in cytoarchitecture could be examined. Finally,

the mechanical effect of fluid flow in PPP and MD was evaluated with COMSOL models of velocity, pressure, and shear stress.

Results from all studies indicated that low-flow PPP caused no more, usually less, brain tissue damage than MD. Since microdialysis has been a valuable tool for neurochemical monitoring, data supports the widespread use of low-flow push-pull perfusion for elucidating brain function, disease, and treatments through *in vivo* sampling. Furthermore, CV, IHC, and computational methods have the potential to evaluate the tissue response in improved probe designs and sampling conditions, facilitating the advancement of neurochemical sensing technology.

CHAPTER 1

INTRODUCTION

In vivo Neurochemical Monitoring

Measuring chemical activity in the brain allows researchers to study the brain and develop treatments for brain-related disorders. Specifically, measuring neurotransmitter concentrations over time elucidates the chemical signaling inherent to behavior, pharmacology, and pathophysiology (Robinson et al., 2008; Weiss et al., 2000). Neurons in the brain communicate via synaptic transmission (Figure 1-1), whereby signals travel to the pre-synaptic end of a neuron and incite the release of neurotransmitters across the synaptic cleft. These chemical messengers are transported into the postsynaptic neuron where they elicit a response (e.g. gene expression, adjusted membrane potential). Neurons can engage in this point-to-point transmission or volume transmission, in which neurotransmitters activate post-synaptic receptors at a distant site (Zoli et al., 1998).

At present, it is impossible to target synapses and considerably difficult to sample directly from intrasynaptic space. However, extracellular measurements can be used to infer intrasynaptic concentrations. *In vivo* measurements are necessary because the temporal resolution of *ex vivo* methods is insufficient for relating brain chemistry to behavior. Moreover, *ex vivo* artifacts interfere with accurate analysis and interpretation of data (Obrenovitch et al., 1997).

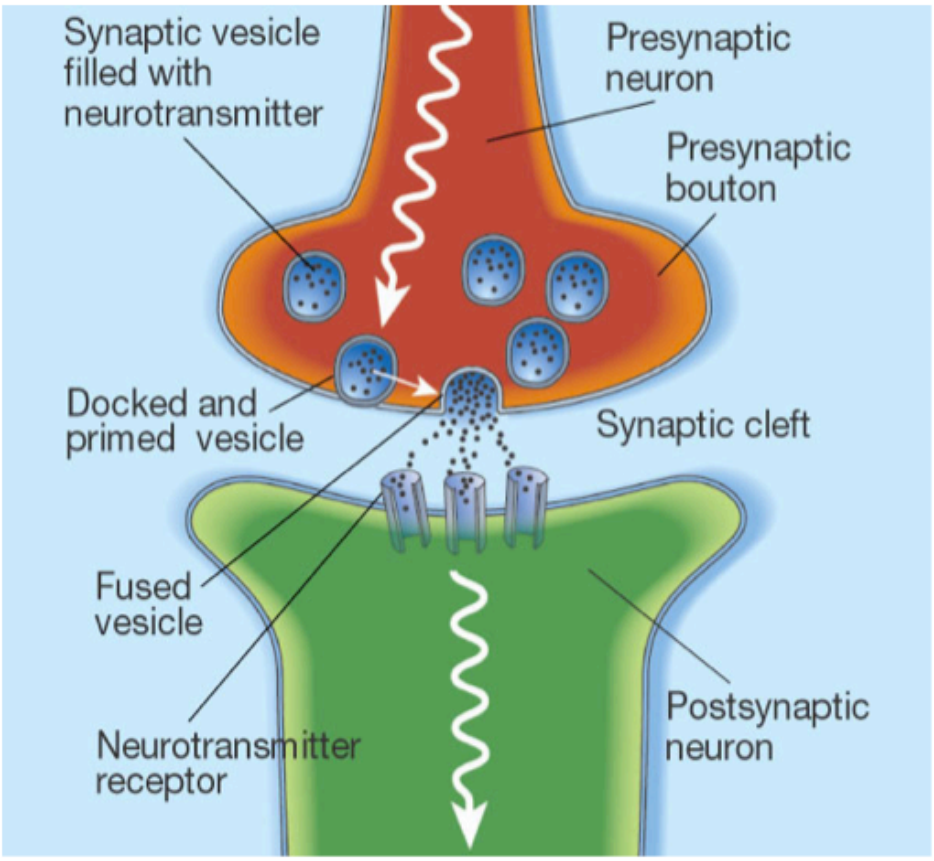

Figure 1-1: Illustration of neuronal communication via synaptic transmission. Neurotransmitters are delivered from pre- to post-synaptic neuron to propagate chemical signals, which are then terminated by reuptake into pre-synaptic neurons or enzymatic degradation in the extracellular space. Sampling and subsequent analysis of the extracellular fluid provides valuable information on behavior, pharmacology, and pathophysiology (Dobrunz and Garner, 2002).

By monitoring neurochemical levels *in vivo*, the "language" of the brain can be better understood, and regulated can with chemical stimuli. For example, schizophrenia has been associated with abnormally low levels of glutamate (Kim et al., 1980). Since neurochemical monitoring provides a window into how the disease is operating, a framework for drug design can be established to normalize glutamate levels, reducing symptoms. Recent clinical advances in neurochemical sensing include monitoring conditions of severe brain injury, examining the role of neurotransmitters in tremor during deep brain stimulation, investigating neurometabolic aberrations in epilepsy patients, and detecting catecholamine levels in the context of learning, stress, and memory (Matzneller and Brunner, 2011; Park et al., 2011; Chang et al., 2012). These observations can be made in acute and chronic conditions, although it is more challenging to maintain accurate signal in long-term applications.

In vivo neurochemical monitoring can be divided into two classes: non-invasive and invasive. Non-invasive techniques like positron emission tomography (PET) are usually expensive, unsuitable for animal studies, have poor temporal and spatial resolution (10 s and 1 cm^3 respectively), and are limited to a few analytes (Hans Lundqvist, 1999). Thus, invasive techniques involving probe implantation in brain tissue are a fitting alternative. These include electrochemical and neurochemical methods. Electrochemical sensors offer high temporal and spatial resolution (10 ms and tens of μm^3 respectively), but are limited to a few electroactive neurotransmitters (e.g. dopamine, serotonin). For example, in voltammetry, chemical concentrations are characterized by measuring unique current vs. voltage waveforms over time (Millar et al., 1985). Additionally, these microelectrodes are more susceptible to surface fouling, noise

interference, and failure (Williams et al., 1999). Though spatial and temporal resolution is lower, neurochemical sampling methods can sample multiple analytes simultaneously, and are amenable to various analytical techniques (e.g. high pressure liquid chromatography: HPLC, capillary electrophoresis: CE). The focus of this study will compare the two premier capillary-based neurotransmitter sampling methods: microdialysis (MD) and low-flow push-pull perfusion (PPP), which involves sampling through a microdialysis membrane in MD and directly from the brain tissue in PPP (Delgado et al., 1972; Gaddum, 1961).

Current challenges in MD and PPP, and the invasive neuromolecular monitoring field in general, include optimizing selectivity, or multi-analyte capability; sensitivity; spatial and temporal resolution; and minimizing tissue response. The brain is host to over 100 neurotransmitters and metabolites, therefore high selectivity is needed. Furthermore neurochemical samples have very small volumes/concentrations (μM or less), thus high sensitivity is required. Spatial resolution is important since many brain structures are small and larger structures have heterogeneity that is lost with poor resolution (Mitchell et al., 1994). Moreover, temporal resolution is critical in gaining an accurate timeline of neural activity (Rossell et al., 2003). Finally, there is an acute inflammatory response due to probe insertion, and in our case fluid flow, while extended probe presence itself induces a chronic response associated with glial scar encapsulation (Figure 1-2) (Polikov et al., 2005).

Optimization of these parameters will produce a clearer picture of neurochemical signaling, and thus further the understanding and treatment of brain disorders. Because tissue response is a major barrier to accurate neuro-invasive measurements, it is

A

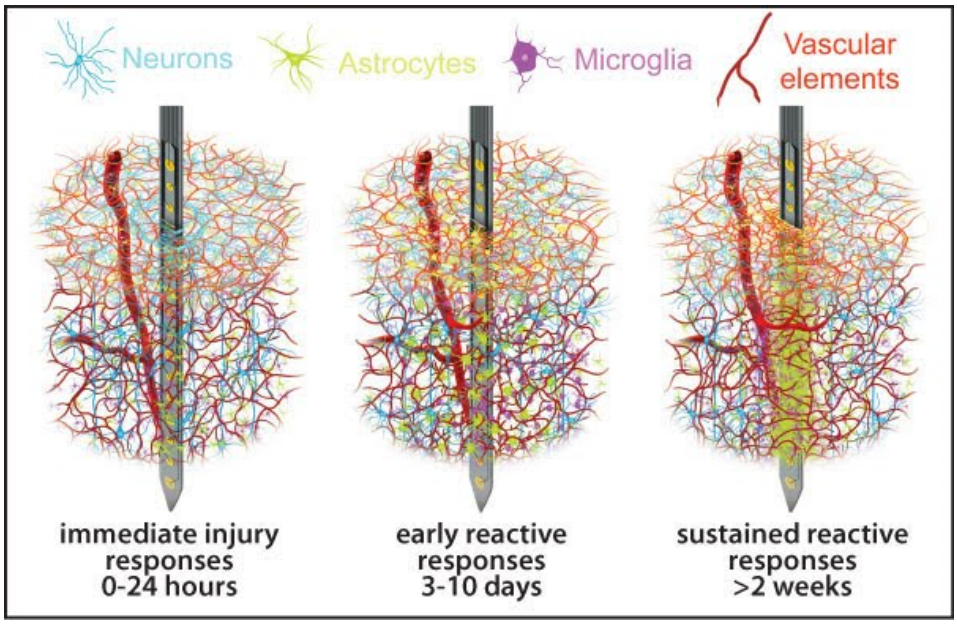

B

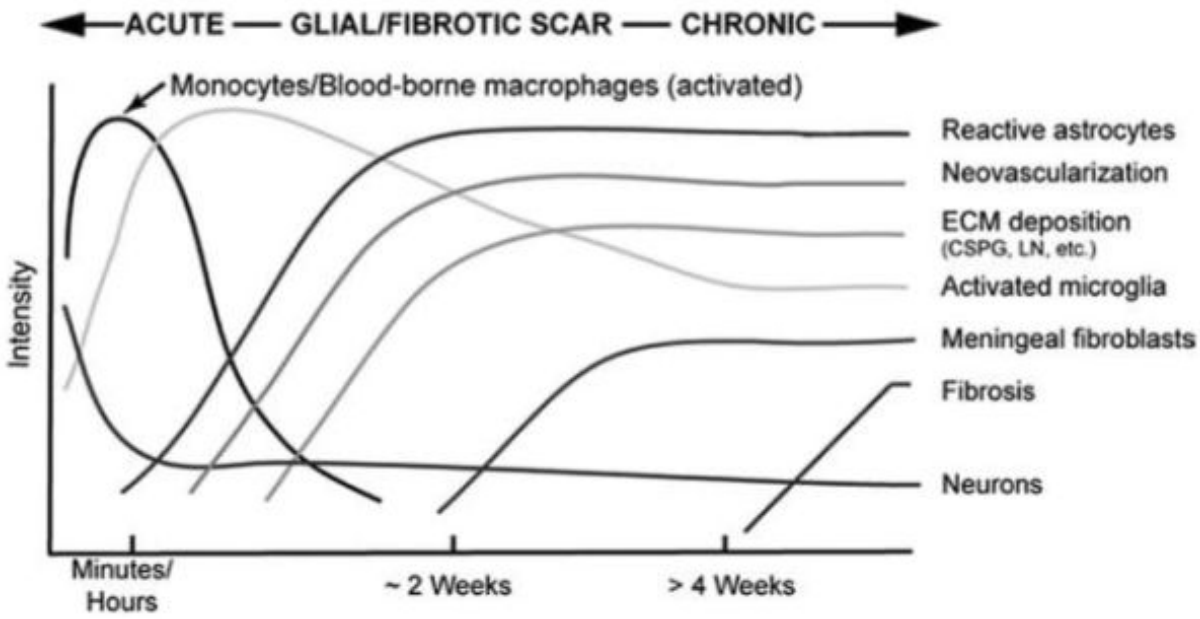

Figure 1-2: Stages (A) and timeline (B) of brain tissue response. Microglia, the resident macrophages of the brain, are the key players during acute, or immediate neuroinflammation. Astrocytes dominate chronic, or sustained responses, forming a protective sheath between foreign bodies and brain tissue (Reichert, 2007).

important to examine this parameter thoroughly (Wisniewski and Reichert, 2000; Liao and Cui, 2007). The focus of this study investigates the relative tissue damage between MD and PPP.

Microdialysis

Microdialysis, the most popular method of neurochemical sampling, works under the following principle. A 200-400 μm diameter by 1-4 mm long hollow-fiber dialysis membrane probe is inserted into the brain (Figure 1-3A). The inside of the fiber is perfused at 0.1-3.0 μL/min with artificial cerebrospinal fluid (aCSF), causing extracellular fluid components to diffuse across the membrane according to their concentration gradient between the inside and outside of the membrane. In general, probe size is limited by the fabrication method and toughness/durability of the probe.

The major advantage of MD is its ability to reliably separate and detect a wide range of compounds, neurotransmitters, metabolites, amino acids, and drugs. Although MD can filter molecules by molecular weight cutoff, it has difficulty collecting high molecular weight species. For example, neuroactive peptides in the brain are found in low concentration and often stick to the dialysis membrane. Furthermore, data is presented as percent recovery rather than absolute values (e.g. ng/mL), which can distort the actual change in quantity of solutes in a dialysate series (Myers et al., 1998).

Accuracy in MD is also limited in terms of space and time resolution. Spatial resolution (~0.1 mm^3) is restricted by the working area of the dialysis membrane, while temporal resolution is usually limited by the minimum sample collection time needed for detection by the analytical technique. For instance, a temporal response of 2 s was

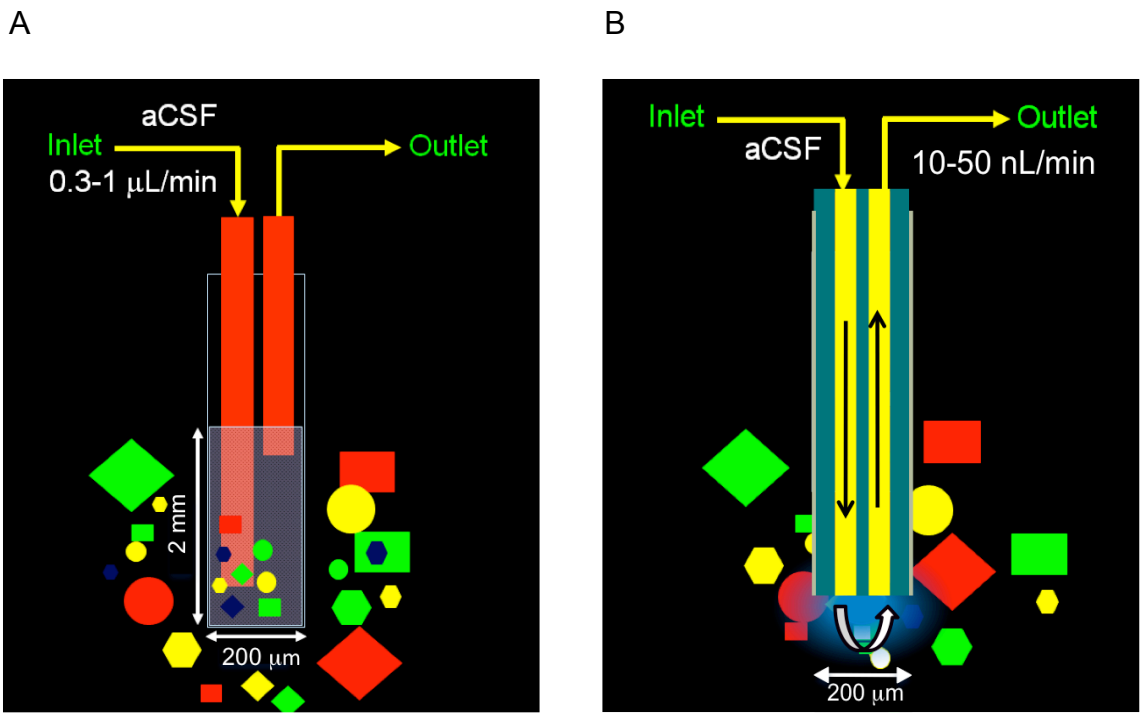

Figure 1-3: Diagrams of microdialysis (MD) (A) and low-flow push-pull perfusion (PPP) (B). In microdialysis, artificial cerebrospinal fluid (aCSF) is infused through a dialysis membrane at 1 µL/min. Analytes are collected via diffusion, according to their concentration gradient. In push-pull perfusion, aCSF is infused directly into the brain at 50 nL/min. Sample is withdrawn via vacuum at the same flow rate (Images courtesy of Dr. Hernan Fuentes).

achieved when coupled to capillary electrophoresis with laser-induced fluorescence (CE-LIF) (Wang et al., 2010).

Low-Flow Push-Pull Perfusion

In contrast to MD, push-pull perfusion is an open system using two side-by-side or concentric capillary probes (Figure 1-3B). Sample is "pulled" from one capillary and aCSF is "pushed" through the other capillary to replace the sampled volume. PPP also has the capability to detect multiple analytes. The high collection efficiencies and direct collection of extracellular fluid in PPP give an enormous advantage over MD for sampling neurochemicals in low volumes and concentrations, particularly neuropeptides (Kohsaka et al., 1999). Most importantly, because the perfusion fluid directly contacts the tissue under study at the tip, spatial resolution is improved substantially. Specifically, there is a 500-fold improvement when comparing the surface area of the 40 μm diameter capillary inlet in low-flow PPP to the 200 μm x 2 mm dialysis membrane in MD (Figure 1-4). Like MD, temporal resolution is also determined by the analytical technique it is coupled to. For example, 7 s resolution was achieved with segmented multi-phase flow (Slaney et al., 2011).

Brain Tissue Response

Acute neurochemical sampling (2-4 hours), namely MD and PPP, elicits an immediate injury response due to the implantation itself. The central nervous system wound healing response is initiated by mechanical trauma. Disruption of blood vessels releases erythrocytes, clotting factors, and inflammatory factors that induce glial cell activation and proliferation. Moreover, activated astrocytes and microglia are recruited

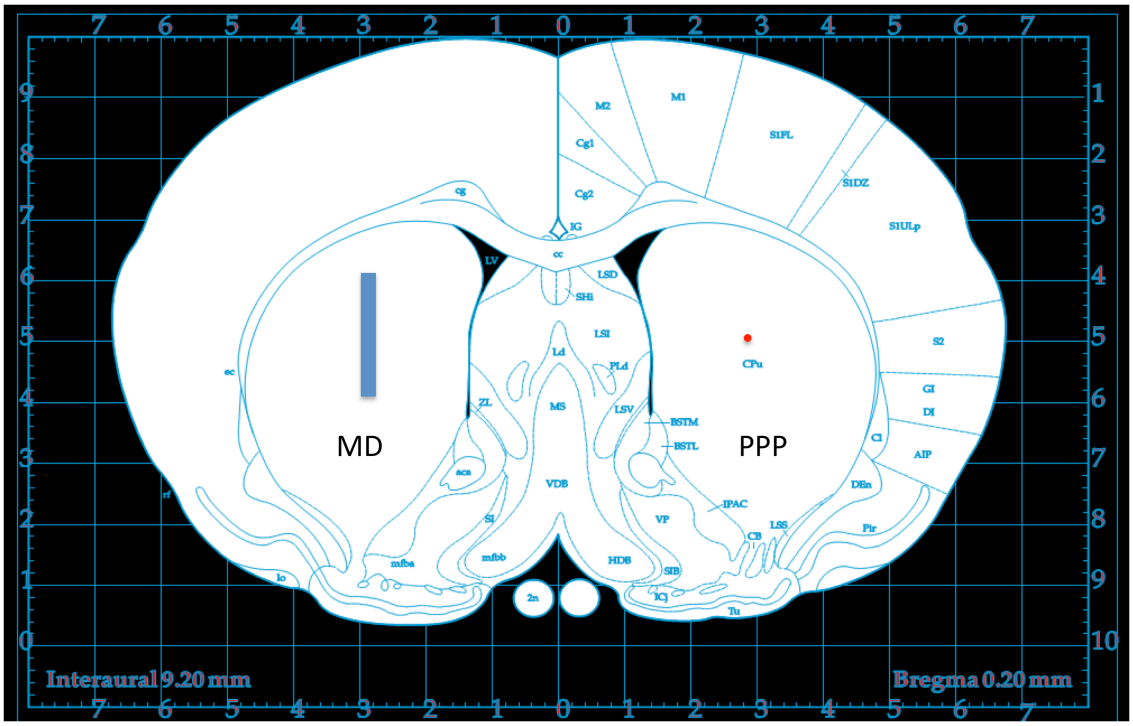

Figure 1-4: Comparison of spatial resolution between MD and low-flow PPP. A rectangle (left) represents the 200 μm x 2 mm surface area of the MD dialysis membrane. A dot (right) represents the 40-μm diameter surface area of the inlet capillary in PPP, which improves spatial resolution approximately 500-fold.

around the inserted probe (Turner et al., 1999). Insertion induced accumulation of fluid and necrotic nervous tissue causes vasogenic edema, further adding to the intracranial pressure surrounding the implant (Barzo et al., 1997).

Among strategies to reduce tissue damage are minimizing device insertion speed and cross-sectional area (Szarowski et al., 2003). The fluid dynamics inherent to infusing and withdrawing sample from the brain add another dimension of potential tissue damage. Fluid flow effects have not been studied effectively in MD and PPP (Dluzen and Ramirez, 1986).

Microdialysis

With respect to tissue response, MD has been shown to negatively influence the sampling environment including altered morphology, microcirculation, metabolism rate, and blood-brain barrier integrity (Morgan et al., 1996). Initial MD tissue damage studies found that cerebral blood flow and local glucose metabolism decreased around the probe within 2 hr of implantation, but normalized within 24 hr (Benveniste et al., 1987). Various histological studies of MD probes implanted for 1-3 days have found regions of damaged, degenerating neurons in the surrounding area of the probe (Tang et al., 2003; Zhou et al., 2002b) Furthermore, a semi-quantitative tissue damage study reported neuronal density decreases up to 400 μm from a 40 h implanted probe, and intercellular disruption up to 1.4 mm from the probe tract (Clapp-Lilly et al., 1999).

Nevertheless, MD has enabled neuroscientists to reliably associate chemical changes from sensory and pharmacological stimuli to behavioral and pathological states. The causative role of adenosine in sleep, the toxic levels of glutamate contributing to brain damage in stroke, and the proportional relationship of glutamate levels to

schizophrenic symptoms were all discovered through microdialysis (Porkka-Heiskanen et al., 1997; Moghaddam and Adams, 1998; Benveniste et al., 2006).

Low-Flow Push-Pull Perfusion

Initially PPP was conducted with flow rates as high as 25 μL/min (Myers and Gurleyorkin, 1985), which often caused considerable tissue lesions, especially if push and pull flow were unbalanced (Redgrave, 1977). This tissue response eclipsed the enhancement of spatial resolution, and decreased the popularity of PPP in the scientific community. Consequently, MD flourished as the prominent neurochemical monitoring method.

Upon the advent of microfluidics in the last decade, the current low-flow PPP method was developed, with infusion/withdrawal of fluid at 10-50 nL/min. Although these lower flow rates may make the probe more susceptible to clogging, they reduce the mechanical disturbances inherent to high-flow PPP, and have been proposed to cause less tissue damage than MD. However, the tissue response in low-flow PPP has not been quantitatively characterized. Our data has expanded upon another group's study that suggested minimal tissue response associated with the PPP probe tip (Kottegoda et al., 2002). The lack of thorough and comprehensive tissue damage studies in capillary-based neurochemical sampling methods prove a major barrier to the widespread use of PPP, and the optimization of neurochemical sensing overall.

Evaluation of Tissue Response

Common practices for analyzing tissue samples include histology and confocal microscopy. Histology involves the microscopic anatomical study of cells and tissue by

sectioning and mounting samples on slides for imaging. Confocal fluorescent microscopy offers high-resolution, high-contrast 3D imaging for quantification of live/damaged cells and delineation of key structures (Pawley, 2008). Histological studies of MD and PPP with light and electron microscopy have provided some insight about the tissue response in neurochemical sampling methods, but comparisons between MD and PPP remain inconclusive.

Cell viability stains and immunohistochemistry (IHC) are reliable tools for molecular biology and neuroscience applications. Furthermore, analytical models are valuable for guiding and validating experimental methods. For cell viability, live/dead cell stains have been infused through microfluidic channels of neural microelectrode implants to quantify damage due to device insertion (Retterer et al., 2008). For IHC, antibodies and molecular stains have been used to label glial cells and vasculature to assess cellular responses to neuroprosthetic devices (Spataro et al., 2005). For computational modeling, mechanical loading and fluid flow in biodegradable scaffolds have been reproduced with finite element analysis (FEA) and computational fluid dynamics (CFD) (Milan et al., 2009).

By performing low-flow PPP and MD, labeling the brain tissue with cell viability and IHC stains, and imaging via confocal fluorescent microscopy, the research described herein explores the relative tissue damage between MD and PPP, and establishes a baseline of probe designs and procedures to minimize tissue response. Moreover, by modeling the neurochemical sampling in COMSOL, force distributions in MD and PPP can be compared to each other and to experimental data. This dissertation is organized in the following ways.

Dissertation Overview

In Chapter 2, we examined the effect of PPP and MD on cells in the surrounding brain tissue by identifying healthy and damaged cells within reach of the perfusate. This was achieved by *in vivo* infusion of a fluorescent cell marker cocktail through the probes. The cocktail consisted of the nucleic acid stains Hoechst 33342 (H342), which crosses all cell membranes, and Sytox Orange (SO), which can only cross the compromised plasma membrane of non-viable cells. The extent of SO-labeled versus the double-labeled (H342 & SO) cells indicated how well the neurochemical sampling method was tolerated by the affected cells. The results from PPP were compared to MD to allow evaluation of cell viability in the sampling regions of both methods.

In Chapter 3, we described using 3-D spectral confocal microscopy and subsequent image analysis to identify changes in the distribution and morphology of cells involved in brain tissue response, following PPP and MD. IHC was used to identify cell bodies (H342), neurons (NeuroTrace), vasculature (endothelial barrier antigen; EBA), and microglia (ionized calcium binding adaptor molecule 1; Iba1). The visualization and quantitative analysis of these histological markers indicated how the neurochemical sampling methods affected cellular organization and activation.

In Chapter 4, we investigated the computational modeling of neurochemical sampling. By inputting known parameters (e.g., material properties of the brain and pertinent fluids) into COMSOL, we graphed the velocity, pressure, and shear stress fields in fluid flow for PPP and MD. Numerical outputs allowed us to validate experimental data and gain insight into fluid force distributions in terms of tissue damage.

In Chapter 5, we conclude that low-flow PPP causes no more, mostly less, tissue damage than MD. Therefore, the continued research and development of low-flow PPP for neurochemical sampling is encouraged. Furthermore, the studies described herein enable minimization of tissue damage, and thus optimization of neurochemical measurements. Such advancements not only give a better understanding of the neural signaling involved in behavior, pharmacology, and pathophysiology, but also have great impacts on effective treatments for brain disorders.

References

Barzo P, Marmarou A, Fatouros P, Hayasaki K, Corwin F. Contribution of vasogenic and cellular edema to traumatic brain swelling measured by diffusion-weighted imaging. J. Neurosurg., 1997; 87: 900-7.

Benveniste H, Drejer J, Schousboe A, Diemer NH. Elevation of the extracellular concentrations of glutamate and aspartate in rat hippocampus during transient cerebral ischemia monitored by intracerebral microdialysis. Journal of Neurochemistry, 2006; 43: 1369-74.

Chang S-Y, Kim I, Marsh MP, Jang DP, Hwang S-C, Van Compel JJ, Goerss SJ, Kimble CJ, Bennet KE, Garris PA, Blaha CD, Lee KH. Wireless fast-scan cyclic voltammetry to monitor adenosine in patients with essential tremor during deep brain stimulation. Mayo Clinic Proceedings, 2012; 87: 760+.

Clapp-Lilly KL, Roberts RC, Duffy LK, Irons KP, Hu Y, Drew KL. An ultrastructural analysis of tissue surrounding a microdialysis probe. Journal of Neuroscience Methods, 1999; 90: 129-42.

Delgado JM, DeFeudis FV, Roth RH, Ryugo DK, Mitruka BM. Dialytrode for long term intracerebral perfusion in awake monkeys. Archives internationales de pharmacodynamie et de therapie, 1972; 198: 9-21.

Dluzen DE, Ramirez VD. A miniaturized push-pull cannula for use in conscious, unrestrained animals. Pharmacology Biochemistry and Behavior, 1986; 24: 147-50.

Dobrunz LE, Garner CC. Priming plasticity. Nature, 2002; 415: 277-8.

Gaddum J. Push-pull cannulae. J. Physiol, 1961; 155.

Hans Lundqvist ML, Vladimir Tolmachev, Anna Lövqvist, Anders Sundin, Soheir Beshara, Alexander Bruskin, Jörgen Carlsson, Jan-Erik Westlin. Positron Emission Tomography and Radioimmunotargeting: General Aspects. Acta Oncologica, 1999; 38: 335-41.

Kim J, Kornhuber H, Schmid-Burgk W, Holzmüller B. Low cerebrospinal fluid glutamate in schizophrenic patients and a new hypothesis on schizophrenia. Neuroscience Letters, 1980; 20: 379-82.

Kohsaka A, Watanobe H, Kakizaki Y, Suda T. A comparative study of the effects of nitric oxide and carbon monoxide on the in vivo release of gonadotropin-releasing hormone and neuropeptide Y from rat hypothalamus during the estradiol-induced luteinizing hormone surge: Estimation by push-pull perfusion. Neuroendocrinology, 1999; 69: 245-53.

Kottegoda S, Shaik I, Shippy SA. Demonstration of low flow push-pull perfusion. Journal of Neuroscience Methods, 2002; 121: 93-101.

Liao W, Cui XT. Reagentless aptamer based impedance biosensor for monitoring a neuro-inflammatory cytokine PDGF. Biosensors & bioelectronics, 2007; 23: 218.

Matzneller P, Brunner M. Recent advances in clinical microdialysis. TrAC Trends in Analytical Chemistry, 2011; 30: 1497-504.

Milan JL, Planell JA, Lacroix D. Computational modelling of the mechanical environment of osteogenesis within a polylactic acid-calcium phosphate glass scaffold. Biomaterials, 2009; 30: 4219-26.

Millar J, Stamford JA, Kruk ZL, Wightman RM. Electrochemical, pharmacological and electrophysiological evidence of rapid dopamine release and removal in the rat caudate nucleus following electrical stimulation of the median forebrain bundle. European Journal of Pharmacology, 1985; 109: 341-8.

Mitchell K, Oke AF, Adams RN. In-vivo dynamics of norepinephrine release reuptake in multiple terminal field regions of rat-brain. Journal of Neurochemistry, 1994; 63: 917-26.

Moghaddam B, Adams BW. Reversal of phencyclidine effects by a group II metabotropic glutamate receptor agonist in rats. Science, 1998; 281: 1349-52.

Morgan ME, Singhal D, Anderson BD. Quantitative assessment of blood-brain barrier damage during microdialysis. J. Pharmacol. Exp. Ther., 1996; 277: 1167-76.

Myers RD, Adell A, Lankford MF. Simultaneous comparison of cerebral dialysis and push-pull perfusion in the brain of rats: A critical review. Neuroscience and Biobehavioral Reviews, 1998; 22: 371-87.

Myers RD, Gurleyorkin L. New micro push-pull catheter system for localized perfusion of diminutive structures in brain. Brain Research Bulletin, 1985; 14: 477-83.

Obrenovitch TP, Hardy AM, Urenjak J. High extracellular glycine does not potentiate N-methyl-d-aspartate-evoked depolarization in vivo. Brain Research, 1997; 746: 190-4.

Park J, Takmakov P, Wightman RM. In vivo comparison of norepinephrine and dopamine release in rat brain by simultaneous measurements with fast-scan cyclic voltammetry. Journal of Neurochemistry, 2011; 119: 932-44.

Pawley J. Handbook of Biological Confocal Microscopy, Third Edition. Journal of Biomedical Optics, 2008; 13: 029902-.

Polikov VS, Tresco PA, Reichert WM. Response of brain tissue to chronically implanted neural electrodes. Journal of Neuroscience Methods, 2005; 148: 1-18.

Porkka-Heiskanen T, Strecker RE, Thakkar M, Bjørkum AA, Greene RW, McCarley RW. Adenosine: a mediator of the sleep-inducing effects of prolonged wakefulness. Science, 1997; 276: 1265-8.

Redgrave P. A modified push-pull system for the localised perfusion of brain tissue. Pharmacology Biochemistry and Behavior, 1977; 6: 471-4.

Reichert WM. Indwelling neural implants: strategies for contending with the in vivo environment. CRC, 2007.

Retterer ST, Smith KL, Bjornsson CS, Turner JN, Isaacson MS, Shain W. Constant pressure fluid infusion into rat neocortex from implantable microfluidic devices. Journal of Neural Engineering, 2008; 5: 385-91.

Robinson DL, Hermans A, Seipel AT, Wightman RM. Monitoring Rapid Chemical Communication in the Brain. Chemical Reviews, 2008; 108: 2554-84.

Rossell S, Gonzalez LE, Hernandez L. One-second time resolution brain microdialysis in fully awake rats - Protocol for the collection, separation and sorting of nanoliter dialysate volumes. Journal of Chromatography B-Analytical Technologies in the Biomedical and Life Sciences, 2003; 784: 385-93.

Slaney TR, Nie J, Hershey ND, Thwar PK, Linderman J, Burns MA, Kennedy RT. Push-Pull Perfusion Sampling with Segmented Flow for High Temporal and Spatial Resolution in Vivo Chemical Monitoring. Analytical Chemistry, 2011; 83: 5207-13.

Spataro L, Dilgen J, Retterer S, Spence AJ, Isaacson M, Turner JN, Shain W. Dexamethasone treatment reduces astroglia responses to inserted neuroprosthetic devices in rat neocortex. Experimental Neurology, 2005; 194: 289-300.

Szarowski DH, Andersen MD, Retterer S, Spence AJ, Isaacson M, Craighead HG, Turner JN, Shain W. Brain responses to micro-machined silicon devices. Brain Research, 2003; 983: 23-35.

Tang A, Bungay PM, Gonzales RA. Characterization of probe and tissue factors that influence interpretation of quantitative microdialysis experiments for dopamine. Journal of Neuroscience Methods, 2003; 126: 1-11.

Turner JN, Shain W, Szarowski DH, Andersen M, Martins S, Isaacson M, Craighead H. Cerebral astrocyte response to micromachined silicon implants. Experimental Neurology, 1999; 156: 33-49.

Wang M, Slaney T, Mabrouk O, Kennedy RT. Collection of nanoliter microdialysate fractions in plugs for off-line in vivo chemical monitoring with up to 2 s temporal resolution. Journal of Neuroscience Methods, 2010; 190: 39-48.

Weiss DJ, Lunte CE, Lunte SM. In vivo microdialysis as a tool for monitoring pharmacokinetics. TrAC Trends in Analytical Chemistry, 2000; 19: 606-16.

Williams JC, Rennaker RL, Kipke DR. Long-term neural recording characteristics of wire microelectrode arrays implanted in cerebral cortex. Brain Research Protocols, 1999; 4: 303-13.

Wisniewski N, Reichert M. Methods for reducing biosensor membrane biofouling. Colloids and Surfaces B: Biointerfaces, 2000; 18: 197-219.

Zhou F, Braddock JF, Hu Y, Zhu XW, Castellani RJ, Smith MA, Drew KL. Microbial origin of glutamate, hibernation and tissue trauma: an in vivo microdialysis study. Journal of Neuroscience Methods, 2002; 119: 121-8.

Zoli M, Torri C, Ferrari R, Jansson A, Zini I, Fuxe K, Agnati LF. The emergence of the volume transmission concept. Brain Research Reviews, 1998; 26: 136-47.

CHAPTER 2

ASSESSMENT OF CELL VIABILITY IN MICRODIALYSIS AND LOW-FLOW PUSH-PULL PERFUSION

Introduction

In vivo neurochemical monitoring is an important tool for studying the brain and neural disorders such as Alzheimer's, depression, and addiction (Robinson et al., 2008; Weiss et al., 2000). Such measurements of extracellular neurotransmitter concentrations over time correlate chemical signaling to behavior, pharmacology, and pathophysiology. Non-invasive *in vivo* monitoring techniques like positron emission tomography (PET) are powerful, but their expense, requirements for immobilized subjects, and limitations to a few neurotransmitters precludes their use for many basic neuroscience studies (Kessler et al., 1984). Invasive techniques involving probe insertion into brain tissue are a widely used alternative. Electrochemical methods offer high temporal and spatial resolution (as good as 10 ms and tens of μm^3, respectively) but are also limited to a few neurotransmitters.

Microdialysis (MD) sampling is another popular method for *in vivo* monitoring (Delgado et al., 1972). An advantage of MD is the ability to collect a wide range of compounds that can then be reliably determined by different analytical techniques (Nandi and Lunte, 2009). Spatial resolution in MD is restricted by the active length of the dialysis membrane (1-2 mm), while temporal resolution is usually determined by the minimum sample collection time needed for detection by the analytical technique (Davies

et al., 2000; Wang et al., 2010). MD has been essential in advancing the fields of neuro-pharmacology, -anatomy, and -physiology. The dependence of dopamine release on tetrodotoxin (TTX), and the role of serotonin in behavior such as sleep and feeding has been clarified in animal studies (Santiago and Westerink, 1990; Rueter et al., 1997). Certainly, microdialysis proves a valuable interface between in vitro cellular models of drug activity and their behavioral effects in vivo.

A less frequently used method of sampling is push-pull perfusion (PPP) (Gaddum, 1961). This method uses an open fluidic system consisting of two side-by-side or concentric capillaries. Sample is "pulled" from one capillary and aCSF is "pushed" through the other capillary to replace sampled volume. Because sampling occurs at the tip, spatial resolution is improved relative to microdialysis. This improvement is vital for studying small brain nuclei or smaller subjects (like mice) (Mitchell et al., 1994). PPP may also have an advantage for collecting high molecular weight compounds since collected molecules do not cross a membrane (Kohsaka et al., 1999; Mizuno et al., 2000).

While MD has usually been performed at 1-2 μL/min, early forms of PPP were typically conducted at 10 μL/min. These relatively high flow rates were perceived to cause substantial tissue damage (Redgrave, 1977). Low-flow PPP, which uses flow rates of 10-50 nL/min, has recently become possible (Kottegoda et al., 2002). This technique has been coupled with segmented flow and microscale analytical techniques to achieve temporal resolution of a few seconds (Slaney et al., 2011). The combination of versatile measurement, high temporal resolution, and high spatial resolution may cause low-flow push-pull perfusion to become an important alternative to sensors and microdialysis.

A key consideration of any invasive technique is the tissue damage caused and how it affects the measurements being made. Acute insertion (2-4 hours) of any device into the brain elicits an immediate injury response due to mechanical disruption (Polikov et al., 2005). Breakage of blood vessels releases erythrocytes, clotting factors, and inflammatory factors that induce glial cell activation and proliferation. As a result activated astrocytes and microglia are recruited around the inserted probe (Turner et al., 1999). Insertion also induces accumulation of fluid and necrotic nervous tissue causing vasogenic edema, further adding to the intracranial pressure and brain tissue volume surrounding the implant (Barzo et al., 1997).

Strategies to reduce tissue damage include minimizing device insertion speed and cross-sectional area (Szarowski et al., 2003). Furthermore, the fluid dynamics inherent to infusing and withdrawing sample from the brain are an additional dimension of potential tissue damage. These fluid flow effects have not been studied effectively (Dluzen and Ramirez, 1986).

Tissue damage associated with microdialysis has been extensively researched. Initial studies found that cerebral blood flow and local glucose metabolism decreased around the probe within 2 h of implantation, but normalized within 24 h (Benveniste et al., 1987). Histological studies of MD probes implanted for 1-3 days have found regions of damaged, degenerating neurons in the surrounding area of the probe (Tang et al., 2003; Zhou et al., 2002a). Finally, a semi-quantitative tissue damage study reported neuronal density decreases up to 400 μm and intercellular disruption up to 1.4 mm from a 40 h implanted probe (Clapp-Lilly et al., 1999).

The tissue response in low-flow PPP has been investigated much less. An initial study suggested the absence of considerable tissue damage (Kottegoda et al., 2002); however, no follow up studies have been reported. Since levels of cellular damage in low-flow PPP may be similar to that of MD, the absence of comprehensive tissue response data on low-flow PPP is a barrier to its potential widespread use.

To further elucidate the damage associated with low-flow push-pull perfusion, we infused live/dead cell stains during sampling and then imaged the brain slices around the sampling tip with confocal microscopy. These studies allowed determination of the relative fraction of cells that were damaged around the probe. The results were compared to analogous studies in microdialysis.

Materials and Methods

All reagents were purchased from Invitrogen, unless otherwise specified. Fused silica capillaries were from Polymicro (Phoenix, AZ). All animal care, housing, and operative procedures were conducted in accordance with the National Institutes of Health Guide for the Care and Use of Laboratory Animals (National Institutes of Health publication 85-23, 1985). Rats were housed in a pathogen-free facility at the University of Michigan, given food and water ad libitum, and exposed to a 12-hour light/dark cycle. The University Committee on the Use and Care of Animals approved the experimental protocol.

Probe Fabrication

Side-by-side PPP probes were constructed as described elsewhere (Cellar and Kennedy, 2006). Briefly, two 15-cm long 40 μm inner diameter (i.d.) x 100 μm outer

diameter (o.d.) capillaries were threaded through a 26-gauge stainless steel needle (BD, Franklin Lakes, NJ). The ends of these capillaries were attached to 2 cm-long 180 μm i.d. x 360 μm o.d. capillaries for connection to 360 μm fittings. All probe sections were glued together with cyanoacrylate adhesive (Duro Super Glue, Henkel, Rocky Hill, CT). The needle tip extended approximately 1 mm below the capillary tips in these needle-sheathed PPP probes (Figure 2-1 A), and vice versa in miniaturized PPP probes (Figure 2-1 B).

Side-by-side MD probes were constructed by inserting two 10-cm long 40 μm i.d. x 100 μm o.d. capillaries into a ~200 μm-diameter regenerated cellulose membrane, as previously described (Parsons and Justice, 1992). The inlet extended past the outlet capillary to form a 2-mm sampling length (Figure 2-1 C). The inlet capillary end was attached to a 2-cm length of 180 μm i.d. x 360 μm o.d. capillary adapter.

Animal Surgery and Neurochemical Sampling

Male Sprague-Dawley rats weighing 300-400 g were anesthetized with isoflurane and mounted in a stereotaxic frame (n=4). The probes were inserted into the striatum at the following coordinates: 1.0 mm anterior to bregma, +2.6 mm lateral to midline, and 5.5 (MD) / 4.5 (PPP) mm ventral to dura (Paxinos and Watson, 2005). In PPP, aCSF (145 mM NaCl, 2.68 mM KCl, 1.01 mM MgSO4, 1.22 mM CaCl2, 1.55 mM Na2HPO4, 0.45 mM NaH2PO4, pH 7.4) was infused and sample withdrawn at 50 nL/min. In MD, aCSF was infused at 1 μL/min (Tucci et al., 1997).

The push-pull perfusion set-up consisted of a syringe pump (Fusion 400, Chemyx, Stafford, TX) that infused aCSF into the rat brain via the "push" line of the probe, and a vacuum pump (GAST DOA-P704-AA) that withdrew sample from the rat brain via the "pull" line of the probe. The push line began with a 25 μL syringe (Gastight, Hamilton

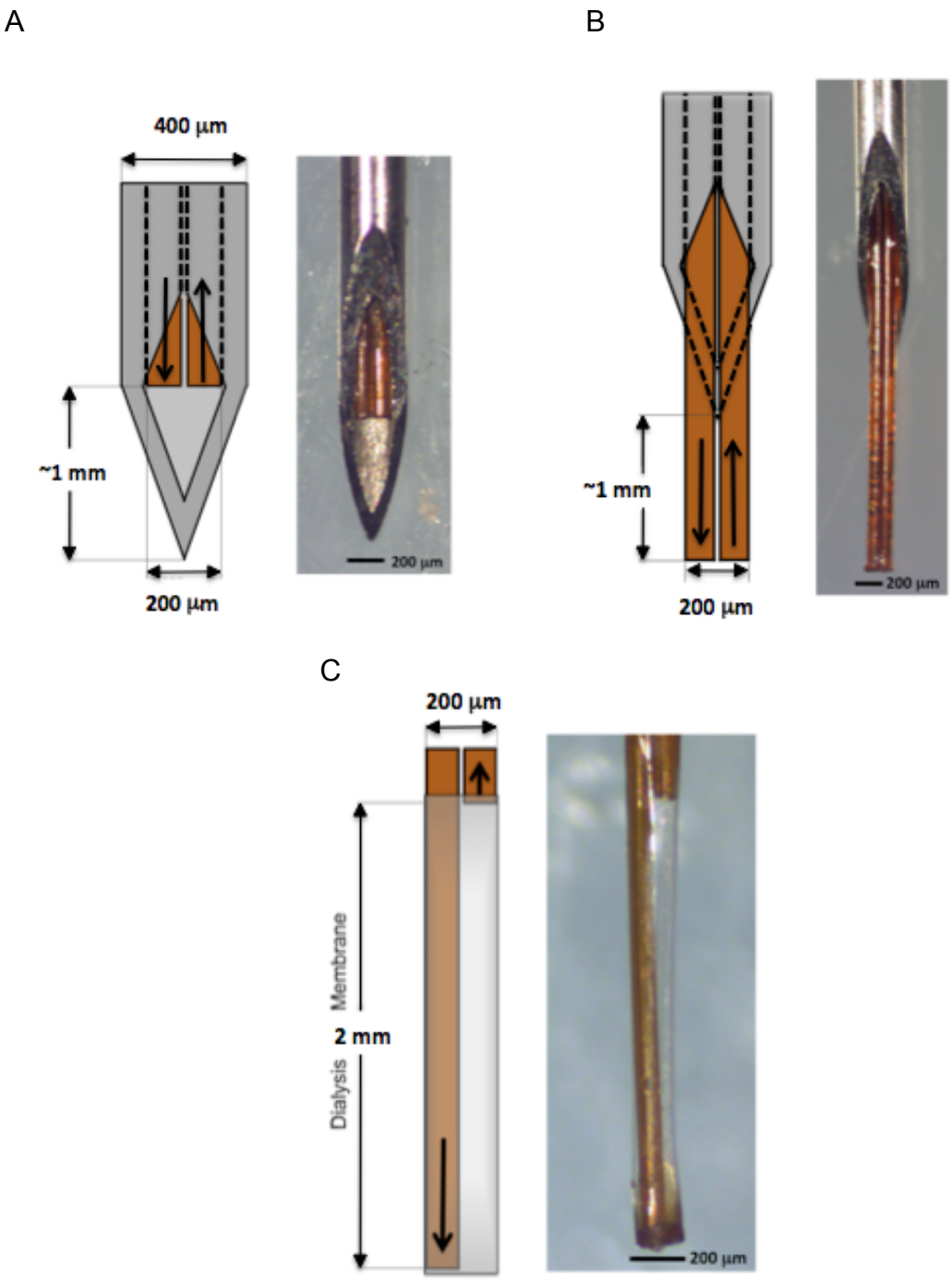

Figure 2-1: Diagrams of probes tested in neurochemcial sampling experiments. Drawings on the left of each probe photo illustrate dimensions and direction of flow. Needle-sheathed PPP probes (A) minimized clogging but decreased spatial resolution, when compared to miniaturized PPP probes (B). Flow in PPP occurs directly at the capillary tips, which improves spatial resolution as much as 500-fold, compared to MD probes (C). In MD, flow area is limited by the dialysis membrane. Scale bars are 200 µm.

Co., Reno, NV), in a syringe pump and continued downstream in the following order: Valco ZU1XC union, 15-cm long 40 μm i.d. x 360 μm o.d. capillary, Upchurch P-772 union, and inlet capillary of the probe. Similarly, in the direction of flow, the pull line consisted of the outlet capillary of the probe, a liquid flow meter (Sensirion SLG1430-025), and a 10-cm long 20 μm i.d. x 360 μm o.d. capillary.

The pull capillary was initially connected to a 25 μL syringe, as in the push line. First, aCSF was flushed through both probe lines at 500 nL/min to minimize clogging. Upon implantation (approximately 5 s), the flow rate was reduced to 50 nL/min over 1 min, and the outlet capillary was switched from syringe to vacuum to begin withdrawing sample. PPP was performed for 3 h 20 min, as pull flow rate at 50 nL/min was confirmed with the liquid flow meter output (Figure 2-2).

The microdialysis set-up, in direction of flow, consisted of a 1 mL syringe, a Valco union, a 15-cm long 40 μm i.d. x 360 μm o.d. capillary, and the probe inlet. A syringe pump infused aCSF through the probe at 1 μL/min and sample was pushed through the outlet by convection & passive diffusion. MD was performed for 3 h 20 min.

Cell Viability Dye Infusion

A nuclear stain cocktail of 162 μM Hoechst 33342 (H342), which labeled all cells, and 50 μM Sytox Orange (SO), which labeled damaged cells, was prepared by adding 2 μL aliquots of H342 and SO stock solutions to sterile Milli-Q water with glucose to yield 400 μL of isotonic solution. The osmolality of the dye cocktail was adjusted to 285-295 mOsm/kg with glucose to prevent swelling or shrinking of surrounding cells. After 3 h 20 min of neurochemical sampling, the perfusion media was switched from aCSF to the nuclear dye cocktail (Figure 2-3 A). In PPP experiments, the

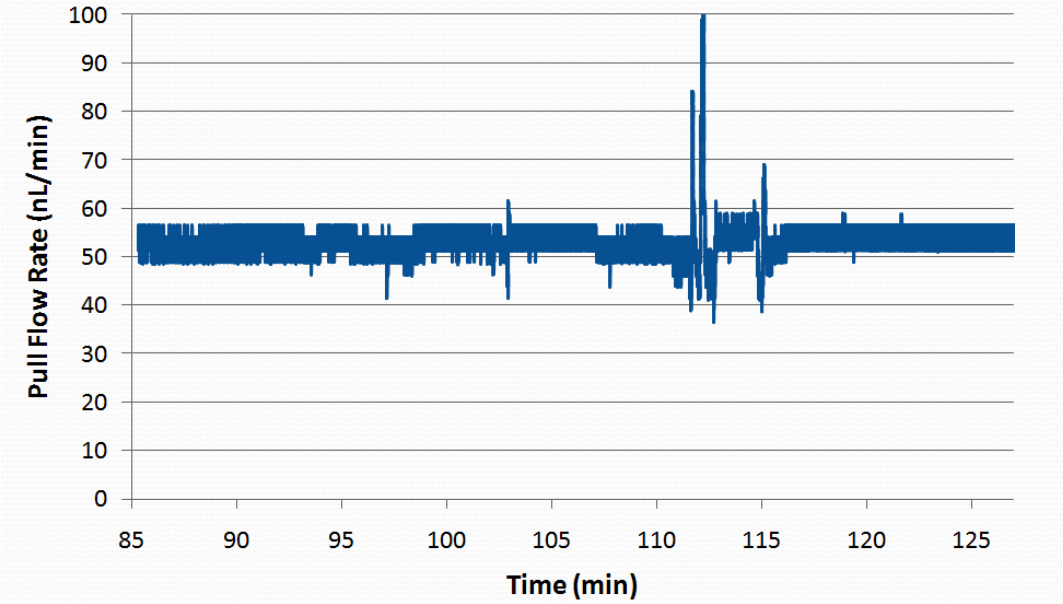

Figure 2-2: Readings from Sensirion liquid flow meter. Pull flow rate in PPP was maintained at 50 nL/min to match push flow rate. Occasionally, vacuum pressure was increased or capillary lines were flushed to counteract clogging and re-establish targeted pull flow rate. In the worst cases, these spikes occurred every 20-30 minutes for less than a minute at a time.

A

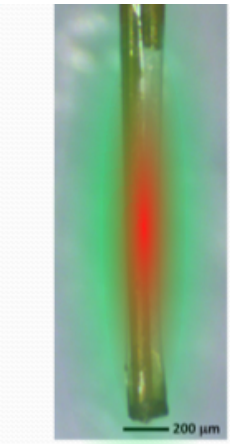

Microdialysis
(Cellulose Membrane)

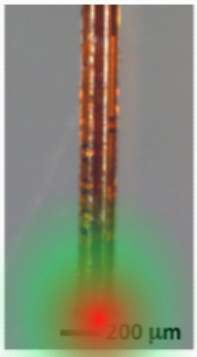

Push-Pull Perfusion
(Fused-Silica Capillaries)

Nuclear Stains

Hoechst 33342

All cells

Sytox Orange

Damaged Cells

Damaged cell count/percentage within reach of nuclear stain cocktail

B

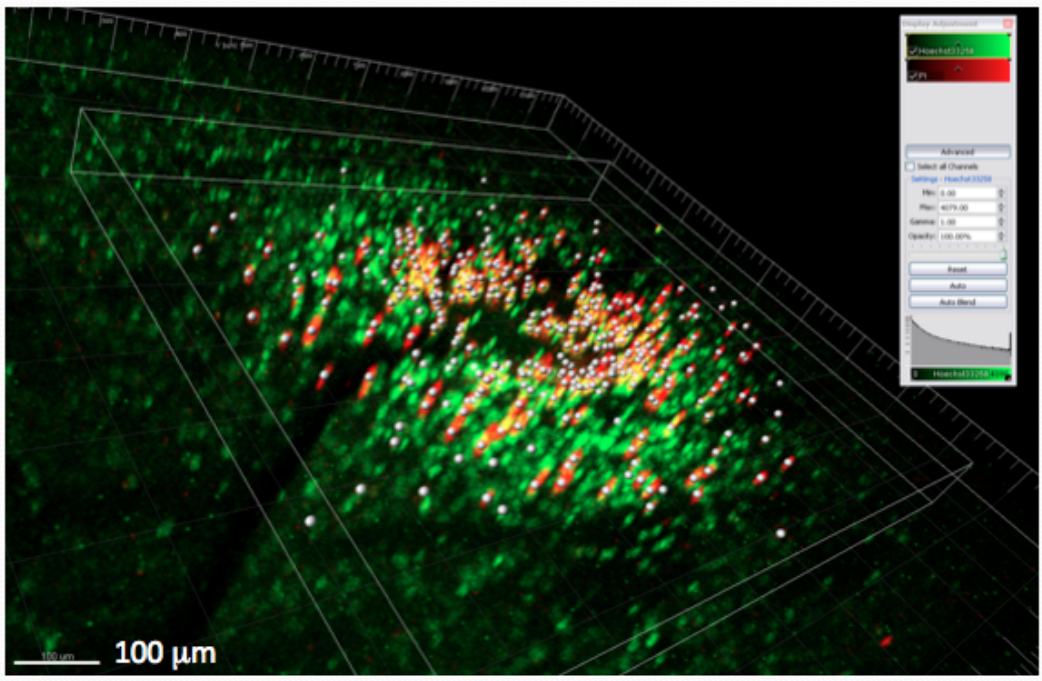

Figure 2-3: Overview of cell viability experiments. (A) After neurochemical sampling, a nuclear stain cocktail labeling all cells (green) and dead cells (red) within reach of the dye was infused into the brain. (B) Cell count and dead/all cell ratio were calculated with Imaris as a metric for tissue damage.

dye was infused at 50 nL/min for 20 min. For a comparable staining radius, the dye was infused at 1 μL/min for 30 min in MD experiments.

Immediately following dye infusion, probes were removed and animals were transcardially perfused with 200 mL phosphate buffered saline, followed by 200 mL of 4% paraformaldehyde using a constant pressure system (Bjornsson et al., 2008). Brains were removed, post-fixed for 24 h, and horizontal 100 μm tissue sections (perpendicular to the probe tract) were collected using a Leica VT1000 vibratome. A series of 50-60 tissue slices were collected from each animal, reaching a depth of 4.5 (PPP) / 5.5 (MD) mm from the dorsal surface of the brain. Alternating tissue slices (every other 100 μm) within the staining range were mounted in ProLong Gold for confocal imaging.

Confocal Imaging and Cell Count Analysis

Images were collected within 48 hours of dye infusion to prevent loss of fluorescent labeling through diffusion. 3-D data sets of 512 x 512 pixel images at 10x from each H342 & SO labeled tissue slice were acquired with an Olympus FV500 laser-scanning confocal microscope (405 nm, 543 nm laser excitations). Images were imported into Imaris (Bitplane, Inc., South Windsor, CT) for quantification of H342 & SO labeling (Figure 2-3 B).

The "count spot" module was selected and filters for cell size and background intensity were set to attain cell count. Because the dyes labeled all cell nuclei bodies, including microglia, astrocytes, and neurons, we set the upper limit of nuclei width to 10 μm, an approximation based on reported values of average neuron nuclei widths (3 to 18 μm) and visually matching labeled spot size to perceived average nuclei size (West et al., 1991). The percentage of non-viable cells (SO-labeled) within total cells in reach of the

dye cocktail (H342-labeled) was calculated to determine the extent of damage due to neurochemical sampling.

Results

In this study we evaluated three styles of sampling probes (Figure 2-1) for dye infusion with and without neurochemical sampling/flow (n=4 for each of the six conditions): low-flow push-pull perfusion ensheathed in a stainless-steel needle (PPP), "miniaturized" low-flow push-pull perfusion (mini PPP) without a needle at the probe tip, and "side-by-side" microdialysis (MD). Sampling tips in PPP probes had a cross sectional area of 0.063 mm^2 (needle encasing two 100 μm side-by-side capillaries), while sampling tips in the mini PPP probes had a cross sectional area of ~0.015 mm^2 (two 100 μm side-by-side capillaries). MD probes had a cross sectional area of ~0.018 mm^2 (dialysis membrane encasing two 100 μm side-by-side capillaries).

To evaluate acute tissue damage, H342/SO dye cocktail was infused through the probe after sampling. H342 stained all cells, while SO stained cells that had been damaged by probe implantation and sampling flow. By comparing the number of cells that had been stained by these two dyes, it was possible to determine the fraction of cells damaged in the sampling region. All probes resulted in some dead cells around the probe during the 3 h 20 min sampling period. Small effects of flow were seen. The relatively small sphere of damage associated with the PPP probes suggest that this technique can be effectively used.

Confocal Fluorescent Microscopy Images

After sampling, the brain tissue was sliced to 100 μm thick sections perpendicular to the probe track. Every other 100 μm section along the length of the probe was collected and imaged. Collapsed 3-D stacks were separated into H342 (green) and SO (red) channels, displaying total cells and dead cells, respectively, for PPP, mini PPP, and MD (Figure 2-4). For each probe style, experiments were performed with and without sampling flow to allow determination of the effect of flow on tissue response. This approach allowed assessment of damage radiating away from probes at different depths relative to probe insertion.

For both PPP designs, the section with the largest cell count, or signal, was determined to be near the sampling tip (0.0) (Retterer et al., 2008). The Z-range of staining was approximately -0.6 – +0.8 mm in needle-sheathed PPP, and -0.2 – +0.8 in mini PPP, with respect to the probe tip (0.0). Staining range was more limited in mini PPP, likely due to direct tissue contact at the probe tip, constricting flow. The needle in the initial PPP design cleared some tissue at the sampling area upon implantation, and may have created more space for flow and dye infusion. In the plane parallel to the probes, dye infusion areas appeared to be mostly circular for needle-sheathed PPP and teardrop-shaped for mini PPP. For both PPP probes, the fluorescent signal gradually decreased moving away from the probe tips.

In MD, the staining area coincided with the active length of the dialysis membrane. Since the inlet capillary was at the vertical bottom of the membrane, the last ventral stained section was labeled as the probe tip (0.0). Because dye flows through the active length in MD, the Z- range of staining was approximately 0.0 – +2.0 mm with

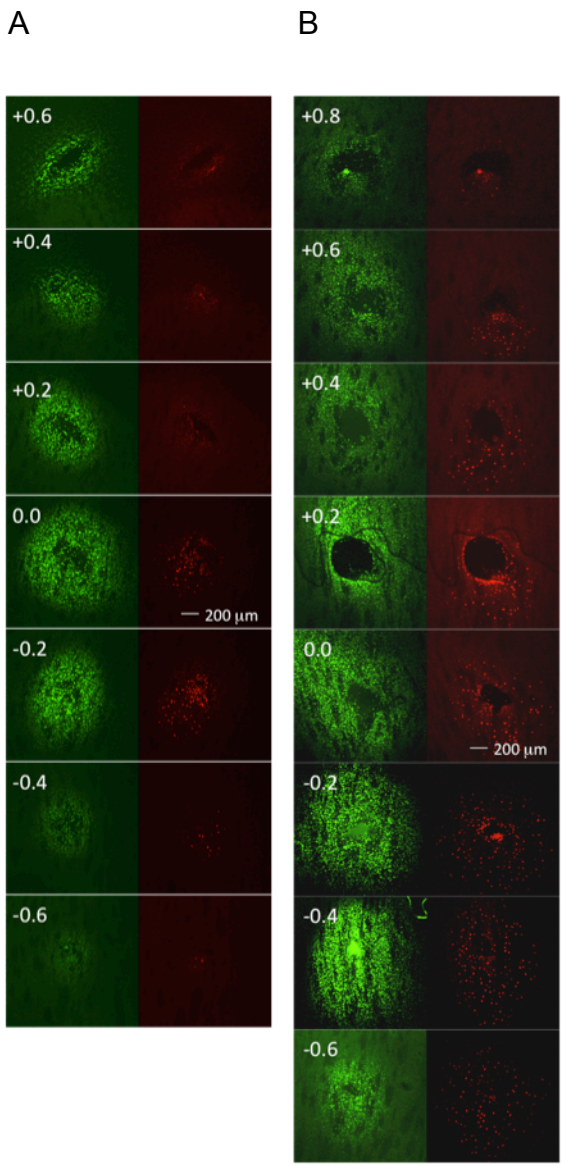

Figure 2-4: Fluorescent images (10x, voxel size 2.5 x 2.5 x 3.2 µm) of cell viability-stained 100 µm horizontal sections in PPP no flow (A), PPP flow (B), mini PPP no flow (C), mini PPP flow (D), MD no flow (E), and MD flow (F) (n=4 for each condition). All cells within reach of the dye cocktail were stained green by H342, while damaged cells were stained red by SO. Sections are labeled according to their relative vertical distance from the sampling tip (0.0) in mm. Scale bars are 200 µm.

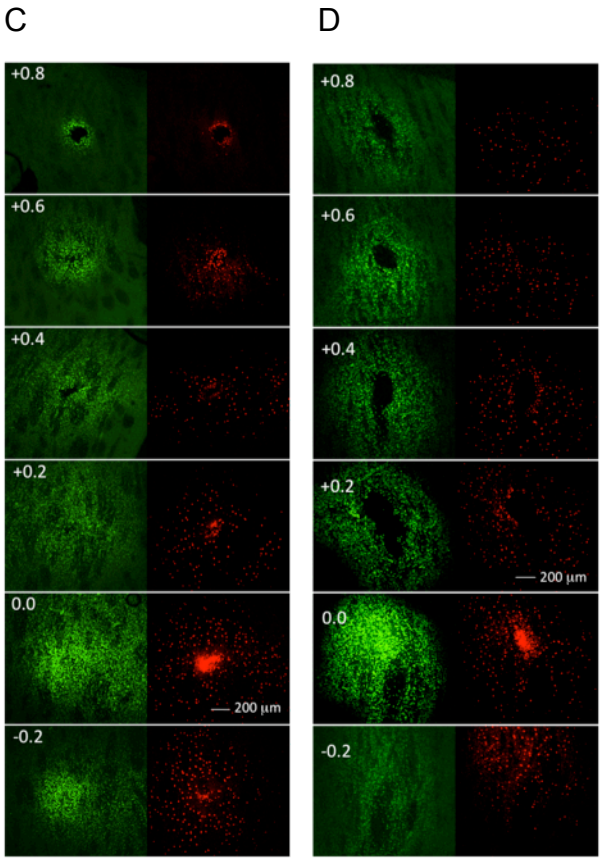
C
D
+0.8
+0.6
+0.4
+0.2
0.0
-0.2
200 µm

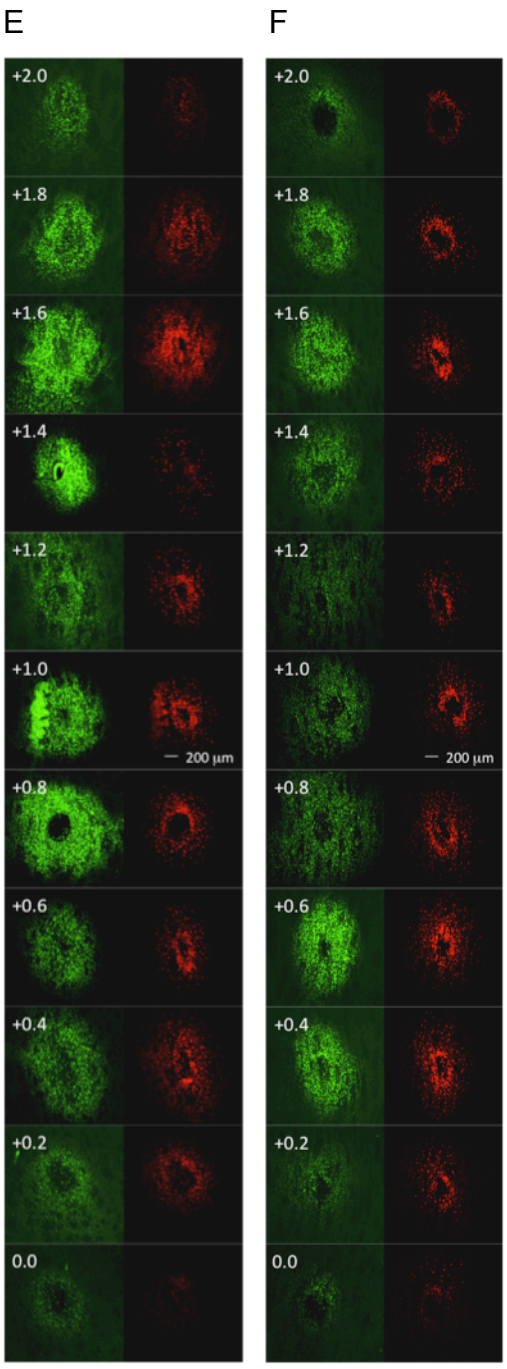
E
F
+2.0
+1.8
+1.6
+1.4
+1.2
+1.0
200 µm
+0.8
+0.6
+0.4
+0.2
0.0

respect to the probe tip. In the plane parallel to the probes, dye infusion areas appeared oval-shaped for MD. Compared to PPP, the fluorescent signal in MD remained relatively consistent throughout the dye stained area.

Overall Cell Count and Dead/Total Cell Ratio

To further assess tissue damage, image analysis software was used to count total cells labeled by H342 and SO within reach of the dye at each section (n=4 for each condition). As mentioned above, cell count or dye distribution patterns in PPP and MD appeared spherical/teardrop and oval shaped, with the center at 0.0 and +1.0 mm from the probe tip, respectively. This trend was expected from the point source flow in PPP and the uniform flow defined by the dialysis membrane in MD. Dead/total cell ratio was also calculated for each stained section (Figure 2-5). By running independent t-tests on sections within each method, significant differences ($p<0.05$) in dead/total cell ratio between flow and no flow conditions were seen in PPP and MD, but not in mini PPP.

In needle-sheathed PPP with flow, the percentage of damaged cells was 15 to 25%. In PPP without flow we found lower dead cell percentage at most positions along the probe with a range of 5 to 20% (Figure 2-5 A). The difference between the flow and no-flow condition was significant at several points ventral to the probe tip. The fraction of cells damaged without flow increased moving dorsal from the probe tip, and seemed to correspond to increasing diameter of the probe, from the narrow needle point up to full needle width. With flow however, the added tissue damage was greater ventral to the probe so that the percentage of damaged cells was relatively constant along the probe track. This result suggests that flow can contribute to tissue damage in PPP and that the wider bore of the probe does add to tissue disruption.

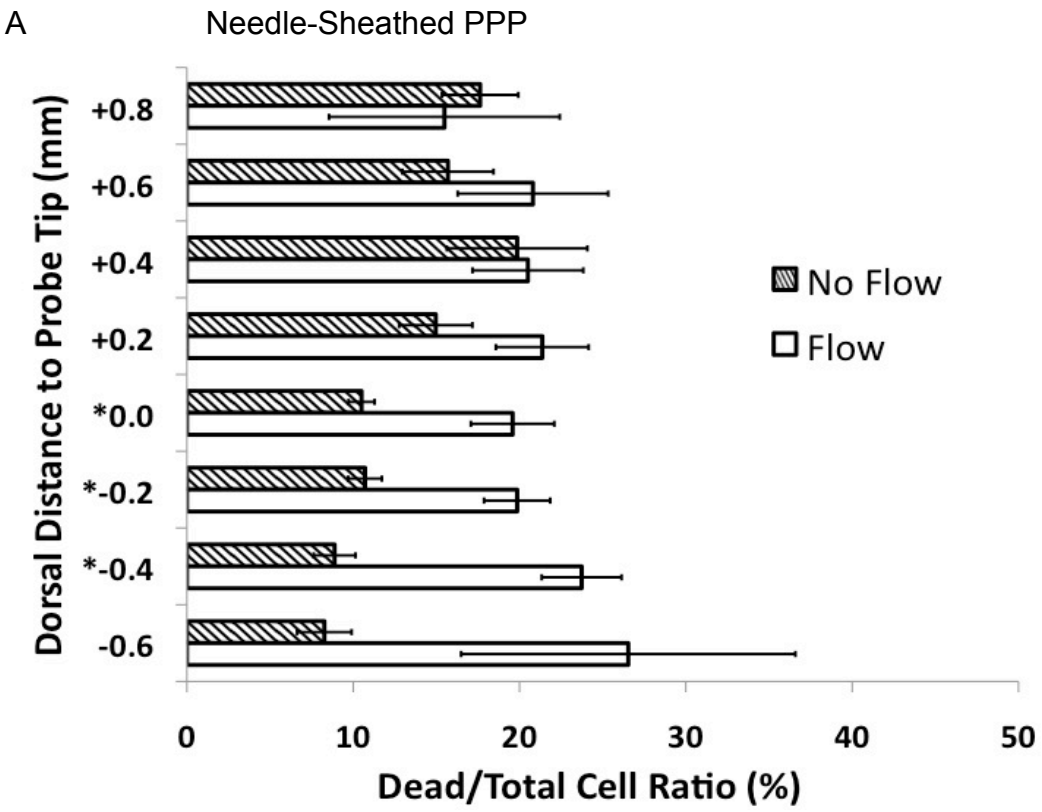

Figure 2-5: Dead/total cell ratio in needle-sheathed PPP (A), mini PPP (B), and MD (C) for flow & no flow conditions, as calculated from H342 & SO cell counts. Sections with significant differences ($p<0.05$) in dead/total cell ratio are labeled with an asterisk. (A) in needle-sheathed PPP, significant differences ($p<0.05$) existed between flow and no flow for sections in the sampling region (0.0 thru 0.4 mm below the probe tip), where the needle displaced tissue. (B) In mini PPP, no such differences existed. (C) In MD, significant differences ($p<0.05$) between flow and no flow were located at non-consecutive sections (0.6 and 1.8 mm above the probe tip). Error bars are standard error.

B Miniaturized PPP

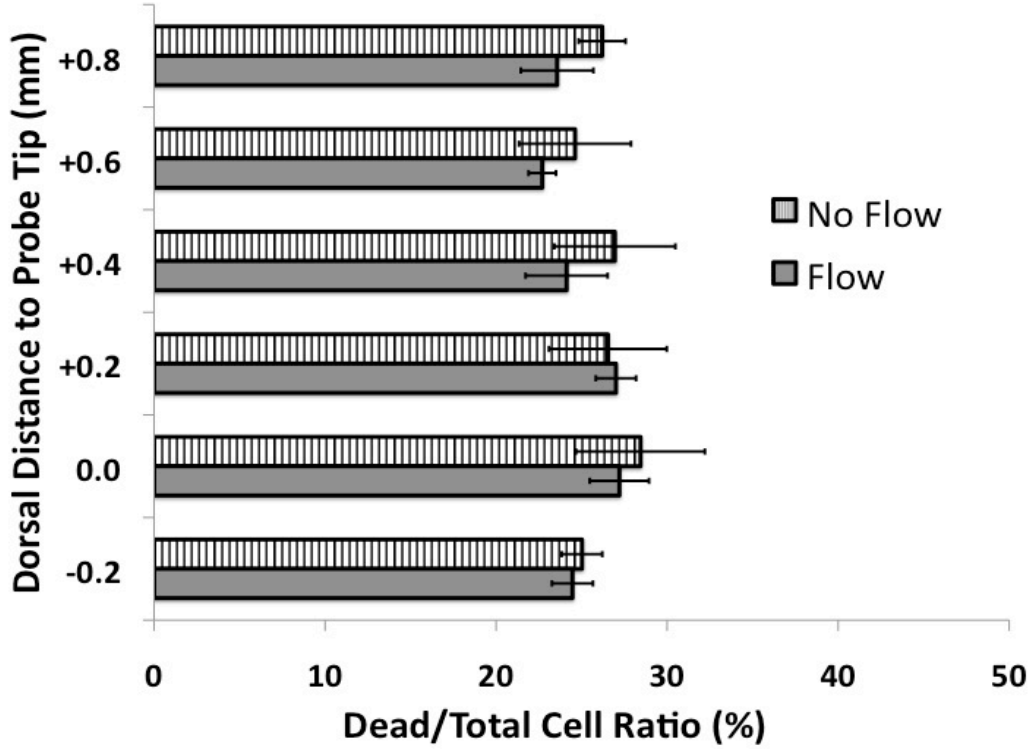

C Microdialysis

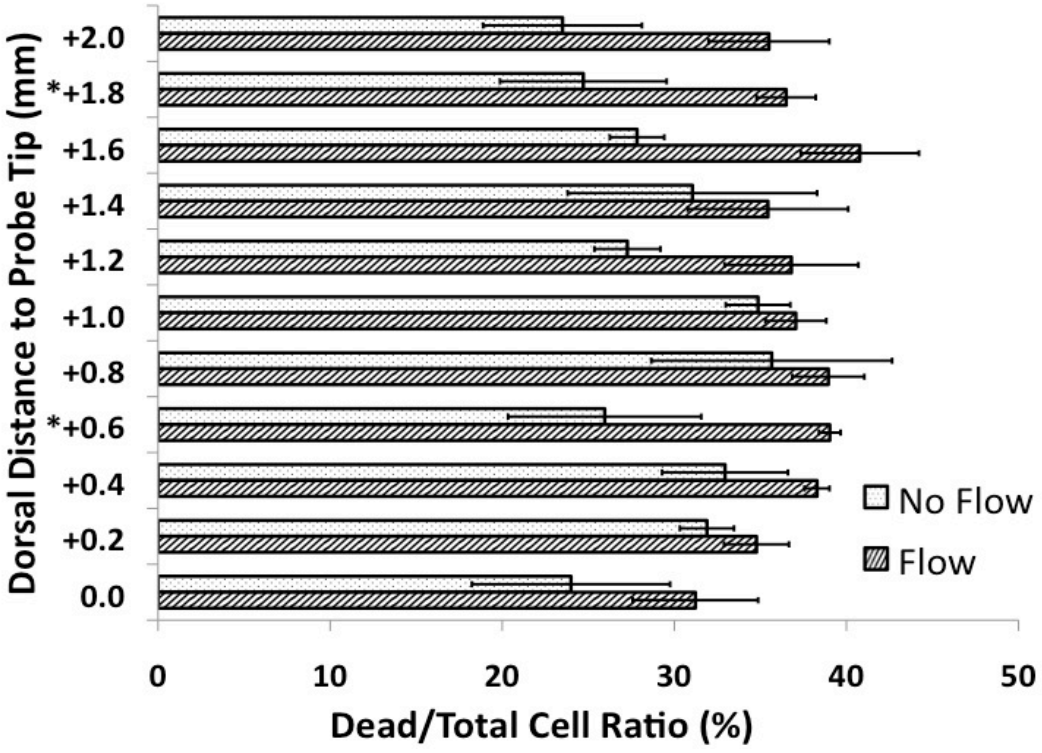

For mini-PPP, the percentage of damaged cells was consistent along the narrower probe. Interestingly, relatively little effect of flow was observed (Figure 2-5 B). This result suggests that an interaction between the needle tip and flow contributed to cell damage in PPP (e.g., the insertion of the needle tip into the tissue made the cells more vulnerable to the effects of flow) and that low flow rates per se, such as at the tip of a mini-PPP, are not especially damaging. This is an important point for PPP as exposure of cells to flow is an obvious potential source of tissue damage. Of course, in all our experiments some flow is required to deliver dye, therefore these experiments evaluate the effect of short bursts of flow versus continuous flow for 3 h 20 min.

Dead/total cell percentage in MD was between 30 and 40% all along the probe (Figure 2-5 C). In general a slightly higher percentage of dead cells was found with flow. For most points along the probe, this difference was not statistically significant ($p>0.05$), but it was at 1.8 and 0.6 mm dorsal of the probe tip. The effect of flow may relate to some outflow from the probe due to ultrafiltration effects or possibly that a component of the aCSF, which would be delivered at a greater concentration with flow, might accelerate cell damage.

In evaluating probes with flow, which is comparable to the actual sampling condition, we found that the percentage of dead cells across areas with dye was 15-20% for PPP, 20-30% for mini PPP, and 30-40% for microdialysis (Figure 2-6). The greater dead/total cell ratio in mini PPP vs. needle-sheathed PPP may be due to the geometry of a tapered needle versus a blunt capillary tip (Li et al., 2011). In particular, the shear force exerted on tissue is more graded, less abrupt in tapered needles, decreasing the likelihood of cell damage. Since flow is restricted to the active length of the membrane, the

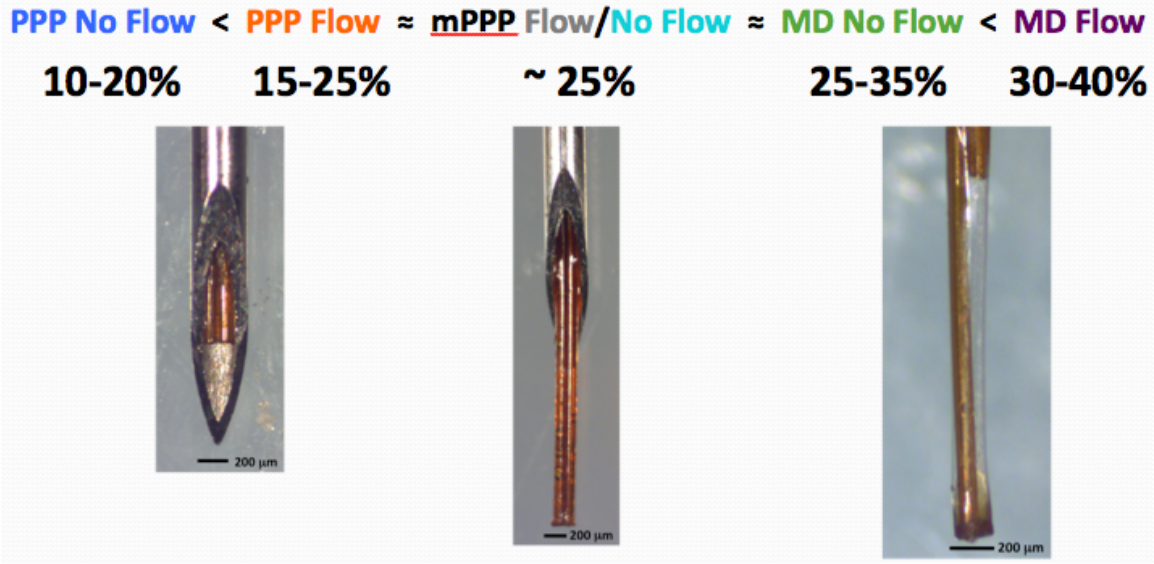

Figure 2-6: Comparison of overall dead/total cell percentages between PPP, mini PPP, and MD. PPP no flow had the lowest dead/total cell ratio, while MD flow had the highest. Most importantly, dead/total cell ratio in PPP flow and mini PPP flow was less than in MD flow ($p<0.05$).

sampling area matches the dyed area in MD. In the region closest to actual sampling points in PPP (0.0 to 0.2 mm ventral to the probe tip), we found that the percentage of dead cells was near 20% for PPP and near 25% for mini PPP. Thus, both PPP and mini-PPP damaged fewer cells in the sampling region and overall than microdialysis, as confirmed by One-Way ANOVA, Tukey test, statistical analysis ($p<0.05$).

Concentric Ring Cell Count and Dead/Total Cell Ratio

To quantify the gradient of damage, cell count was performed within concentric rings of increasing radii with respect to the horizontal probe hole center: at the probe tip (0.0) for the PPP probes and at 1.0 mm dorsal to the probe tip for MD (Figure 2-7). These sections corresponded to the greatest fluorescent signals in cell viability data sets. H342-labeled cells extended as far as approximately 0.7 mm from the probe center, with SO-labeled cells reaching just as far in some sections. However, dead cells were more concentrated near the probe hole.

Because sampling probes were removed from the brain immediately after sampling and before fixation, the probe hole tended to retract towards its original confirmation, normalizing the radial distances in PPP versus MD to some extent. In other words, cell count was performed across a similar spatial distribution, such that concentric rings represented nearly the same regions in MD and PPP. Concentric ring dead/total cell ratio analysis suggested that the overall differences discussed in the previous section were limited to within 250 μm of the probe hole center.

Dead/total cell ratio decreased with radial distance from the probe center. As confirmed by One-Way ANOVA, Tukey test, statistical analysis ($p<0.05$) in each ring, MD groups (flow or no flow) had significantly greater dead/total cell ratio than needle-

A

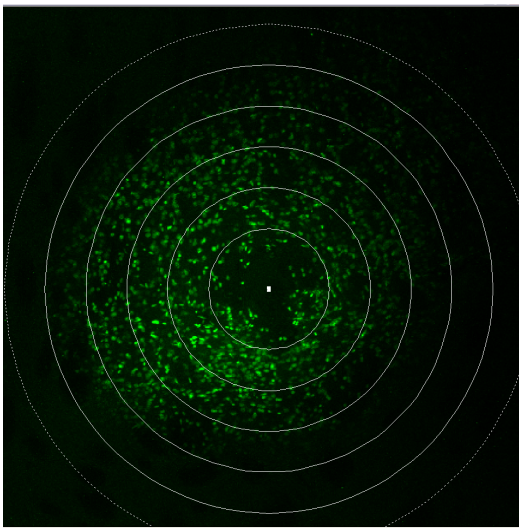

B

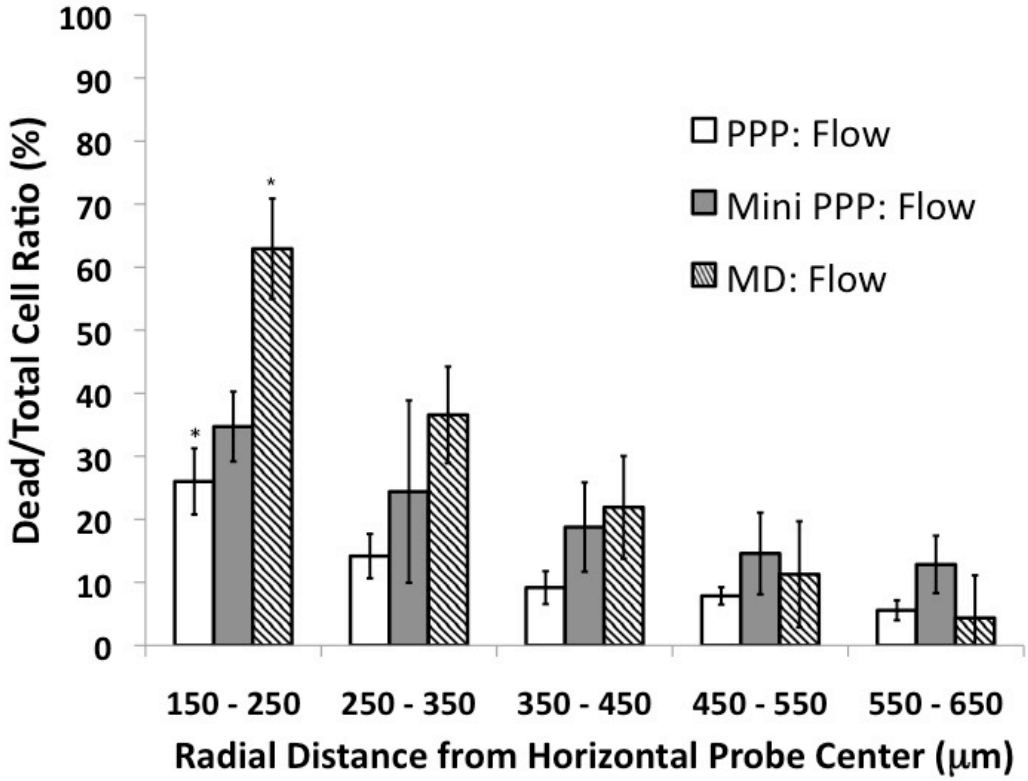

Figure 2-7: The gradient of dead/total cell ratio with respect to the horizontal probe hole center in PPP, mini PPP and MD for flow conditions (n=4 for each group). Cell count was performed within concentric rings of increasing radii (A) at peak cell count sections: at the probe tip (0.0) in PPP, and +1.0 mm from the probe tip in MD. Significant differences ($p<0.05$) between PPP flow and MD flow only existed within 250 μm of the probe hole center (B). Error bars are standard error.

sheathed PPP groups (flow or no flow) in the 2 (out of 5) innermost rings. Specifically, dead/total cell ratio was significantly less in needle-sheathed PPP flow vs. MD flow in only one ring (150-250 μm). Similar to results in overall dead/total cell ratio analysis, no significant differences existed between mini PPP flow & no flow and any other groups.

Discussion

The data on cell viability in MD vs. low-flow PPP presented herein expands on earlier tissue response findings in neurochemical sampling. A previous study comparing MD and high flow PPP (10 μL/min) with cresyl violet staining concluded the damage was the same in the two methods (Myers et al., 1998). Histology at the time gave limited, macroscopic information. In one sample, the diameter of damage caused by MD was determined to be 100-300 μm greater than that caused by PPP, and vice versa in another sample. Data in our study indicates that low-flow PPP causes less tissue damage than MD in flow conditions.

Although information on whole-cell populations was not included, the semi-quantitative study on MD, described previously, illustrated ultrastructural disturbances as far as 400 μm to 1.4 mm from the probe tract (Clapp-Lilly et al., 1999). Similarly, damaged cells were seen approximately 700 μm from the horizontal probe hole center in our results. In 4 hr MD studies labeling blood vessels with fluorescent nanobeads, vasculature viability of less than 10% was reported (Jaquins-Gerstl and Michael, 2009; Jaquins-Gerstl et al., 2011). In contrast, we calculated a cell viability of 60-70%, suggesting that acute microdialysis may not be as detrimental to brain tissue.

The observation that no clear region of damage could be found in low-flow PPP (Kottegoda et al., 2002) was based on visual examination of micrographs stained with

cresyl violet. In a study assessing the tissue damage caused by push-pull electro-osmotic sampling ex vivo, approximately 10% cell death was observed via propidium iodide dead cell staining. (Hamsher et al., 2010). Similarly, low-flow PPP exhibited 10-25% cell damage. Dead/total cell ratio measurements via cell viability staining in PPP, mini PPP, and MD have enabled the visualization and analysis of whole-cell environments in the sampling area. We determined that PPP does in fact elicit a measureable tissue response, though less than that caused by MD.

Through statistical analysis ($p<0.05$), we determined which sampling groups had significantly different overall dead/total cell ratio means, namely less in PPP flow vs. MD flow. A possible explanation for this difference between MD and needle-sheathed PPP may be because of higher volumetric flow rate through the membrane/tissue interface in MD. Moreover, there may be more micromotion in MD due to higher flow rate and sampling area. Another potential source of the extent of damage is the relatively poor biocompatibility of the regenerated cellulose membrane in MD (Miyamoto et al., 1989) vs. the polyimide and stainless-steel interface in needle-sheathed PPP (Jacobs and Oloff, 1985; Wang et al., 2006). Since MD has been invaluable for measuring, analyzing, and manipulating neurochemical levels in a variety of physiological states, it follows that PPP can also be a versatile tool for neurochemical monitoring.

Tissue response data, as measured by dead/total cell ratio, can be used as a baseline from which to improve probe designs/procedures to minimize brain injury and optimize chemical monitoring. Anti-inflammatory reagents delivered through the probe could counteract the immune response to the foreign body probe. Another strategy to

minimize tissue response is to coat or make the probe out of more biocompatible materials like titanium.

Probe construction and operation should be considered when performing neurochemical sampling experiments. Push-pull probes were easier to construct than microdialysis probes, with the former completed in 1 day, and the latter in 3 days. Yet, in terms of sampling, MD was considerably easier to perform than PPP. If the probe worked in vitro, the success rate of *in vivo* flow was close to 100% in MD, and near 75% for PPP. Moreover, the miniaturized PPP probes were more susceptible to clogging, lowering the sampling success rate to around 50%. Needle-sheathed probe size was restricted by the smallest needle inner-diameter in which capillaries could fit. Overall, PPP and MD probe size is limited by fluid back pressure, temporal resolution, volume of sample collected, durability, ease of use, and fabricating technology. Considering the trade-offs between probe construction and operation, MD was easier to execute than PPP overall.

Conclusions

This study confirmed a difference in tissue response between low-flow push-pull perfusion and microdialysis. Needle-sheathed PPP and mini PPP exhibited less overall damage than MD in flow conditions, as measured by dead/total cell % ($p<0.05$). PPP caused more localized damage, while MD caused more uniform damage. Compared to no flow conditions, tissue damage during flow in needle-sheathed PPP was pronounced at and directly below the sampling tip. Sections with greater dead/total cell % in MD flow vs. no flow were not associated with a particular region. For mini PPP, no significant differences ($p>0.05$) existed in flow vs. no flow. Nor were there differences for mini PPP overall vs. PPP flow and MD no flow. Thus for PPP sampling, we recommend the

miniaturized design since spatial resolution is improved compared to needle-sheathed PPP. Undoubtedly, low-flow PPP has dramatically reduced the tissue damage caused by the higher-flow rates in earlier iterations. These tissue response findings validate low-flow push-pull perfusion as a suitable alternative to microdialysis, and encourage the use and development of PPP for engineering and neuroscience applications.

References

Barzo P, Marmarou A, Fatouros P, Hayasaki K, Corwin F. Contribution of vasogenic and cellular edema to traumatic brain swelling measured by diffusion-weighted imaging. J. Neurosurg., 1997; 87: 900-7.

Benveniste H, Drejer J, Schousboe A, Diemer NH. Regional cerebral glucose phosphorylation and blood-flow after insertion of a microdialysis fiber through the dorsal hippocampus in the rat. Journal of Neurochemistry, 1987; 49: 729-34.

Bjornsson CS, Lin G, Al-Kofahi Y, Narayanaswamy A, Smith KL, Shain W, Roysam B. Associative image analysis: A method for automated quantification of 3D multi-parameter images of brain tissue. Journal of Neuroscience Methods, 2008; 170: 165-78.

Cellar NA, Kennedy RT. A capillary-PDMS hybrid chip for separations-based sensing of neurotransmitters in vivo. Lab on a Chip, 2006; 6: 1205-12.

Clapp-Lilly KL, Roberts RC, Duffy LK, Irons KP, Hu Y, Drew KL. An ultrastructural analysis of tissue surrounding a microdialysis probe. Journal of Neuroscience Methods, 1999; 90: 129-42.

Davies MI, Cooper JD, Desmond SS, Lunte CE, Lunte SM. Analytical considerations for microdialysis sampling. Advanced Drug Delivery Reviews, 2000; 45: 169-88.

Delgado JM, DeFeudis FV, Roth RH, Ryugo DK, Mitruka BM. Dialytrode for long term intracerebral perfusion in awake monkeys. Archives internationales de pharmacodynamie et de therapie, 1972; 198: 9-21.

Dluzen DE, Ramirez VD. A miniaturized push-pull cannula for use in conscious, unrestrained animals. Pharmacology Biochemistry and Behavior, 1986; 24: 147-50.

Gaddum J. Push-pull cannulae. J. Physiol, 1961; 155.

Hamsher AE, Xu H, Guy Y, Sandberg M, Weber SG. Minimizing Tissue Damage in Electroosmotic Sampling. Analytical Chemistry, 2010; 82: 6370-6.

Jacobs AM, Oloff LM. Podiatric metallurgy and the effects of implanted metals on living tissues. Clinics in Podiatry, 1985; 2: 121-41.

Jaquins-Gerstl A, Michael AC. Comparison of the brain penetration injury associated with microdialysis and voltammetry. Journal of Neuroscience Methods, 2009; 183: 127-35.

Jaquins-Gerstl A, Shu Z, Zhang J, Liu Y, Weber SG, Michael AC. Effect of Dexamethasone on Gliosis, Ischemia, and Dopamine Extraction during Microdialysis Sampling in Brain Tissue. Analytical Chemistry, 2011; 83: 7662-7.

Kessler RM, Ellis Jr JR, Eden M. Analysis of emission tomographic scan data: limitations imposed by resolution and background. Journal of computer assisted tomography, 1984; 8: 514.

Kohsaka A, Watanobe H, Kakizaki Y, Suda T. A comparative study of the effects of nitric oxide and carbon monoxide on the in vivo release of gonadotropin-releasing hormone and neuropeptide Y from rat hypothalamus during the estradiol-induced luteinizing hormone surge: Estimation by push-pull perfusion. Neuroendocrinology, 1999; 69: 245-53.

Kottegoda S, Shaik I, Shippy SA. Demonstration of low flow push-pull perfusion. Journal of Neuroscience Methods, 2002; 121: 93-101.

Lee GJ, Park JH, Park HK. Microdialysis applications in neuroscience. Neurological Research, 2008; 30: 661-8.

Li M, Tian X, Schreyer DJ, Chen X. Effect of needle geometry on flow rate and cell damage in the dispensing-based biofabrication process. Biotechnology Progress, 2011; 27: 1777-84.

Millan M, Panayi F, Rivet J, Cara BD, Cistarelli L, Billiras R, Girardon S, Gobert A. .1 The role of microdialysis in drug discovery: focus on antipsychotic agents. Handbook of Behavioral Neuroscience, 2006; 16: 485-511.

Mitchell K, Oke AF, Adams RN. In-vivo dynamics of norepinephrine release reuptake in multiple terminal field regions of rat-brain. Journal of Neurochemistry, 1994; 63: 917-26.

Miyamoto T, Takahashi S-i, Ito H, Inagaki H, Noishiki Y. Tissue biocompatibility of cellulose and its derivatives. Journal of Biomedical Materials Research, 1989; 23: 125-33.

Mizuno M, Gearing M, Terasawa E. The Role of Neuropeptide Y in the Progesterone-Induced Luteinizing Hormone-Releasing Hormone Surge in Vivo in Ovariectomized Female Rhesus Monkeys. Endocrinology, 2000; 141: 1772-9.

Myers RD, Adell A, Lankford MF. Simultaneous comparison of cerebral dialysis and push-pull perfusion in the brain of rats: A critical review. Neuroscience and Biobehavioral Reviews, 1998; 22: 371-87.

Nandi P, Lunte SM. Recent trends in microdialysis sampling integrated with conventional and microanalytical systems for monitoring biological events: A review. Analytica Chimica Acta, 2009; 651: 1-14.

Parsons LH, Justice JB. Extracellular Concentration and In Vivo Recovery of Dopamine in the Nucleus Accumbens Using Microdialysis. Journal of Neurochemistry, 1992; 58: 212-8.

Paxinos G, Watson C. The rat brain in stereotaxic coordinates. Elsevier Academic Press: Amsterdam ; Boston, 2005.

Polikov VS, Tresco PA, Reichert WM. Response of brain tissue to chronically implanted neural electrodes. Journal of Neuroscience Methods, 2005; 148: 1-18.

Redgrave P. A modified push-pull system for the localised perfusion of brain tissue. Pharmacology Biochemistry and Behavior, 1977; 6: 471-4.

Retterer ST, Smith KL, Bjornsson CS, Turner JN, Isaacson MS, Shain W. Constant pressure fluid infusion into rat neocortex from implantable microfluidic devices. Journal of Neural Engineering, 2008; 5: 385-91.

Robinson DL, Hermans A, Seipel AT, Wightman RM. Monitoring Rapid Chemical Communication in the Brain. Chemical Reviews, 2008; 108: 2554-84.

Rueter LE, Fornal CA, Jacobs BL. A critical review of 5-HT brain microdialysis and behavior. Reviews in the Neurosciences, 1997; 8: 117-38.

Santiago M, Westerink B. Characterization of the in vivo release of dopamine as recorded by different types of intracerebral microdialysis probes. Naunyn-Schmiedeberg's archives of pharmacology, 1990; 342: 407-14.

Slaney TR, Nie J, Hershey ND, Thwar PK, Linderman J, Burns MA, Kennedy RT. Push-Pull Perfusion Sampling with Segmented Flow for High Temporal and Spatial Resolution in Vivo Chemical Monitoring. Analytical Chemistry, 2011; 83: 5207-13.

Szarowski DH, Andersen MD, Retterer S, Spence AJ, Isaacson M, Craighead HG, Turner JN, Shain W. Brain responses to micro-machined silicon devices. Brain Research, 2003; 983: 23-35.

Tang A, Bungay PM, Gonzales RA. Characterization of probe and tissue factors that influence interpretation of quantitative microdialysis experiments for dopamine. Journal of Neuroscience Methods, 2003; 126: 1-11.

Tucci S, Rada P, Sepúlveda MJ, Hernandez L. Glutamate measured by 6-s resolution brain microdialysis: capillary electrophoretic and laser-induced fluorescence detection application. Journal of Chromatography B: Biomedical Sciences and Applications, 1997; 694: 343-9.

Turner JN, Shain W, Szarowski DH, Andersen M, Martins S, Isaacson M, Craighead H. Cerebral astrocyte response to micromachined silicon implants. Experimental Neurology, 1999; 156: 33-49.

Wang M, Slaney T, Mabrouk O, Kennedy RT. Collection of nanoliter microdialysate fractions in plugs for off-line in vivo chemical monitoring with up to 2 s temporal resolution. Journal of Neuroscience Methods, 2010; 190: 39-48.

Wang X, Xu J, Zhu Y, Cooper KL, Wang A. All-fused-silica miniature optical fiber tip pressure sensor. Opt. Lett., 2006; 31: 885-7.

Weiss DJ, Lunte CE, Lunte SM. In vivo microdialysis as a tool for monitoring pharmacokinetics. TrAC Trends in Analytical Chemistry, 2000; 19: 606-16.

West M, Slomianka L, Gundersen HJG. Unbiased stereological estimation of the total number of neurons in the subdivisions of the rat hippocampus using the optical fractionator. The Anatomical Record, 1991; 231: 482-97.

Zhou F, Braddock JF, Hu Y, Zhu X, Castellani RJ, Smith MA, Drew KL. Microbial origin of glutamate, hibernation and tissue trauma: an in vivo microdialysis study. Journal of Neuroscience Methods, 2002; 119: 121-8.

CHAPTER 3

CHARACTERIZATION OF CYTOARCHITECTURE IN MICRODIALYSIS AND LOW-FLOW PUSH-PULL PERSUION

Introduction

The brain is a host to millions of neurons and glial cells, exchanging hundreds of neurotransmitters and metabolites (Bear et al., 2001). The spatial and morphological organization, or cytoarchitecture, of brain tissue is reflective of its physiological state. Moreover, analysis of the extracellular environment provides valuable chemical information that can be correlated to behavior, pharmacology, and pathophysiology (Weiss et al., 2000). *In vivo* neurochemical sampling is thus essential to understanding the brain and providing treatment to treat neural disorders e.g. Alzheimer's, Parkinson's (Robinson et al., 2008). Non-invasive techniques like positron emission tomography (PET) are usually expensive, unsuitable for animal studies, have poor temporal and spatial resolution, and are limited to a few neurotransmitters (Hans Lundqvist, 1999). Invasive sampling techniques involving probe implantation can measure multiple analytes with improved resolution. Therefore, the latter methods are a fitting alternative for neurochemical monitoring.

The most established method of neurochemical sampling is microdialysis, in which a 200-400 μm diameter by 1-4 mm long hollow-fiber dialysis membrane probe is inserted into the brain (Delgado et al., 1972). The inside of the fiber is perfused at 0.1-3.0 μL/min with artificial cerebrospinal fluid (aCSF). Extracellular fluid components diffuse

across the membrane according to their concentration gradient between the inside and outside of the membrane. A major advantage of microdialysis (MD) is its ability to reliably separate and detect a wide range of compounds, neurotransmitters, metabolites, amino acids, and drugs (Watson et al., 2006). Furthermore, it can filter molecules by molecular weight cutoff, but has difficulty collecting high molecular weight species (Myers et al., 1998).

In contrast to MD, push-pull perfusion (PPP) is an open system using two side-by-side or concentric capillary probes (Gaddum, 1961). The perfusion fluid directly contacts the tissue under study at the tip, thereby providing a 500-fold improvement in spatial resolution. Sample is "pulled" from one capillary and aCSF is "pushed" through the other capillary to replace the sampled volume. Initially PPP was conducted with flow rates as high as 25 μL/min (Myers and Gurleyorkin, 1985), but the current low-flow PPP method infuses/extracts fluid at 10-50 nL/min. PPP also has the capability to detect multiple analytes, and the temporal resolution can be improved by integrating segmented multi-phase flow (Slaney et al., 2011). The high collection efficiencies and direct collection of extracellular fluid in PPP give a tremendous advantage for sampling neurochemicals in low concentration, particularly neuropeptides (Mizuno et al., 2000).

Acute neurochemical sampling (2-4 hours) elicits an immediate injury response due to probe insertion itself, similar to peripheral wound reactions (Berkenbosch, 1992). The central nervous system wound healing response is initiated by mechanical trauma, with disruption of blood vessels releasing erythrocytes, clotting factors, and inflammatory factors that induce glial cell activation and proliferation. Insertion induced accumulation of fluid and necrotic nervous tissue causes vasogenic edema, further adding to the

intracranial pressure and brain tissue volume surrounding the implant (Barzo et al., 1997). Injured neurons send signals to recruit microglia (the resident macrophages of the brain) and astrocytes (glial cells that provide regulatory, structural, and nutritional support) to the wound site (Kreutzberg, 1995; Turner et al., 1999).

Normally, microglia have elongated, ramified processes for immune surveillance. Upon activation, cell body size and process diameters increase, and processes retract. Microglia migrate to the damaged structures, displace synaptic input, and proliferate (Blinzinger and Kreutzberg, 1968; Graeber et al., 1988). Neuronal cell death stimulates phagocytosis in microglia to eliminate neural debris (Streit and Kreutzberg, 1988). Astrocytes also undergo a graded, stereotypic immune response, by forming a barrier between the foreign body and the cellular environment (Eddleston and Mucke, 1993). However, these structural changes are pronounced after acute injury and are not covered in the studies herein. In response to brain injury, vasculature engages in occasional mitosis, but no substantial proliferation (Raivich et al., 1994). Facilitated transport across the endothelium, however, increases significantly (Raivich et al., 1998). In addition to such biological interference caused by probe insertion, fluid flow is another contributing factor to tissue damage that has not been examined thoroughly.

Initial MD tissue damage studies found that cerebral blood flow and local glucose metabolism decreased around the probe within 2 hr of implantation, but normalized within 24 hr (Benveniste et al., 1987). Various histological studies of MD probes implanted for 1-3 days have found regions of damaged, degenerating neurons in the surrounding area of the probe (Tang et al., 2003; Zhou et al., 2002a). A semi-quantitative tissue damage study reported neuronal density decreases up to 400 μm from a 40 hr

implanted probe, and intercellular disruption up to 1.4 mm from the probe tract (Clapp-Lilly et al., 1999). However, information on whole cell populations was not determined. There is still a need for characterization of cytoarchitecture in MD.

Tissue response studies are lacking in current PPP. Low-flow PPP has reduced mechanical disturbances inherent to high-flow PPP, and has been proposed to cause less tissue damage than MD. Yet, the tissue response in PPP has not been thoroughly characterized or compared to other methods. Another group's study suggested the minimal tissue damage (Kottegoda et al., 2002), which statistical data ($p<0.05$) in the previous chapter confirmed. Still, further tissue response studies would be helpful in defining PPP efficiency.

Histological studies with light and electron microscopy have provided some insight about the tissue response in neurochemical sampling methods, but comparisons between PPP and MD remain inconclusive (Myers et al., 1998). Confocal fluorescent microscopy offers high-resolution, high-contrast 3D imaging for quantifying location and distribution of cells, and delineation of key structures (Pawley, 2008). Immunohistochemistry (IHC) is useful for labeling specific cell types through antibody-antigen complexes. Through IHC, antibodies and molecular stains have been used to label glial cells and vasculature to assess cellular responses to neuroprosthetic devices (Spataro et al., 2005). By performing low-flow PPP and MD, labeling the brain tissue with IHC stains, imaging via confocal fluorescent microscopy, and performing image analysis, the research described in this chapter explores the relative changes in cell architecture between MD and low-flow PPP (Figure 3-1).

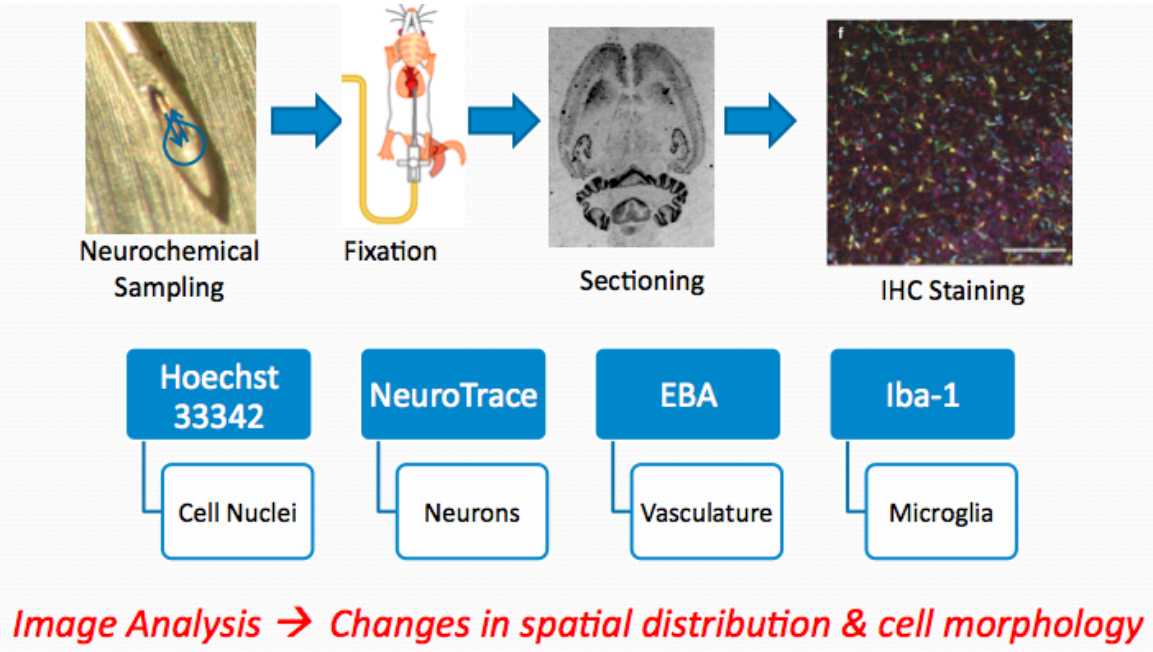

Figure 3-1: Overview of cytoarchitecture experiments. After neurochemical sampling, transcardial fixation, and sectioning, a 3 day IHC staining protocol was applied to brain sections to label cell nuclei, neurons, vasculature, and microglia. Image J was then used to quantify changes in cell architecture.

Materials and Methods

All reagents were purchased from Invitrogen, unless otherwise specified. Fused silica capillaries were obtained from Polymicro (Phoenix, AZ). All animal care, housing, and operative procedures were conducted in accordance with the Guide for the Care and Use of Laboratory Animals (National Institutes of Health publication 85-23, 1985). Rats were housed in a pathogen-free facility at the University of Michigan, given food and water ad libitum, and exposed to a 12-hour light/dark cycle. The University Committee on the Use and Care of Animals approved the experimental protocol.

Probe Fabrication

Side-by-side PPP probes were constructed by threading two 15-cm long 40 μm inner diameter (i.d.) x 100 μm outer diameter (o.d.) capillaries through a 26-gauge stainless steel needle (BD, Franklin Lakes, NJ), as described elsewhere (Cellar and Kennedy, 2006). The ends of these capillaries were attached to 2 cm-long 180 μm i.d. x 360 μm o.d. capillaries for connection to 360 μm fittings. All probe sections were glued together with cyanoacrylate adhesive (Duro Super Glue, Henkel, Rocky Hill, CT). The needle tip extended approximately 1 mm below the capillary tips in these needle-sheathed PPP probes (Figure 2-2 A). Miniaturized PPP probes, with the capillaries extending approximately 1 mm past the needle tip, were not tested. In previous studies comparing the dead/total cell ratio between needle-sheathed PPP, mini PPP, and MD, both PPP designs caused significantly less damage than MD ($p<0.05$), with a larger difference between needle-sheathed PPP and MD (Cepeda et al., in preparation).

Side-by-side MD probes with regenerated cellulose membranes were constructed as previously described (Parsons and Justice, 1992). Briefly, two 10-cm long 40 μm i.d. x 100 μm o.d. capillaries were inserted into a 200 μm-diameter regenerated cellulose membrane to form a 2-mm sampling length (Figure 2-2 C). The inlet capillary end was attached to a 2-cm length of 180 μm i.d. x 360 μm o.d. capillary adapter.

Animal Surgery and Neurochemical Sampling

Male Sprague-Dawley rats weighing 300-400 g were anesthetized with isoflurane and mounted in a stereotaxic frame. The probes were inserted into the striatum at the following coordinates: 1.0 mm anterior to bregma, ±2.6 mm lateral to midline, and 4.5 (PPP) / 5.5 (MD) mm ventral to dura (Paxinos and Watson, 2005). In PPP, aCSF (145 mM NaCl, 2.68 mM KCl, 1.01 mM $MgSO_4$, 1.22 mM $CaCl_2$, 1.55 mM Na_2HPO_4, 0.45 mM NaH_2PO_4, pH 7.4) was infused and sample withdrawn at 50 nL/min. In MD, aCSF was infused at 1 μL/min.

The push-pull perfusion system consisted of a syringe pump (Fusion 400, Chemyx, Stafford, TX) that infused aCSF into the striatum via the "push" arm of the probe, and a vacuum pump (GAST DOA-P704-AA) that withdrew sample from the striatum via the "pull" arm of the probe. In the push line, Valco ZU1XC unions connected a 25 μL syringe (Gastight, Hamilton Co., Reno, NV) to a 15-cm long 40 μm i.d. x 360 μm o.d. capillary, which was attached to the push arm of the probe by an Upchurch P-772 union. In the pull line, the "pull" arm of the probe was attached to a liquid flow meter (Sensirion SLG1430-025), which was attached to a 10-cm long 20 μm i.d. x 360 μm o.d. capillary. The other end of the capillary was initially connected to a 25 μL syringe, as in the push line. During implantation, aCSF was flushed through both

probe lines at 500 nL/min to minimize clogging. After the flow rate was reduced to 50 nL/min, the pull line capillary was switched from syringe to vacuum to begin withdrawing sample. We verified pull flow rate with the liquid flow meter readout. PPP sampling was performed for 3 h 20 min.

The microdialysis set-up consisted of a Valco union connecting a 1 mL syringe to a 15-cm long 40 μm i.d. x 360 μm o.d. capillary, or inlet of the probe. A syringe pump infused aCSF through the probe at 1 μL/min and sample was pushed through the outlet by convection and passive diffusion. MD sampling was performed for 3 h 20 min.

Brain Sectioning

After acute neurochemical sampling, probes were withdrawn, the brain tissue was fixed by transcardial perfusion with 4% paraformaldehyde (PFA), and brains were removed. Following post-fix at 4C in 4% PFA overnight, brains were rinsed 4x in HEPES buffered Hanks solution (HBHS) with sodium azide (90g/L). Brains were sliced in 100 μm sections perpendicular to the probe track, and stored in HBHS with sodium azide until ready for IHC staining. Two sections in PPP and one section in MD were used for this experiment: near the probe tip (approximately 4.5 mm ventral to the dura) and slightly below the probe tip (approximately 4.7 mm deep) in PPP, and at the vertical midpoint of the dialysis membrane in the MD probe (1.0 mm dorsal to the probe tip, approximately 4.5 mm deep). These sections, where the degree of flow was the greatest, were collected in flow (n=4) and no flow conditions (n=4) to compare the effect of probe insertion with sampling versus without sampling (Cepeda et al., in preparation). Additionally, a control site without probe insertion (n=4) was collected approximately 4.5 mm ventral to the dura.

Immunohistochemistry

Tissue slices were processed using the following IHC procedure. All incubations were followed by washes in HBHS with sodium azide. Slices were incubated with 5% sodium borohydride, solubilized with 0.2% Triton X-100 in HBHS, and incubated overnight in 5% bovine serum albumin in HBHS to block non-specific antibody binding. The following day slices were first incubated with 0.3% hydrogen peroxide to block endogenous peroxidase activity, followed by an overnight incubation with primary antibodies identifying vasculature (mouse anti-EBA, 1:300 dilution, Sternberger Monoclonals Inc.) and microglia (rabbit anti-Iba-1, 1:800 dilution, WAKO). The next day, samples were washed and incubated overnight with a cocktail of secondary antibodies (Alexa 488 goat anti-mouse and Alexa 546 goat anti-rabbit, 1:200 dilution), a nuclear stain (Hoechst 33342: H342, 0.1 mg/ml), and a Nissl substance (640/660 NeuroTrace, 1:150 dilution). Samples were washed before mounting in ProLong Gold for confocal imaging.

Confocal Microscopy Imaging

1024 x 1024 pixel images at 25x were collected as 3-D data sets on a Leica TCS SP5 confocal scanning microscope using emissions from four lasers (405 nm, 488 nm, 543 nm and 633 nm) and a 20x objective lens at 1.25 zoom. This yielded a voxel resolution of 0.6 x 0.6 x 1.5 µm. Data collection conditions were adjusted for tissue samples from each IHC run so that color level differences in the final images reflected changes in signal intensities. Collapsed stacks, or maximum projections, were created so that the entire Z dimension of the sample could be represented in one plane. Images were imported into Image J for image analysis.

Cytoarchitecture Analysis

Concentric circle masks were created in Metamorph to isolate 500, 750, and 1000 pixel diameter central regions (Figure 3-2 A). Spatial dimensions could then be measured in the 500 pixel diameter circle, in the ring between the 500 and 750 pixel diameter circles, and the ring between the 750 and 1000 pixel diameter circles. For all maximum projection images (n=4), we counted cell nuclei, neurons, and microglia in each circle/ring to calculate the differences in cell density with respect to the image center.

Using NIH Image J software, the scale was set to 1.644 pixels/μm to match the 1024 x 1024 pixel area. The maximum projection images were binarized, and cells were counted with the "analyze particle" feature. The area filter was set to 0-150 μm^2 for cell nuclei, 0-300 μm^2 for neurons, and 20-500 μm^2 for microglia. Cell density was calculated by dividing the cell count by the corresponding circle or ring area in mm^2 (n=4).

Because microglia area and process, or branch, length are related to the degree of activation, we measured average microglial area and used the "skeletonize" function in Image J to derive topological branch skeletons from the binary images (Fontainhas et al., 2011). The "analyze skeleton" Image J plugin was then applied to the skeletonized images (Figure 3-2 B), and average branch length was calculated as a metric for tissue damage (n=4) (Arganda-Carreras et al., 2010). Moreover, by circumscribing the region of activated microglia in each image with the freehand selection tool (Figure 3-2 C), we estimated the ratio of activated microglia area to total image area (n=4). The zone of abnormally-shaped activated microglia, circulating the probe site, was easily distinguished from uniformly distributed resting microglia. It is important to note that

A

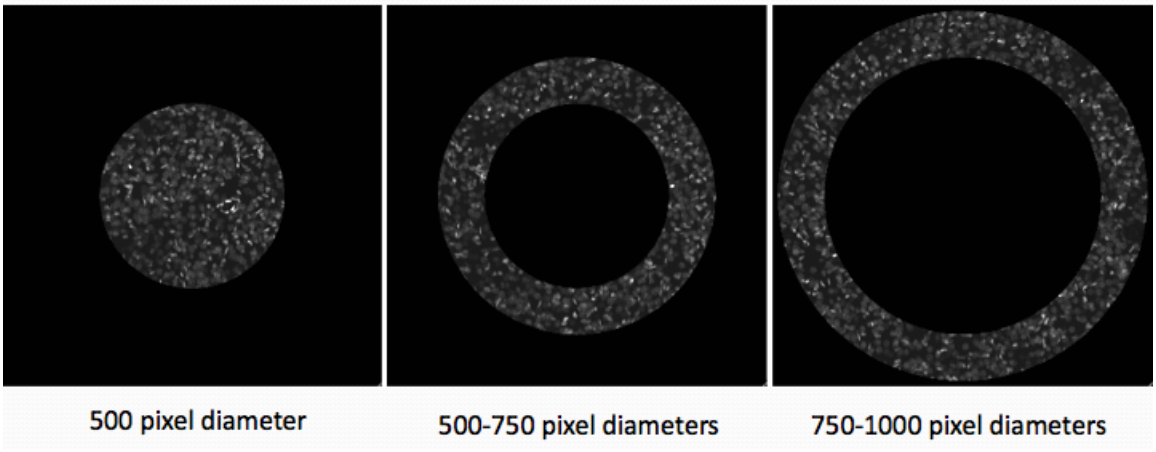

Figure 3-2: Cytoarchitecture measurement methods. (A) Concentric rings (500 pixel diameter circle, ring between 500 & 750 pixel diameter circle, and ring between diff b/t 750 & 1000 pixel diameter circle) were constructed in Metamorph to calculate cell density. (B) The "analyze skeleton" function in Image J was used to determine average branch length. (C) The freehand selection tool in Image J was used to circumscribe the region of activated microglia to estimate the ratio of activated microglia area to total image area.

B

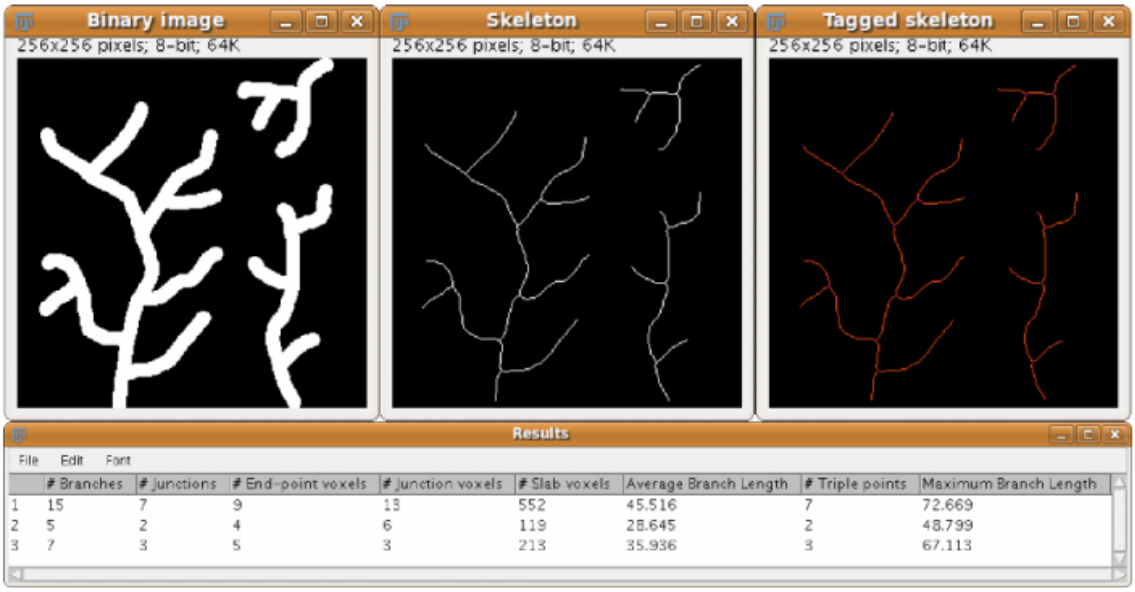

	# Branches	# Junctions	# End-point voxels	# Junction voxels	# Slab voxels	Average Branch Length	# Triple points	Maximum Branch Length
1	15	7	9	13	552	45.516	7	72.669
2	5	2	4	6	119	28.645	2	48.799
3	7	3	5	3	213	35.936	3	67.113

C

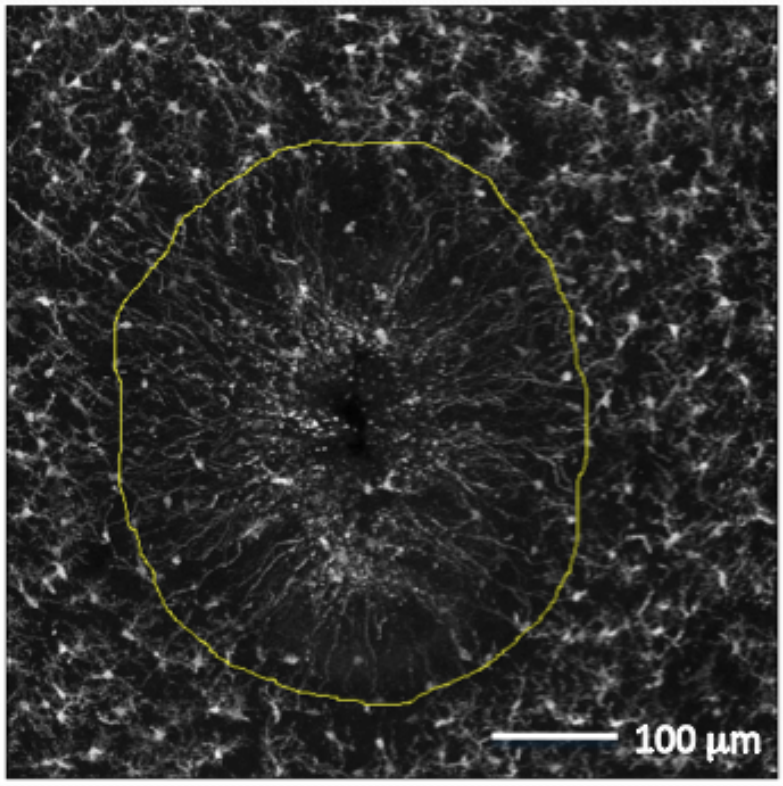

dimensions between PPP and MD were fairly normalized because probes were removed before fixation and IHC staining.

Results and Discussion

We used 3-D confocal microscopy and computational image analysis to compare changes in cellular organization in probe insertion with and without PPP/MD flow, and no insertion samples. IHC molecular stains were used to identify cell nuclei (H342), neurons (NeuroTrace), microglia (Iba1), and vasculature (EBA). With visualization and computational analysis of these bio-markers, we described morphological and population changes in the early reactive response to neurochemical sampling.

Confocal Fluorescent Microscopy Images

Cell nuclei, neurons, microglia and vasculature were labeled in IHC images (n=4) for PPP and MD (Figure 3-3). In PPP, sections at and ~200 mm below the probe tip were analyzed in flow and no flow conditions. Cellular displacement was evident in both, and to a greater degree in PPP flow. Neurons encircled the probe uniformly in PPP no flow, but seemed more disorganized in PPP flow, likely because sampling dislocated neurons and impeded them from conforming to probe shape. Similarly, microglia reorganized into a starburst pattern with elongated processes radiating from the probe, uniformly in PPP no flow, and more distant and random in PPP flow. Finally, vasculature was displaced by the probe in PPP no flow, and more so in PPP flow.

In MD, sections at 1.0 mm above the probe tip were investigated. More cellular displacement and numerous cell fragments were evident around the insertion sites in both MD flow and no flow. Neurons formed a concentric pattern around the insertion sites,

A

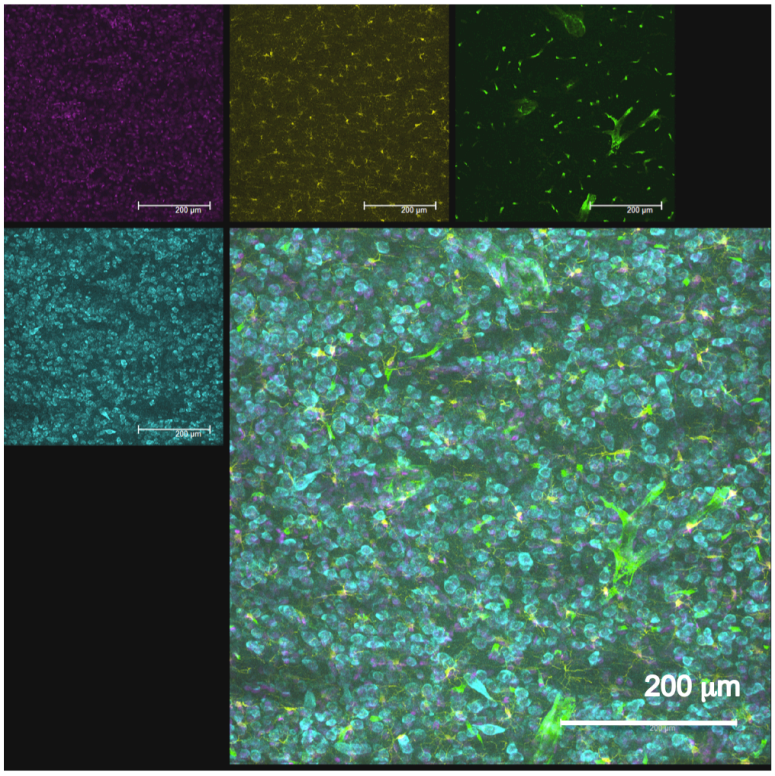

Figure 3-3: Fluorescent images (25x, voxel size 0.6 x 0.6 x 1.5 µm) of cell nuclei (purple), microglia (yellow), vasculature (green), neurons (blue), and composite in no insertion (A), PPP no flow at tip (B), PPP flow at tip (C), MD no flow (D), and MD flow (E) (n=4 for each condition). Scale bars are 200 µm.

B

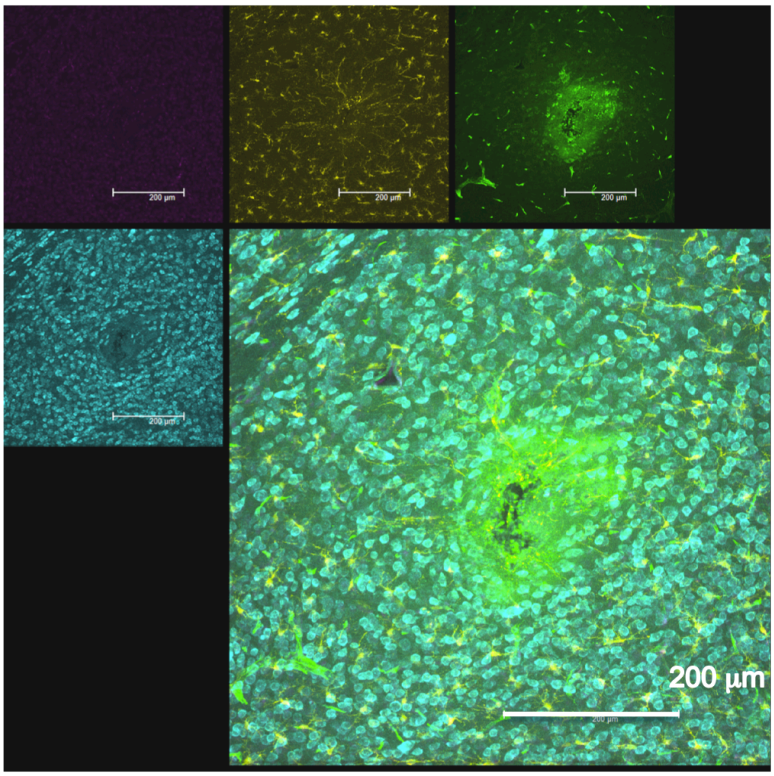

C

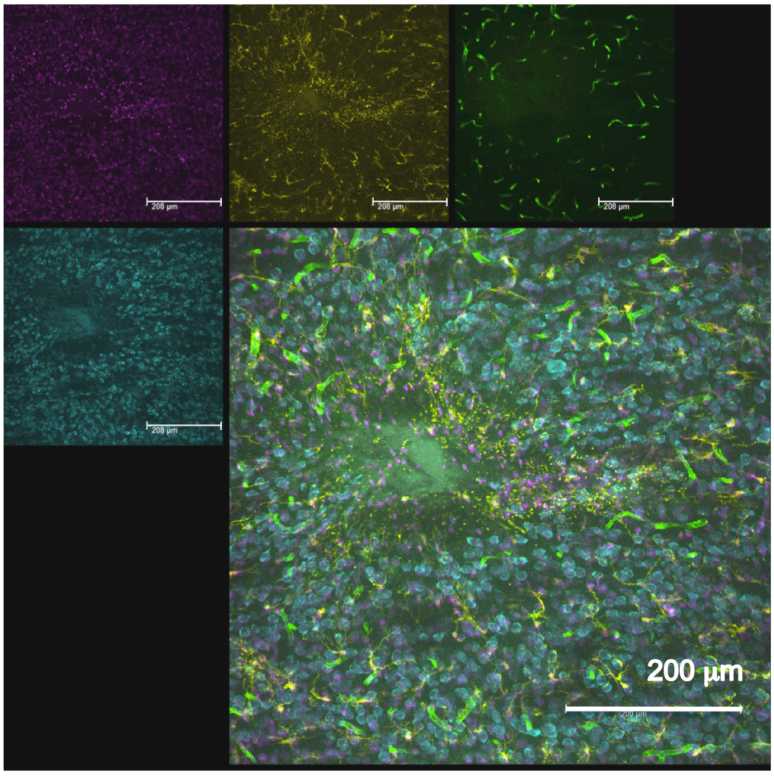

D

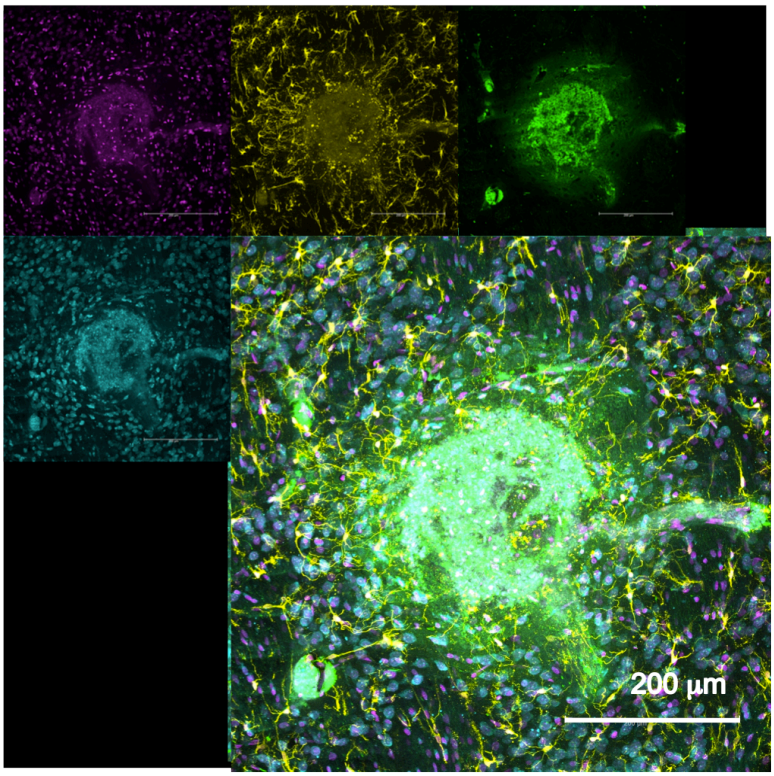

E

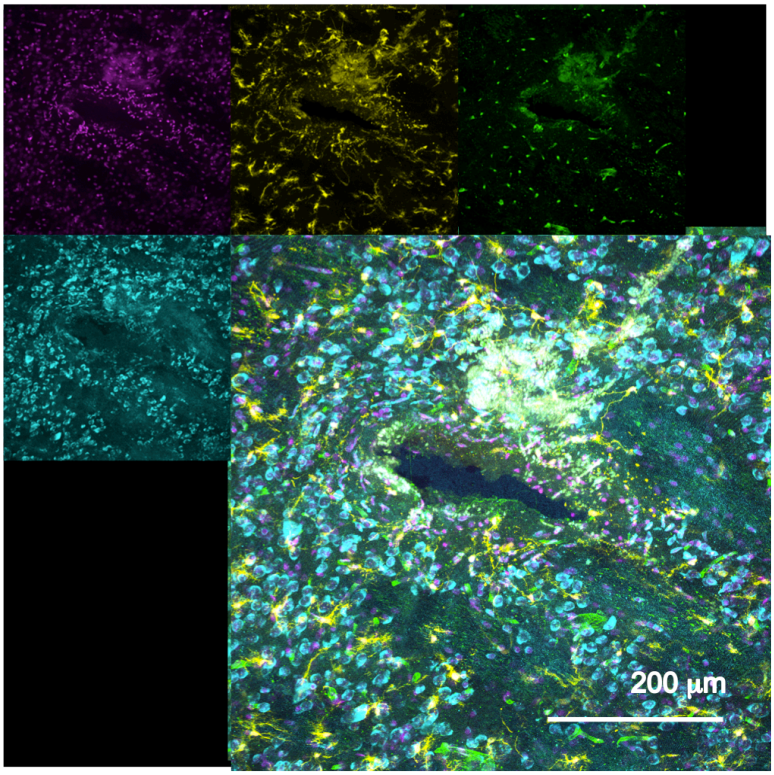

conforming to probe shape. Moreover, activated microglia and loss of vasculature appeared greater around insertion sites. In some no flow samples, blood remained at the probe site after fixation and IHC treatment (Figure 3-3 B & D). However, these artifacts did not interfere with cell counting as the contrast between cells and blood was sufficient for image analysis software to delineate structures. Like in PPP, cell displacement and activation was more pronounced in MD flow vs. no flow conditions.

Disregarding blood artifacts in the no flow samples, overall changes in cytoarchitecture in the IHC images appeared proportional to the degree of treatment (no insertion < probe insertion without flow < probe insertion with flow), as expected. Changes in cell morphology and spatial distribution appeared less salient in PPP vs. MD. These changes were quantitatively characterized in terms of cell density and morphology.

Cell Nuclei, Neuron, and Microglia Density

Cell count was performed within 500 pixel diameter circles, and rings between 500 & 750 and 750 & 1000 pixel diameter circles (Figure 3-2 A). Cell density was then calculated for cell nuclei, neurons, and microglia within each region in PPP and MD IHC images (Figure 3-4 A-C). Although brain injury is associated with proliferation of some cell types, namely microglia, data suggests that acute probe insertion and flow (both PPP and MD) was not enough to significantly increase the number of cells (cell nuclei, neurons, and microglia) per unit area ($p<0.05$). This may be a temporal effect, with cell density changes occurring in the long-term.

Although we found no changes in neuron density, we must consider that the IHC stain, NeuroTrace, labels the Nissl bodies in both live and dead neurons; therefore, live neurons may be reduced around the probes. Because Nissl bodies breakdown and

A

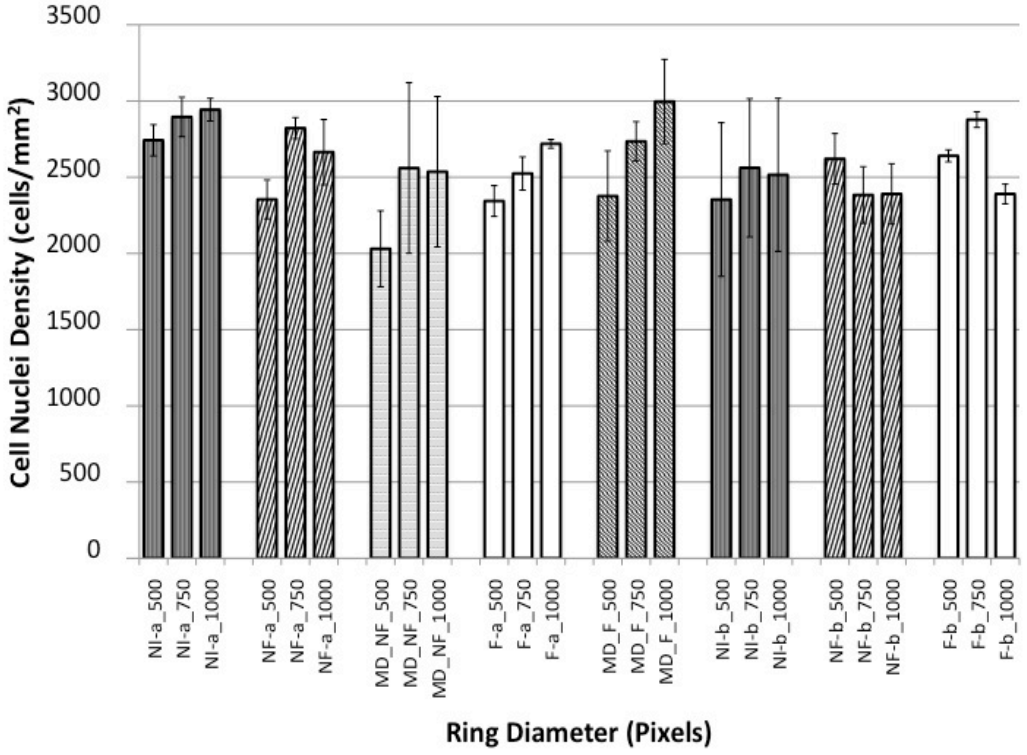

Figure 3-4: Density of cell nuclei (A), neurons (B), and microglia (C); and average microglial area (D) for no insertion at tip (NI_a), no insertion below tip (NI_b), PPP no flow at tip (NF_a), PPP flow at tip (F_a), PPP no flow below tip (NF_b), PPP flow below tip (F_b), MD no flow (MD_NF), and MD flow (MD_F) (n=4 for each group). No significant differences in cell nuclei, neuron, or microglia density; or microglia area were found among groups ($p>0.05$). Error bars are standard error.

B

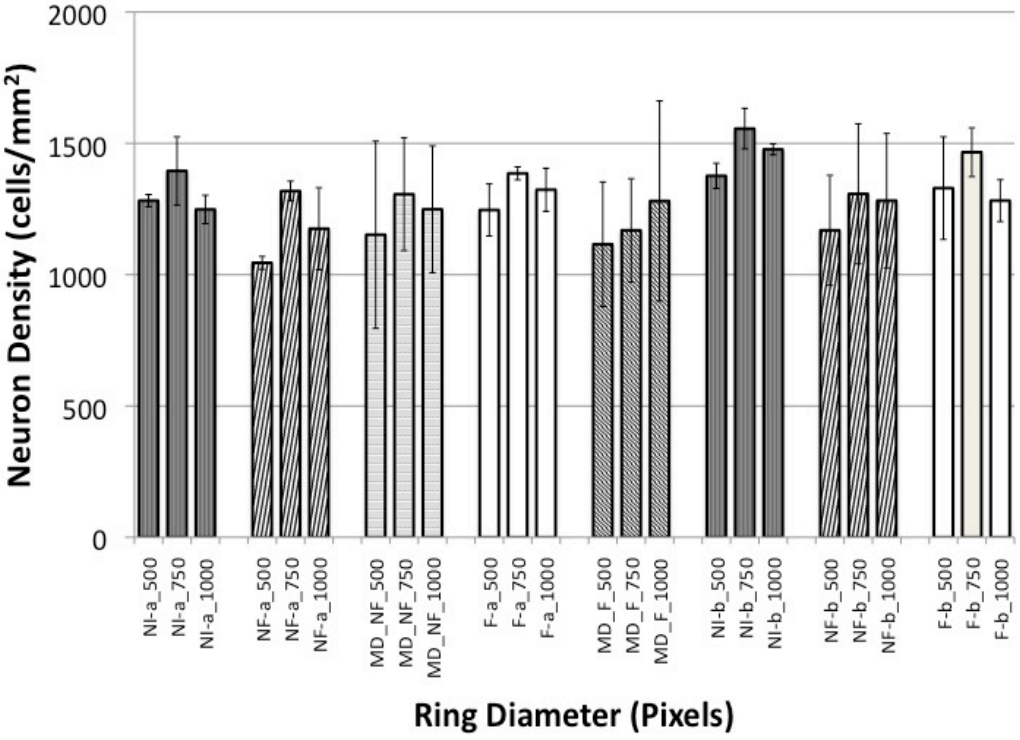
2000
1500
1000
500
0
Neuron Density (cells/mm²)
NI-a_500
NI-a_750
NI-a_1000
NF-a_500
NF-a_750
NF-a_1000
MD_NF_500
MD_NF_750
MD_NF_1000
F-a_500
F-a_750
F-a_1000
MD_F_500
MD_F_750
MD_F_1000
NI-b_500
NI-b_750
NI-b_1000
NF-b_500
NF-b_750
NF-b_1000
F-b_500
F-b_750
F-b_1000
Ring Diameter (Pixels)

C

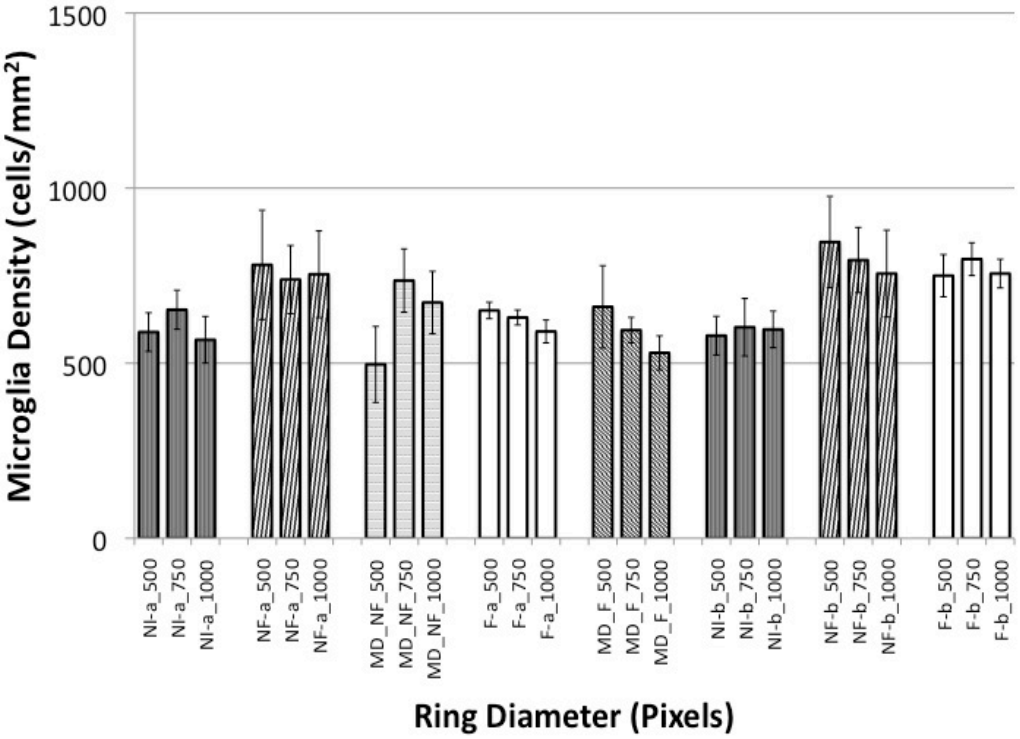
1500
1000
500
0
Microglia Density (cells/mm²)
NI-a_500
NI-a_750
NI-a_1000
NF-a_500
NF-a_750
NF-a_1000
MD_NF_500
MD_NF_750
MD_NF_1000
F-a_500
F-a_750
F-a_1000
MD_F_500
MD_F_750
MD_F_1000
NI-b_500
NI-b_750
NI-b_1000
NF-b_500
NF-b_750
NF-b_1000
F-b_500
F-b_750
F-b_1000
Ring Diameter (Pixels)

D

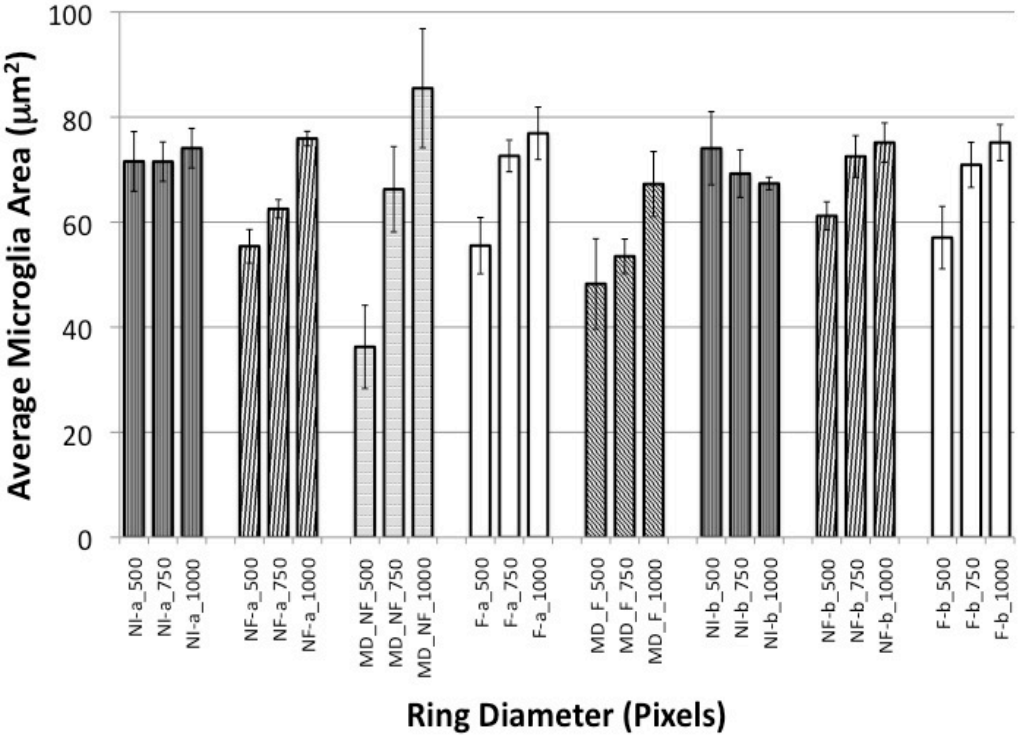
Average Microglia Area (µm²)
100
80
60
40
20
0
NI-a_500
NI-a_750
NI-a_1000
NF-a_500
NF-a_750
NF-a_1000
MD_NF_500
MD_NF_750
MD_NF_1000
F-a_500
F-a_750
F-a_1000
MD_F_500
MD_F_750
MD_F_1000
NI-b_500
NI-b_750
NI-b_1000
NF-b_500
NF-b_750
NF-b_1000
F-b_500
F-b_750
F-b_1000
Ring Diameter (Pixels)

rearrange at the periphery of the cells, neuron viability can potentially be quantified with higher resolution images and more sophisticated image analysis. Although more significant during chronic long-term tissue response, the changes in shape and arrangement of astrocytes, which form a physical barrier between damaged and healthy tissue, would also be of interest.

Microglial Morphology and Degree of Activation

Resting microglia have a ramified, or branched, structure, while activated microglia have an ameboid-like shape with increased area, and retracted branches. Thus, average microglial cell area (Figure 3-4 D) and branch length (Figure 3-5 A) were measured as a point of comparison in MD and PPP IHC images. Furthermore, the ratio of the area of activated microglia to total microglia image area (0.388 mm^2) was determined in each image as a metric for tissue response (Figure 3-5 B). No significant differences in microglia area were found among samples ($p>0.05$). As in the previous section, acute neurochemical sampling did not exhibit enough damage to induce a measurable increase in microglial dimensions.

Contrary to established and hypothesized results, the average branch length increased in probe insertion samples, compared to no insertion, for both PPP and MD. Specifically, branch lengths in both MD samples (flow and no flow) were significantly greater than all other groups ($p<0.05$). Displacement and stretching of tissue due to the probe penetration injury may account for the elongation of microglial processes, radiating from the insertion site (Jaquins-Gerstl and Michael, 2009). Assuming extended microglial branches are indicative of acute activation, PPP causes less tissue disturbance than MD.

A

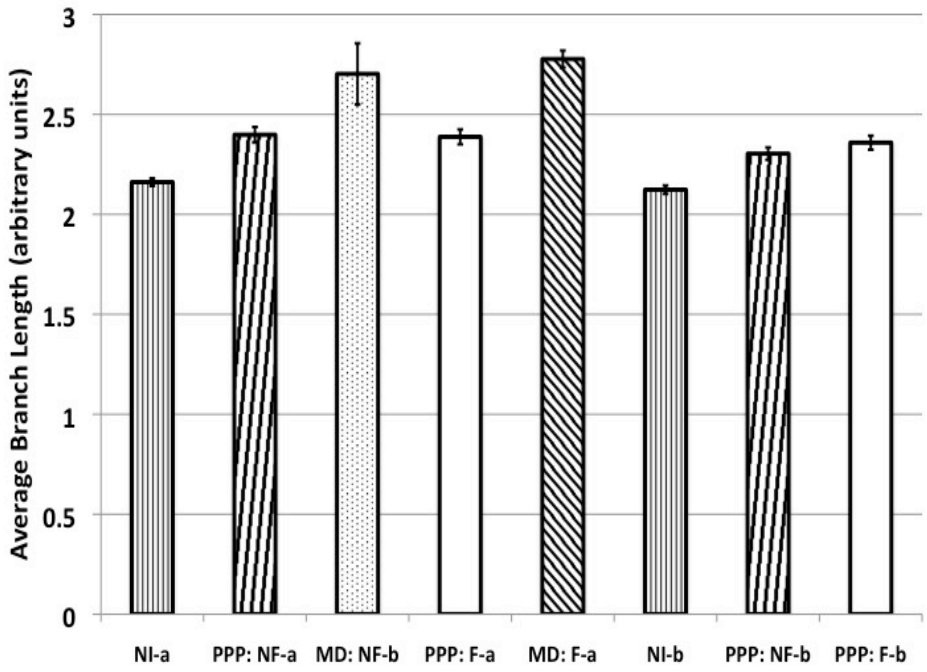

Figure 3-5: The changes in average branch length (A), and area percentage of activated microglia (B) for no insertion at tip (NI_a), no insertion below tip (NI_b), PPP no flow at tip (NF_a), PPP flow at tip (F_a), PPP no flow below tip (NF_b), PPP flow below tip (F_b), MD no flow (MD_NF), and MD flow (MD_F) (n=4 for each group). Both MD flow and no flow had significantly greater branch lengths than all other groups ($p<0.05$). PPP flow at tip had a greater area of activated microglia than PPP no flow ($p<0.05$). MD flow had significantly greater area of activated microglia than all other groups ($p<0.05$). Error bars are standard error.

B

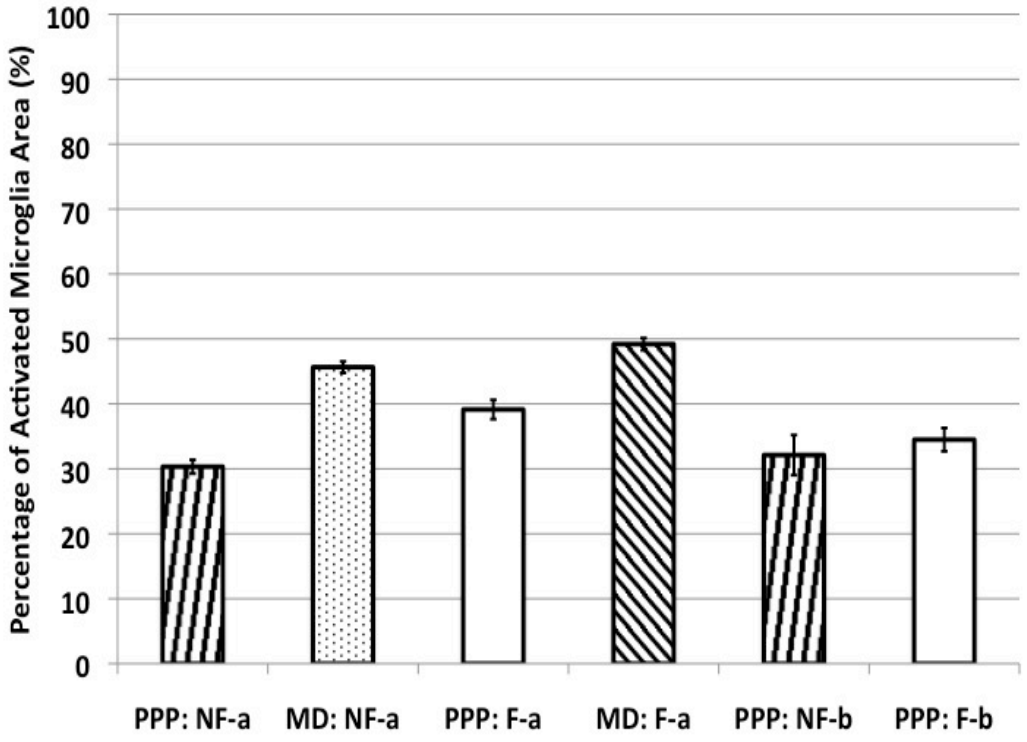
Percentage of Activated Microglia Area (%)
100
90
80
70
60
50
40
30
20
10
0
PPP: NF-a
MD: NF-a
PPP: F-a
MD: F-a
PPP: NF-b
PPP: F-b

Microglia likely convert to their activated ameboid shape with retracted processes after the experimental 3-4 h period of acute immune response.

The area of activated microglia, however, was proportional to degree of treatment, following a normal trend. Specifically, the percentage of activated to total microglia area was significantly greater in PPP flow vs. no flow, MD no flow vs. all other groups (except PPP flow, and MD flow), and MD flow vs. all other groups (except MD no flow) ($p<0.05$). Like the results on average branch length, these findings suggest that PPP induces less microglial activation than MD.

Conclusions

By labeling neural cells and structures (non-specific cell nuclei, neurons, microglia, and vasculature) with IHC stains, we examined the changes in cellular distribution and morphology following acute neurochemical sampling (PPP and MD). Probe insertion with and without flow did not cause a significant change in density for cell nuclei, neurons, or microglia compared to no insertion. Nor were variations in microglial area observed. PPP caused significantly less change in microglial average branch length, and degree of activation than MD flow.

Since these factors are associated with the extent of brain injury, it follows that PPP causes no more brain tissue damage than MD. Since MD is an established tool for neurochemical monitoring, the results herein support the more widespread use of PPP. This cytoarchitecture data establishes a reference point of cellular measurements to minimize tissue response, thereby improving neurochemical sensing. Mini PPP could also be investigated, although it will also likely cause less damage than MD. Future work can build upon this study by characterizing other intrinsic measurements like spatial

locations, branching patterns, vessel width variation, and membranous area surfaces. Moreover, associative measurements quantifying the relationships between two or more structures would provide further insight on the cellular dynamics of brain injury (Bjornsson et al., 2008).

References

Arganda-Carreras I, Fernández-González R, Muñoz-Barrutia A, Ortiz-De-Solorzano C. 3D reconstruction of histological sections: Application to mammary gland tissue. Microscopy Research and Technique, 2010; 73: 1019-29.

Barzo P, Marmarou A, Fatouros P, Hayasaki K, Corwin F. Contribution of vasogenic and cellular edema to traumatic brain swelling measured by diffusion-weighted imaging. J. Neurosurg., 1997; 87: 900-7.

Bear MF, Connors BW, Paradiso MA. Neuroscience: exploring the brain. Lippincott Williams & Wilkins: Baltimore, Md., 2001.

Benveniste H, Drejer J, Schousboe A, Diemer NH. Regional cerebral glucose phosphorylation and blood-flow after insertion of a microdialysis fiber through the dorsal hippocampus in the rat. Journal of Neurochemistry, 1987; 49: 729-34.

Berkenbosch F. Macrophages and Astroglial Interactions in Repair to Brain Injury. Annals of the New York Academy of Sciences, 1992; 650: 186-90.

Bjornsson CS, Lin G, Al-Kofahi Y, Narayanaswamy A, Smith KL, Shain W, Roysam B. Associative image analysis: A method for automated quantification of 3D multi-parameter images of brain tissue. Journal of Neuroscience Methods, 2008; 170: 165-78.

Blinzinger K, Kreutzberg G. Displacement of synaptic terminals from regenerating motoneurons by microglial cells. Cell and tissue research, 1968; 85: 145-57.

Cellar NA, Kennedy RT. A capillary-PDMS hybrid chip for separations-based sensing of neurotransmitters *in vivo*. Lab on a Chip, 2006; 6: 1205-12.

Clapp-Lilly KL, Roberts RC, Duffy LK, Irons KP, Hu Y, Drew KL. An ultrastructural analysis of tissue surrounding a microdialysis probe. Journal of Neuroscience Methods, 1999; 90: 129-42.

Delgado JM, DeFeudis FV, Roth RH, Ryugo DK, Mitruka BM. Dialytrode for long term intracerebral perfusion in awake monkeys. Archives internationales de pharmacodynamie et de therapie, 1972; 198: 9-21.

Eddleston M, Mucke L. Molecular profile of reactive astrocytes: Implications for their role in neurologic disease. Neuroscience, 1993; 54: 15-36.

Fontainhas AM, Wang M, Liang KJ, Chen S, Mettu P, Damani M, Fariss RN, Li W, Wong WT. Microglial Morphology and Dynamic Behavior Is Regulated by Ionotropic Glutamatergic and GABAergic Neurotransmission. PLoS ONE, 2011; 6: e15973.

Gaddum J. Push-pull cannulae. J. Physiol, 1961; 155.

Graeber MB, Tetzlaff W, Streit WJ, Kreutzberg GW. Microglial cells but not astrocytes undergo mitosis following rat facial nerve axotomy. Neuroscience Letters, 1988; 85: 317-21.

Hans Lundqvist ML, Vladimir Tolmachev, Anna Lövqvist, Anders Sundin, Soheir Beshara, Alexander Bruskin, Jörgen Carlsson, Jan-Erik Westlin. Positron Emission Tomography and Radioimmunotargeting: General Aspects. Acta Oncologica, 1999; 38: 335-41.

Jaquins-Gerstl A, Michael AC. Comparison of the brain penetration injury associated with microdialysis and voltammetry. Journal of Neuroscience Methods, 2009; 183: 127-35.

Kottegoda S, Shaik I, Shippy SA. Demonstration of low flow push-pull perfusion. Journal of Neuroscience Methods, 2002; 121: 93-101.

Kreutzberg GW. 19. Reaction of the neuronal cell body to axonal damage. Oxford University Press, 1995: 355-74.

Mizuno M, Gearing M, Terasawa E. The Role of Neuropeptide Y in the Progesterone-Induced Luteinizing Hormone-Releasing Hormone Surge *in vivo* in Ovariectomized Female Rhesus Monkeys. Endocrinology, 2000; 141: 1772-9.

Myers RD, Adell A, Lankford MF. Simultaneous comparison of cerebral dialysis and push-pull perfusion in the brain of rats: A critical review. Neuroscience and Biobehavioral Reviews, 1998; 22: 371-87.

Myers RD, Gurleyorkin L. New micro push-pull catheter system for localized perfusion of diminutive structures in brain. Brain Research Bulletin, 1985; 14: 477-83.

Parsons LH, Justice JB. Extracellular Concentration and *In vivo* Recovery of Dopamine in the Nucleus Accumbens Using Microdialysis. Journal of Neurochemistry, 1992; 58: 212-8.

Pawley J. Handbook of Biological Confocal Microscopy, Third Edition. Journal of Biomedical Optics, 2008; 13: 029902-.

Paxinos G, Watson C. The rat brain in stereotaxic coordinates. Elsevier Academic Press: Amsterdam ; Boston, 2005.

Raivich G, Jones LL, Kloss CU, Werner A. Immune surveillance in the injured nervous system: T-lymphocytes invade the axotomized mouse facial motor nucleus and aggregate around sites of neuronal degeneration. The Journal of Neuroscience, 1998; 18: 5804-16.

Raivich G, Moreno-Flores MT, Möller JC, Kreutzberg GW. Inhibition of Posttraumatic Microglial Proliferation in a Genetic Model of Macrophage Colony-Stimulating Factor Deficiency in the Mouse. European Journal of Neuroscience, 1994; 6: 1615-8.

Robinson DL, Hermans A, Seipel AT, Wightman RM. Monitoring Rapid Chemical Communication in the Brain. Chemical Reviews, 2008; 108: 2554-84.

Slaney TR, Nie J, Hershey ND, Thwar PK, Linderman J, Burns MA, Kennedy RT. Push-Pull Perfusion Sampling with Segmented Flow for High Temporal and Spatial Resolution *in vivo* Chemical Monitoring. Analytical Chemistry, 2011; 83: 5207-13.

Spataro L, Dilgen J, Retterer S, Spence AJ, Isaacson M, Turner JN, Shain W. Dexamethasone treatment reduces astroglia responses to inserted neuroprosthetic devices in rat neocortex. Experimental Neurology, 2005; 194: 289-300.

Streit WJ, Kreutzberg GW. Response of endogenous glial cells to motor neuron degeneration induced by toxic ricin. The Journal of Comparative Neurology, 1988; 268: 248-63.

Tang A, Bungay PM, Gonzales RA. Characterization of probe and tissue factors that influence interpretation of quantitative microdialysis experiments for dopamine. Journal of Neuroscience Methods, 2003; 126: 1-11.

Turner JN, Shain W, Szarowski DH, Andersen M, Martins S, Isaacson M, Craighead H. Cerebral astrocyte response to micromachined silicon implants. Experimental Neurology, 1999; 156: 33-49.

Watson CJ, Venton BJ, Kennedy RT. *In vivo* measurements of neurotransmitters by microdialysis sampling. Analytical Chemistry, 2006; 78: 1391-9.

Weiss DJ, Lunte CE, Lunte SM. *In vivo* microdialysis as a tool for monitoring pharmacokinetics. TrAC Trends in Analytical Chemistry, 2000; 19: 606-16.

Zhou F, Braddock JF, Hu Y, Zhu X, Castellani RJ, Smith MA, Drew KL. Microbial origin of glutamate, hibernation and tissue trauma: an *in vivo* microdialysis study. Journal of Neuroscience Methods, 2002; 119: 121-8.

CHAPTER 4

COMPUTATIONAL MODELING OF FLUID FLOW IN MICRODIALYSIS AND LOW-FLOW PUSH-PULL PERFUSION

Introduction

Neurochemical measurements are essential to understanding the brain and developing treatments to alleviate neural disorders e.g. addiction, depression (Robinson et al., 2008; Watson et al., 2006). Invasive techniques involving probe implantation in brain tissue remain superior for *in vivo* neurochemical sensing. However, the brain's immune response to *in vivo* sampling interferes with signal sensitivity and resolution. Computer modeling can provide valuable information on the theoretical mutliphysics involved in tissue damage, guiding and validating experimental methods.

Acute neurochemical sampling (2-4 hours) elicits an immediate injury response due to the implantation itself. Disruption of blood vessels releases clotting and inflammatory factors that recruit activated astrocytes and microglia around the inserted probe (Turner et al., 1999). Some strategies to reduce tissue damage include minimizing device insertion speed and cross-sectional area (Shain et al., 2003; Szarowski et al., 2003). Yet, the probe implantation and fluid flow intrinsic to invasive neurochemical sampling have not been modeled effectively.

Microdialysis (MD), as previously described, is a powerful tool for monitoring and analysis of multiple neurotransmitters simultaneously (Watson et al., 2006). Briefly, a wide range of extracellular analytes diffuse across a dialysis membrane of a MD probe

according to their concentration gradient. Since artificial cerebrospinal fluid (aCSF) is infused through a semi-permeable boundary, the initial flow rate (0.1-3.0 μL/min) is reduced to some unknown degree in the sampling area. Yet, the flow at the membrane/tissue interface may still be forceful enough to cause some damage. In addition to the quantitative MD tissue response described in Chapters 2 and 3, neuronal density decreases up to 400 μm from a 40 hr implanted MD probe, and intercellular disruption up to 1.4 mm from the probe tract were reported in a semi-quantitative tissue damage study (Clapp-Lilly et al., 1999).

Similar to MD, push-pull perfusion (PPP) can sample an extensive array of neurochemicals for separations-based sensing (Cellar and Kennedy, 2006). Because extracellular fluid is withdrawn directly at the probe tip, not through a dialysis membrane, PPP offers a remarkable advantage in spatial resolution and collecting high molecular weight species, like neuropeptides (Kohsaka et al., 1999). Initially PPP was performed at relatively high flow rates (10-25 μL/min) and caused obvious tissue lesions (Myers and Gurleyorkin, 1985; Redgrave, 1977), consequently reducing its popularity in the scientific community. In the last decade, low-flow PPP (10-50 nL/min) was developed in part to minimize corresponding brain injury. No regions were associated with significant tissue damage in one PPP study (Kottegoda et al., 2002). Nevertheless, data in Chapters 2 and 3 reported measurable tissue response in PPP.

Previous data chapters compared the relative tissue response in low-flow PPP and MD. In Chapter 2, dead/total cell ratio calculated from cell viability stained brain sections indicated that PPP caused approximately 10% less damage (dead/total cell ratio) than MD. In Chapter 3, cytoarchitecture analysis from immunohistochemical images

determined that PPP caused approximately 10% less cell morphology changes (e.g. % of activated microglia area) than MD, but both methods did not cause major changes in cell spatial distribution. These findings emphasize some overall effects of *in vivo* sampling, but the degree to which insertion and flow contribute to this damage needs to be clarified.

Dynamic and static compression are involved in all facets of neurochemical sampling. Implanting the probe causes time-dependent shear and deformation, or strain. The probe continues to cause static pressure as it remains in the brain during use. Finally, the fluid flow causes some dynamic pressure and shear stress in the sampling microenvironment. Since the flow rate is constant in PPP and MD, time dependence is not as critical as in probe insertion. As noted above, mechanical loading and fluid flow rupture cells through two main distributions of force: pressure and shear stress.

High hydrostatic pressure in cells causes ribosome denaturation, membrane alterations, enzyme inactivation, changes in the nucleoid, and inhibition of transcription and protein synthesis (Bartlett, 1992; Niven et al., 1999). Pressure promotes membrane lipid gelation and tighter packing of the acyl chains (Macdonald, 1984). Moreover, physical damage to the bacterial cell membrane has been demonstrated by increased uptake of fluorescent dyes such as propidium iodide, which labels membrane-compromised cells (Shigehisa et al., 1991), and as leakage of ATP or UV-absorbing material from bacterial cells subjected to pressure (Smelt et al., 1994). Finally, loss of cell membrane functionality due to pressure treatment has been reported. In *Lactobacillus plantarum*, pressure treatment reduced the ability of cells to maintain a ΔpH, and impaired the acid efflux mechanism (Wouters et al., 1998).

Shear stress causes cell death through a few proposed mechanisms: turbulent eddy-cell interactions, cell-cell collisions, and net laminar shear force in a cell (Vickroy et al., 2007). Furthermore, shear stress induces biochemical changes that alter cell behavior. Endothelial-leukocyte cross-talk is facilitated to respond to pro-inflammatory stimuli and endothelial cell proliferation is inhibited. Also, protein expression in the cytosol, nucleus, and membrane decreases, while that of the cytoskeleton increases (Cucullo et al., 2011).

Computational modeling has been helpful in investigating such relationships between biological environments and foreign objects/stimuli (Patrachari et al., 2012). In biodegradable scaffolds designed for bone regeneration, mechanical loading and fluid flow has been reproduced with finite element analysis (FEA) and computational fluid dynamics (CFD) (Milan et al., 2009). Flow patterns in bioreactors, which provide mechanical and biochemical stimuli for *in vitro* cell cultures, have been mathematically characterized with CFD (Hutmacher and Singh, 2008). FEA has been used to simulate displacement, mean stress, and shear stress of the rat brain during impact (El Sayed et al., 2008; Peña et al., 2005). Most relevant to probe implantation, needle insertion and corresponding soft tissue deformation has been simulated (DiMaio and Salcudean, 2003).

Computational simulations provide major advantages, including efficient analysis of multiple interdependent systems, simple manipulation of variables once the model is created, and time/cost reduction. However, interpreting results should be done carefully. Multiple factors and their degree of influence may not be fully represented in user-defined models.

By modeling mechanical force fields during neurochemical sampling in COMSOL (COMSOL Inc., Burlington, MA), the relative extent of damage in PPP and MD due to probe insertion and flow can be resolved, facilitating the interpretation of experimental data. In the context of the work described herein, probe implantation involves more boundary conditions, degrees of freedom, time-dependent dynamics, and unknown variables. In contrast, fluid properties are better defined. Due the complexity of the solid mechanics involved in probe physics, we focused on simulating fluid flow in neurochemical sampling.

Materials and Methods

In order to gain insight on experimental data and determine the mechanical effect of neurochemical sampling on brain tissue, we used COMSOL to model physics distribution patterns. This was accomplished by creating 2D geometries/blueprints of the MD, miniaturized PPP, and microfabricated PPP probes in the brain; and inputting variables associated with the physical properties of the materials involved (e.g. brain, aCSF). We wanted to compute the worst-case scenario of damage caused by PPP and determine if it was still less than that caused by MD.

Because mini PPP produced more, although not significant, damage than needle-sheathed PPP in cell viability experiments ($p>0.05$), the former was chosen to compare to MD. Furthermore, mini PPP was easier to model than the more complex geometry of needle-sheathed PPP. For mini PPP, we modeled the preparatory (500 nL/min for 10 s) and experimental phase (50 nL/min for 200 min). Initially, we determined the shear stress along the arc length of the flow/tissue interface in mini PPP. This algorithm was applied to larger scales to investigate the amount of damage caused by fluid flow in the sampling

area. Velocity, pressure, and shear stress maps were compared to experimental results summarized in the introduction of this chapter.

Probe Geometries

Drawings of probes were created in COMSOL (Figure 4-1). First, the brain was drawn as a simple 15 x 15 cm square, an area several orders of magnitude greater than the sampling area. For mini PPP, two 4.5 cm side-by-side 100 μm width capillaries with 40 μm width channels were drawn, extending ventrally from the horizontal upper boundary, or surface, of the brain. A smaller, microfabricated version was modeled as a probe with 80 μm width and two parallel 15 μm-width channels (Lee, in preparation). For MD, two side-by-side capillaries were drawn with the same dimensions as mini PP, except the inlet capillary extended 5.5 cm, and the outlet 3.5 cm. This differential space was encased in a 216 μm x ~2 mm rectangle representing the dialysis membrane.

Material Properties

The brain was modeled as an isotropic porous medium with previously reported physical properties (Caicedo et al., 2010; Mace et al., 2010). Specifically, the input physical properties were density (1000 kg/m^3), dynamic viscosity (0.001 Pa·s), permeability (1 x 10^{-11} m^2), porosity (0.4), elastic modulus (7 kPa), and shear modulus (12 kPa). The MD membrane was modeled with a permeability of 2.92 x 10^{-13} m^2 (Bungay et al., 2003). For Dirichlet boundary conditions, the concentration of NaCl, the solute with highest concentration in aCSF (145 mM) was input. The density and dynamic viscosity of aCSF, with properties near identical to water, were entered as 1 kg/m^3 and 8.9 x 10^{-4} Pa·s, respectively.

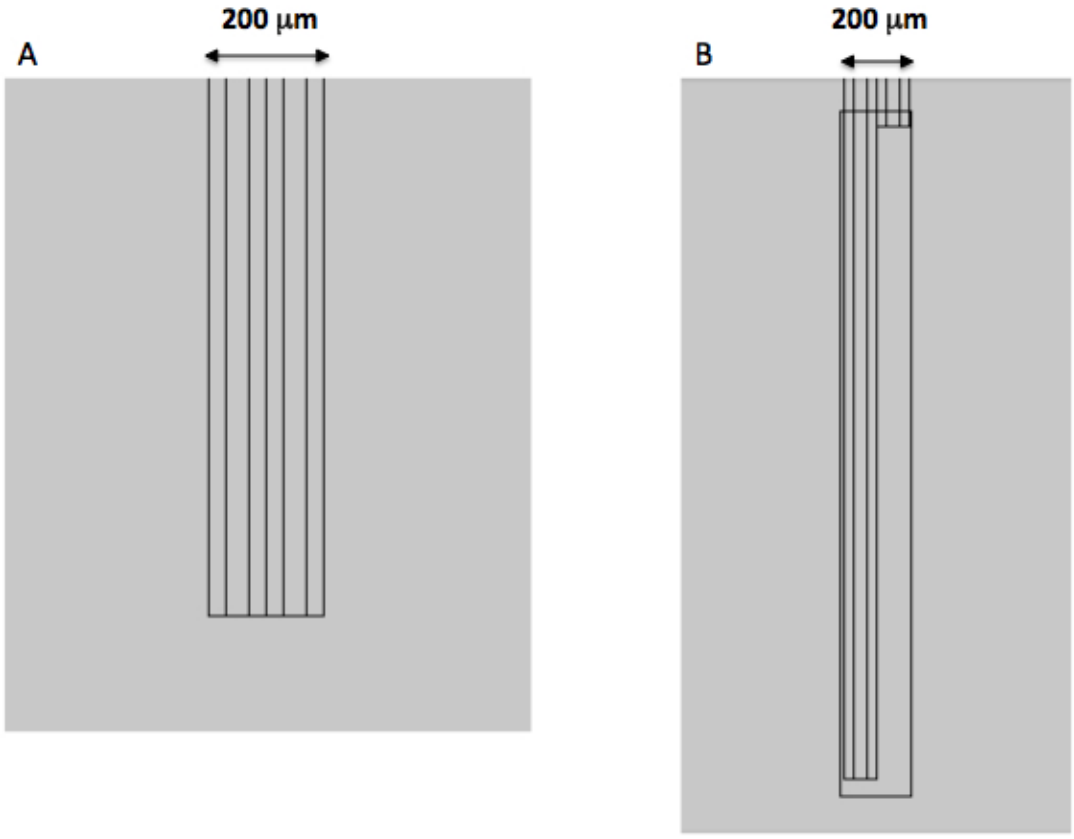

Figure 4-1: COMSOL drawings of mini PPP (A) and MD (B) probe sampling tips. Probes were drawn within a 15 x 15 cm square representing the brain. A microfabricated PPP probe (not shown) had the same layout/proportions as the mini PPP probe with an 80 μm width. Flow occurred directly at the tip in PPP, and was restricted to the surface area of the membrane in MD.

Convection-Diffusion and Laminar Flow

Because the fluid flow in MD and PPP does not cause enough pressure to deform brain tissue, as calculated mathematically and demonstrated experimentally in agar (Slaney, in preparation), a diffusion-based flow model was appropriate. The "convection-diffusion equation" module was chosen to simulate the movement of fluid due to diffusion. All probe walls except for the 40 μm length of inlet (and outlet in mini PPP) were designated with zero flux. For simplicity, all conditions in mini PPP were applied to the counterparts of microfabricated PPP.

The "laminar flow" module was selected to incorporate aCSF properties and flow rate. Laminar inflow was input as 50 nL/min for mini PPP and 1 μL/min for MD. Laminar outflow for mini PPP was also 50 nL/min, and outlet conditions for MD were set as pressure, no viscous stress. A time-dependent study ranging from 0 to 200 min was run to graph velocity, pressure, and shear stress maps for these flow rates. Yet, since flow rate was modeled as constant, time did not play a significant factor in calculated outputs. Because we initially flushed aCSF at 500 nL/min to facilitate pull flow in PPP, this flow rate condition was also modeled for 10 s. We will refer to the 500 and 50 nL/min flow rate periods in PPP as preparatory and experimental, respectively.

Neurochemical Sampling Area

We graphed streamlines that ran tangent along the entire vector field in our mini PPP and MD COMSOL models. To verify that these lines defined the sampling area, MATLAB (Mathworks Inc., Natick, MA) was used to introduce a particle with zero diffusivity into the flow field. This particle was hypothesized to follow the path drawn by

the streamline, thus defining the limits that a particle could travel, or sampling boundaries. The streamlines were assumed to start at the limits of the inlet outlet and connect to the outer limits of the outlet/inlet.

Microdialysis Flow Rate

We were interested in determining fluid dynamics at the membrane perimeter, where cells were directly affected. To get an idea of the recovery and flow rate at the MD membrane/tissue interface, velocity with respect to position along the membrane and inlet/outlet were graphed in MATLAB. To calculate the volumetric flow rate, the areas under the curves were integrated and multiplied by the corresponding circumference.

Results and Discussion

We simulated force distributions caused by fluid flow in mini PPP and MD. Separate maps were graphed for preparatory and experimental mini PPP. COMSOL models of velocity (Figure 4-2), pressure superimposed on velocity (Figure 4-3) and shear stress (Figure 4-4) showed force fields concentrated at the inlets (downward arrow: where aCSF was infused) and outlets (upward arrow: where sample was collected) in both methods.

Mini PPP models displayed the probe tip, with the inlet on the left and the outlet on the right. Preparatory and experimental mini PPP force distribution maps spanned a similar area and displayed comparable gradient patterns. However, major differences were observed in force distribution values between preparatory and experimental PPP, due to the ten-fold difference in flow rates. Notably, all force distribution values were less in experimental PPP than MD. Microfabricated PPP values were greater than mini

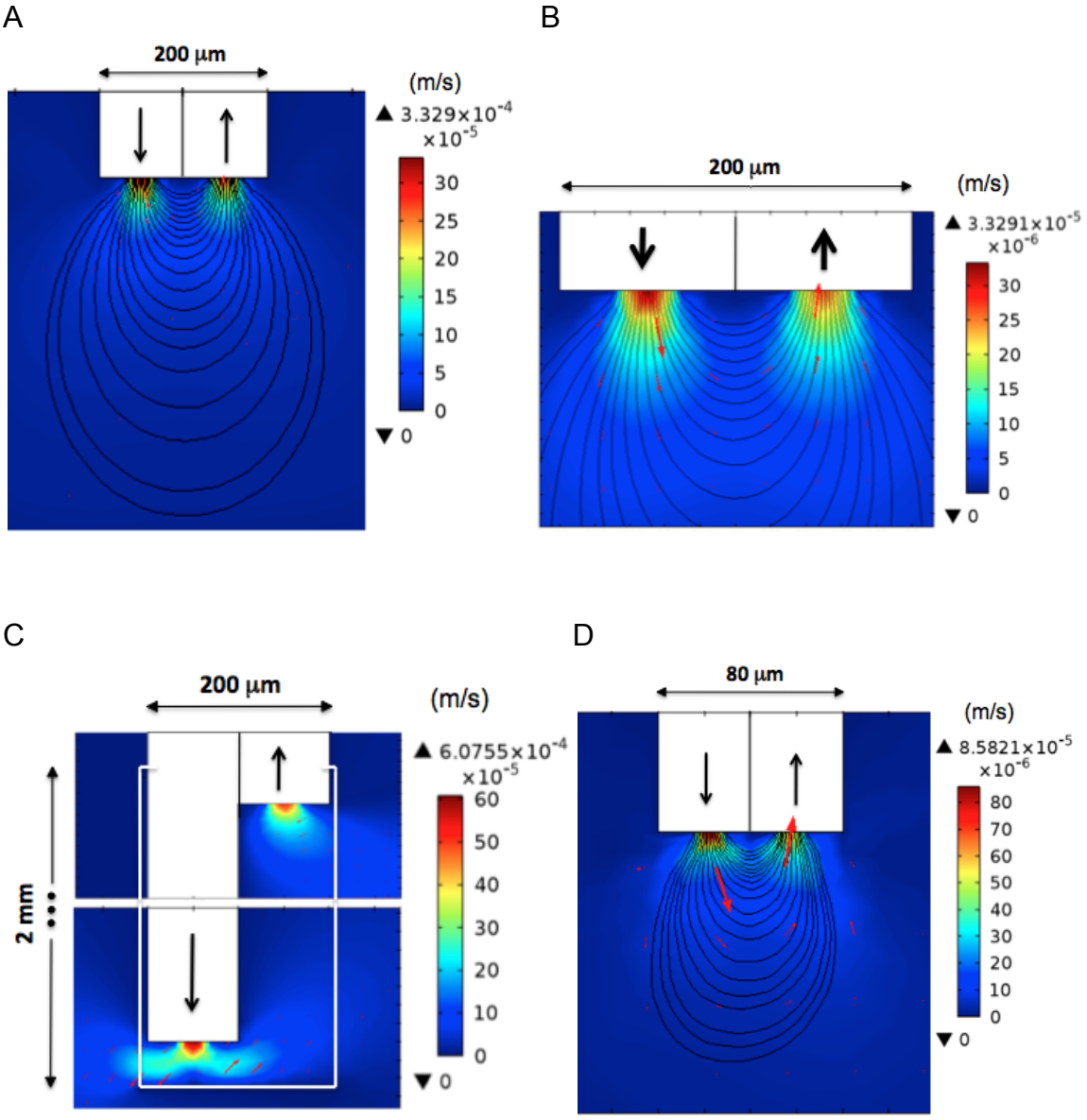

Figure 4-2: COMSOL velocity models for preparatory mini PPP (500 nL/min for 10s) (A), experimental mini PPP (50 nL/min for 200 min) (B), microdialysis (C), and microfabricated PPP (D). aCSF was infused through the inlet (downward arrow) and sample was collected through the outlet (upward arrow). Force field intensity ranged from dark blue (least) to red (greatest).

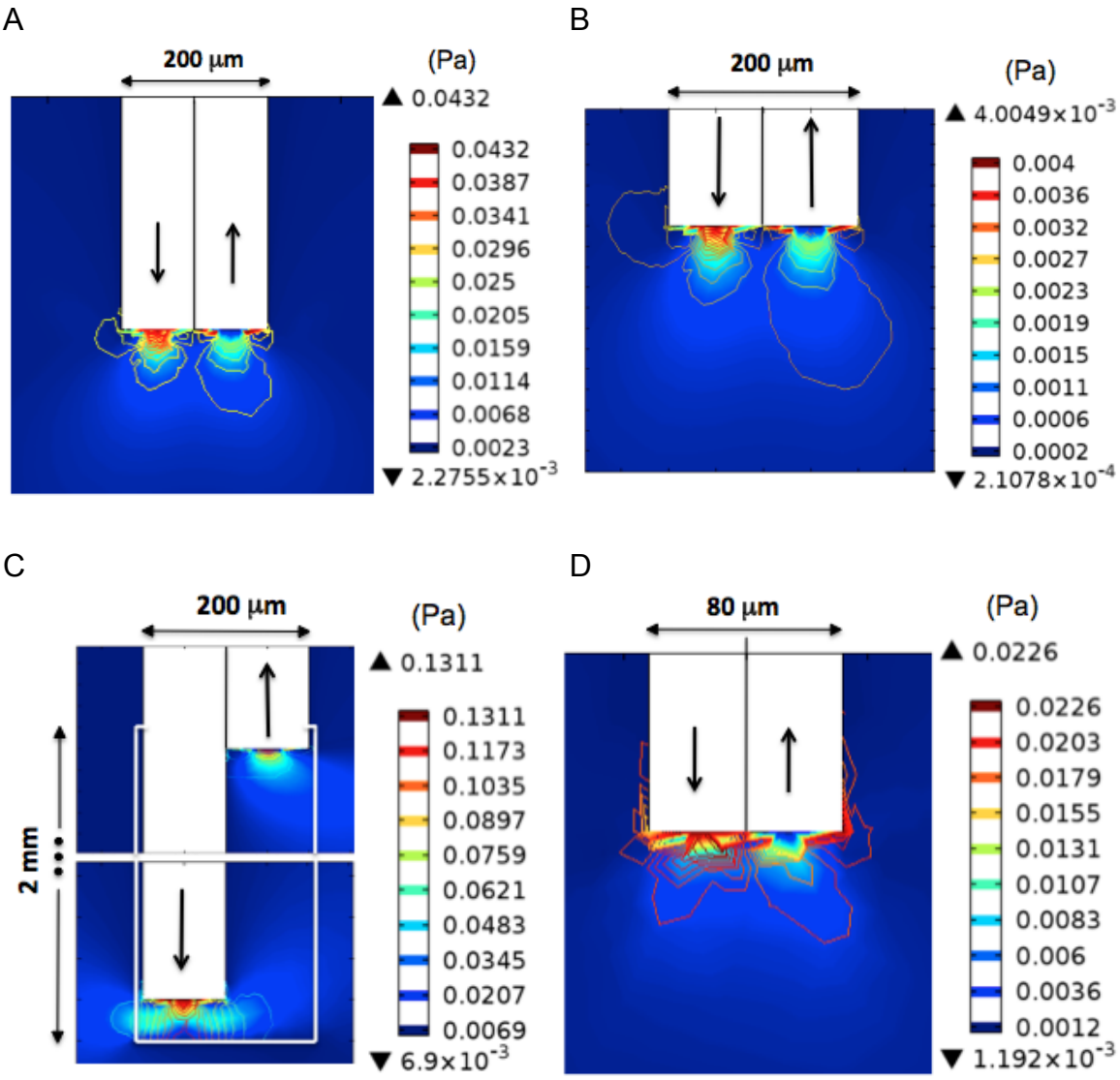

Figure 4-3: COMSOL pressure models for preparatory mini PPP (A), experimental mini PPP (B), MD (C), and microfab PPP (D). All pressure values were well below the threshold pressure required to cause cell death (25 mPa).

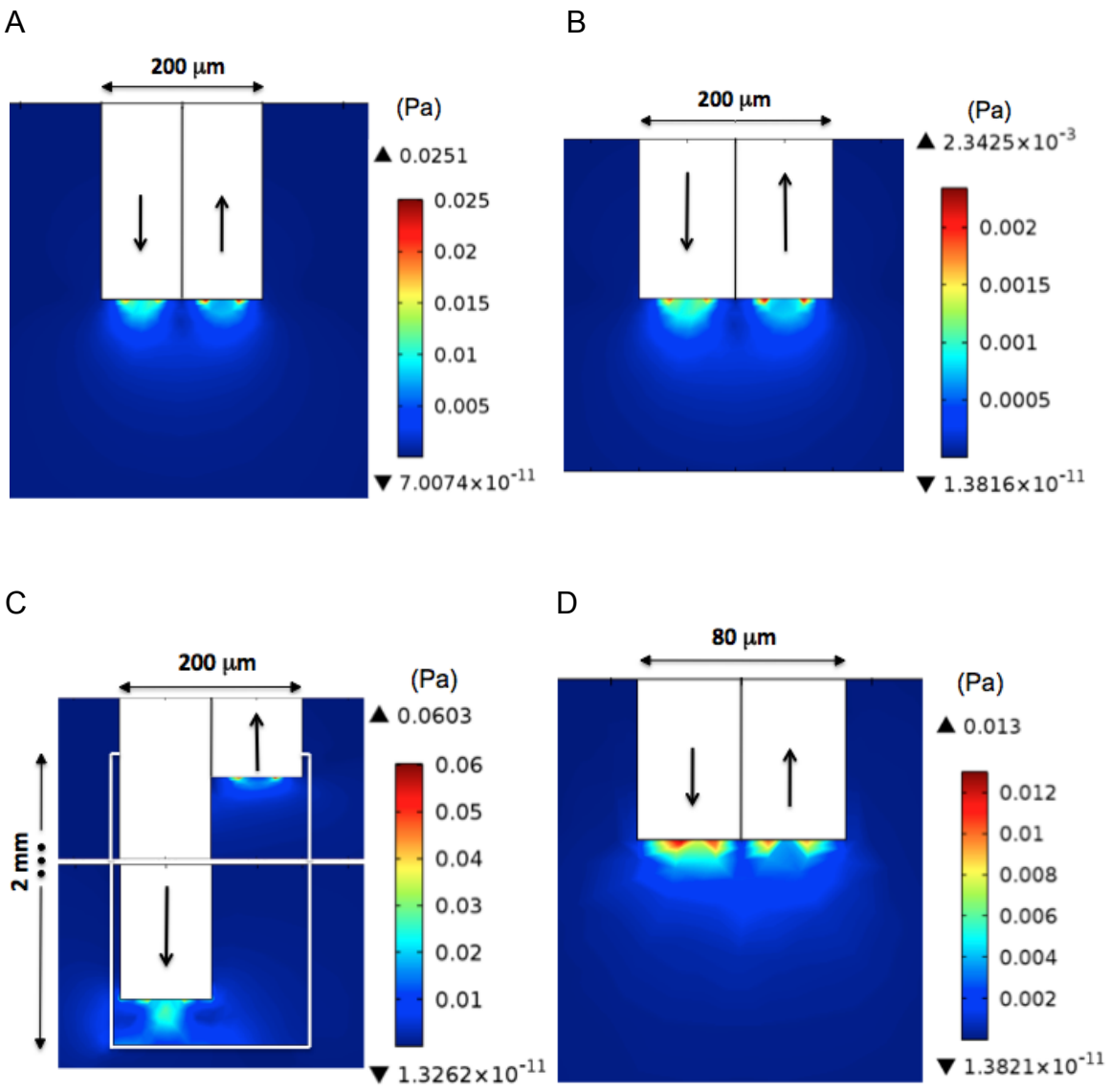

Figure 4-4: COMSOL shear stress models for preparatory mini PPP (A), experimental mini PPP (B), MD (C), and microfab PPP (D). Shear stress values in all but experimental PPP exceeded the threshold required to cause cell death (5 mPa). However, shear stress fields covered a smaller area than that observed experimentally.

PPP, but less than MD. Overall, force distribution maps in mini PPP and MD spanned less of an area than in cell viability and cytoarchitecture results from Chapters 2 and 3, respectively.

Velocity Maps

The velocity map in PPP and MD models showed downward/outward flow at the inlet and upward/inward flow at the outlet (Figure 4-2). For preparatory mini PPP, the maximum velocity was found at the inlet and the endpoints of the outlet with a value of 3.3×10^{-4} m/s. The maximum velocity values for experimental PPP and microfab PPP were 3.3×10^{-5} m/s and 8.6×10^{-5} m/s, respectively. For MD, the maximum velocity was found the inlet and outlet with a value of 6.1×10^{-4} m/s. This maximum velocity field spanned a greater area at the inlet. Velocity at the MD membrane ranged from 1×10^{-4} to 3×10^{-4} m/s.

The maximum velocity for preparatory mini PPP was comparable to that of MD. However, this maximum velocity was carried out for the entirety of MD sampling (200 min) compared to 10 s of pre-sampling in PPP. The greater damage in MD seen in previous data chapters may be due to this prolonged maximum flow rate at the membrane/tissue interface. Specifically, this membrane-restricted flow rate is small compared to the infused flow rate in MD (1 μL/min), but appears to be similar to the preparatory PPP flow rate (500 nL/min), and thus greater than the experimental PPP flow rate (50 nL/min).

Pressure Maps

Pressure contour lines closely matched velocity gradients in the previous section and also illustrated the highest pressure at the probe inlet for mini PPP and MD models (Figure 4-3). The maximum pressure values for preparatory PPP, experimental PPP, MD, and microfab PPP were 44 mPa, 4 mPa, 130 mPa, and 22 mPa respectively. Pressure at the MD membrane perimeter ranged from 10 to 70 mPa. In a comprehensive study characterizing the effect of pressure on various eukaryotic cell types, the lowest value that caused cell death was 5 MPa (Frey et al., 2008). Because pressure values in PPP and MD were several orders of magnitude lower, COMSOL data suggests that fluid flow pressure in neurochemical sampling is not a contributing factor to tissue damage.

Shear Stress Maps

The shear stress map in the PPP models showed a larger overall area of shear stress at the inlet, but a greater area of maximum shear at the perimeter of the outlet (Figure 4-4 A,B,&D). A similar pattern was shown in the MD model, with the shear stress fields constricted by the impermeable bottom of the membrane (Figure 4-4 C), as in velocity and pressure maps. The maximum shear stress values for preparatory PPP, experimental PPP, MD, and microfab PPP were 25 mPa, 2.3 mPa, 60 mPa, and 13, respectively. Shear stress at the membrane perimeter ranged from 10 to 20 mPa. Shear stress values $\geq$ 5 mPa have been shown to be detrimental to cell viability (Milan et al., 2009). This threshold was not reached in experimental mini PPP, but was exceeded in preparatory mini PPP, MD, and microfab PPP.

Therefore, COMSOL data suggests that mini PPP, MD, and microfab PPP may induce enough shear stress to cause tissue damage. However, it is imperative to take the

spatial and temporal factors into account. Spatially, this critical shear stress is observed no more than 25 μm horizontally from the vertical plane of the membrane in MD, and no more than 20 μm ventrally from the probe tip in mini PPP. Also, the shear stress field in mini PPP does not cross the vertical plane of the probe. Temporally, this critical shear stress is only in effect for 10 s in mini PPP and 200 min in MD.

Neurochemical Sampling Area

As expected, streamlines started at the limits of the inlet/outlet and connected to the outer limits of the outlet/inlet. Moreover, the particle with zero diffusivity did in fact follow the path drawn by the streamline, thus defining the sampling area in mini PPP and MD (Figure 4-5). The computational estimates of the sampling areas for mini PPP and MD were 0.04 mm^2 and 62.51 mm^2, respectively. These numbers verified that low-flow push-pull perfusion did indeed sample from a more localized area than microdialysis, thereby significantly improving spatial resolution.

Microdialysis Flow Rate

Net flow rates for the left boundary of the membrane, right boundary, capillary inlet, and outlet were 0.165 μL/min (out of the membrane), 0.166 μL /min (into the membrane), 0.996 μL /min (out of the inlet), and 0.990 μL /min (into the outlet), respectively (Figure 4-6). These values indicate that the volume of aCSF that exited the membrane was approximately the same as the volume of sample that was collected. This numerical data also verifies that the flow rate at the brain/tissue interface in MD is greater than the flow rate in low-flow PPP: ~160 nL/min vs. 50 nL/min, respectively.

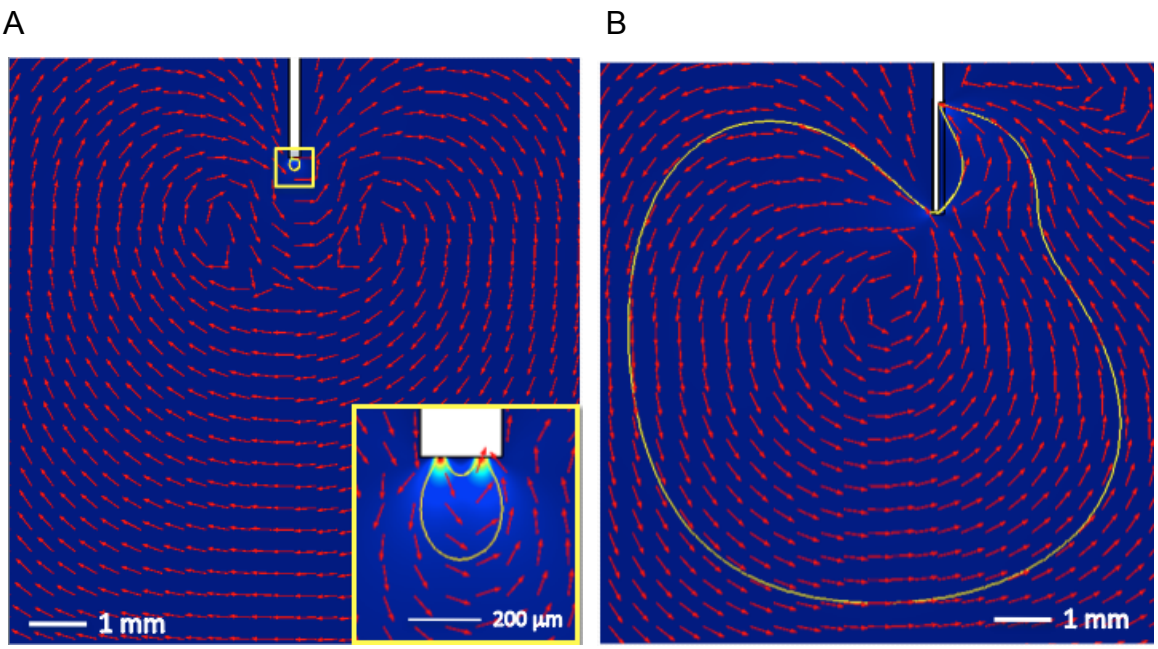

Figure 4-5: Sampling areas in mini PPP (A) and MD (B). Yellow lines extending from the probe tips enclosed the areas where aCSF was infused (left side of the probes) and sample was collected (right side of the probes). Validating the improved spatial resolution in low-flow push-pull perfusion, sampling area in mini PPP was approximately 1,500 times smaller than that in MD.

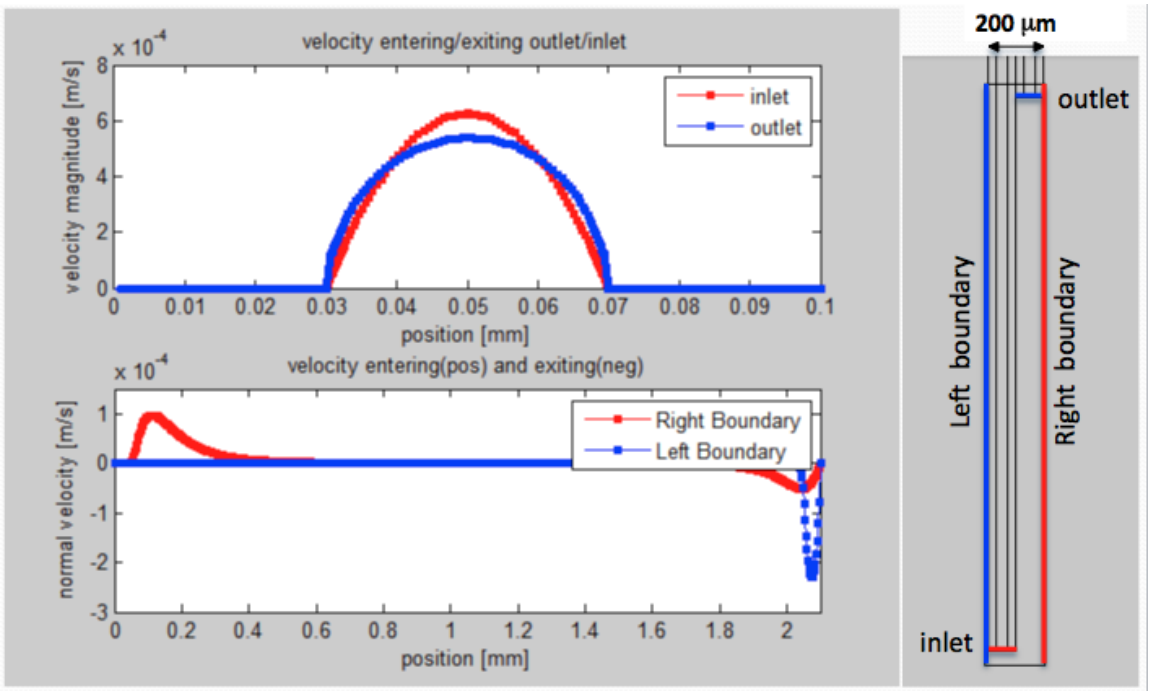

Figure 4-6: MATLAB graph of velocity with respect to position along capillary inlet/outlet and dialysis membrane walls in MD. Volumetric flow rate was calculated by integrating the area under the curves and multiplying by the corresponding circumference (e.g. 100 μm capillary inlet/outlet). Net flow rates indicated that the volume exiting the left boundary equaled the volume entering the right boundary (~0.16 μL/min) and that the volume exiting the inlet equaled the volume entering the outlet (~0.99 μL/min).

Microdialysis vs. Low-Flow Push-Pull Perfusion

Because the force distributions that affect cells are at the membrane/tissue interface in MD, we used these values to compare to those in mini PPP. First, we compared the MD model to the experimental mini PPP model. MD velocity fields were 10 times greater than the maximum velocity in mini PPP. Although the maximum pressure value in experimental mini PPP was approximately 5-50% less than pressure values in MD, fluid flow pressures for both methods were approximately 10^6 times less than lower range cell death thresholds (Frey et al., 2008). The maximum fluid flow shear stress value in mini PPP was 12-25% less than shear stress values in MD. However, only those in MD exceeded the reported shear stress threshold for cell death (Milan et al., 2009). In contrast, the maximum shear stress value in mini PPP was approximately 50% less than the cell death threshold.

When comparing the MD model to the preparatory mini PPP model, force distribution values were in similar ranges. The maximum mini PPP velocity corresponded to the maximum velocity value at the MD membrane perimeter. This implies that the flow rate at the membrane/tissue interface was greater than that found in experimental PPP: > 50 nL/min. This was verified with the MD flow rate calculation in MATLAB. Furthermore, the calculated flow rates indicated that mass was conserved, as the volume of aCSF infused into the brain was nearly equal to the volume of sample collected. Maximum mini PPP pressure fell in between the range of MD pressure values.

Both the maximum shear stress values in preparatory mini PPP and MD surpassed the shear stress cell death threshold by at least 4-fold. Yet, mini PPP inflicts this unfavorable shear stress for 0.008% of the time that MD does. It is essential to note that

cell death and degeneration usually does not occur in seconds or minutes, but hours or days (LaPlaca et al., 1997). Finally, the sampling area in mini PPP was calculated to be 1,500 times smaller than that of MD, further indicating that fluid flow had much less of an impact in mini PPP than MD. All in all, computational data indicates that low-flow push-pull perfusion, executed with mini PPP probes, imposes quantitatively less fluid mechanical effect on brain tissue than microdialysis.

Comparison to Experimental Data

COMSOL models for MD and mini PPP showed pressure and shear stress maps restricted to a smaller area than the cell death and disturbed cytoarchitecture observed in experimental data. Of all the modeled parameters, pressure covered the most area. In MD, pressure and shear stress extended no more than approximately 30 μm horizontally from the dialysis membrane, or 130 μm from the probe center. Moreover, observable pressure and shear stress did not span more than 200 μm vertically along the length of the membrane. From cell viability and IHC data, tissue damage was observed at least 500 μm from the probe center and along the entire 2 mm length of the membrane in MD. In mini PPP, substantial pressure reached no more than 200 μm ventrally from the probe tip and shear stress extended no more than 50 μm below the probe tip. From cell viability and IHC data, tissue damage was observed at least 200 μm ventral to the tip in mini PPP. Clearly, modeled pressure and shear stress fields from fluid flow account for a fraction of the damage shown in Chapters 2 and 3.

As expected, the flow rate in PPP was found to be proportional to the potential for cellular damage. The flow rates used in low-flow PPP (10-50 nL/min) fall under the shear stress threshold shown to cause cell death, and are thus suitable for chemical sampling.

This cell death threshold is exceeded by flow rates of at least 500 nL/min, which is consistent with the macroscopic injury observed in high-flow PPP (10-25 μL/min). A more precise damage-inducing flow rate limit can be investigated analytically.

Taking the spatial and temporal details of experimental and computational data into account, analytical models suggest that a minimal amount of *in vivo* sampling damage is due to flow, and that shear stress is the main contributing factor within fluid flow. Thus, detrimental effects on cell viability and cytoarchitecture are likely due to the dynamic and static compression of probe insertion. More sophisticated algorithms can be developed to study these implantation effects with FEA and CFD.

Microfabricated PPP Probes

Although microfabricated PPP probe force distribution values were less than those in MD, the shear stress in microfab PPP was near double the shear stress threshold value for cell death. The increased resistance resulting from smaller capillary i.d. (15 μm vs. 40 μm in mini PPP) translates to increased pressure and shear stress imposed on brain tissue. A lower flow rate would be needed to decrease the probability of tissue damage. Thus, there is trade off between increased spatial resolution with decreased probe size and decreased temporal resolution with decreased flow rate. However, decreased probe size inherently decreases the area of influence, so less spatial tissue damage than mini PPP may be observed experimentally.

Conclusions

We created models of velocity, pressure, and shear stress during sampling in mini PPP, MD, and microfab PPP to determine the effect of flow on tissue damage. All force

distribution values were greater in the microdialysis sampling area than that of low-flow push-pull perfusion conducted with mini PPP probes, consistent with findings in Chapters 2 and 3. Although preparatory mini PPP force distribution levels were similar to those in MD, the former may not have occurred long enough to cause significant tissue damage.

Effective flow rate and sampling area in MD were determined to be greater than in mini PPP, supporting the findings that low-flow PPP provides higher spatial resolution of chemical signaling and has a more localized effect on brain tissue. Yet, the area of force fields in both methods was much smaller than that observed in cell viability and IHC experiments, suggesting that most of the tissue damage from neurochemical sampling may be due to penetration injury. The shear stress in microfabricated PPP crossed cell death thresholds, but the smaller probe size may reduce the volume of cell death relative to mini PPP.

Future work will involve optimizing models and testing a variety of conditions. For one, flow rates and channel widths in microfabricated PPP probes can be altered to determine the optimal design for high temporal resolution and minimal tissue damage. Needle-sheathed PPP can also be modeled, although the geometry of the needle is more complicated. Moreover, 3D models, with additional mechanical conditions like strain, will provide more accurate information on sampling-induced brain injury. Finally, the solid mechanics of probe insertion can be computed with more advanced calculations. All in all, analytical models can guide future experiments by predicting the amount of damage due to different physical properties and parameters, such as membrane material, probe geometry, and flow rate.

References

Bartlett DH. Microbial life at high-pressures. Science progress (1916), 1992; 76: 479-96.

Bungay PM, Newton-Vinson P, Isele W, Garris PA, Justice JB. Microdialysis of dopamine interpreted with quantitative model incorporating probe implantation trauma. Journal of Neurochemistry, 2003; 86: 932-46.

Caicedo HH, Hernandez M, Fall CP, Eddington DT. Multiphysics simulation of a microfluidic perfusion chamber for brain slice physiology. Biomedical Microdevices, 2010; 12: 761-7.

Cellar NA, Kennedy RT. A capillary-PDMS hybrid chip for separations-based sensing of neurotransmitters *in vivo*. Lab on a Chip, 2006; 6: 1205-12.

Clapp-Lilly KL, Roberts RC, Duffy LK, Irons KP, Hu Y, Drew KL. An ultrastructural analysis of tissue surrounding a microdialysis probe. Journal of Neuroscience Methods, 1999; 90: 129-42.

Cucullo L, Hossain M, Puvenna V, Marchi N, Janigro D. The role of shear stress in Blood-Brain Barrier endothelial physiology. BMC Neuroscience, 2011; 12: 40.

DiMaio SP, Salcudean SE. Needle insertion modeling and simulation. Robotics and Automation, IEEE Transactions on, 2003; 19: 864-75.

El Sayed T, Mota A, Fraternali F, Ortiz M. Biomechanics of traumatic brain injury. Computer Methods in Applied Mechanics and Engineering, 2008; 197: 4692-701.

Frey B, Janko C, Ebel N, Meister S, Schlucker E, Meyer-Pittroff R, Fietkau R, Herrmann M, Gaipl US. Cells Under Pressure - Treatment of Eukaryotic Cells with High Hydrostatic Pressure, from Physiologic Aspects to Pressure Induced Cell Death. Current Medicinal Chemistry, 2008; 15: 2329-36.

Hutmacher DW, Singh H. Computational fluid dynamics for improved bioreactor design and 3D culture. Trends in Biotechnology, 2008; 26: 166-72.

Kohsaka A, Watanobe H, Kakizaki Y, Suda T. A comparative study of the effects of nitric oxide and carbon monoxide on the *in vivo* release of gonadotropin-releasing

hormone and neuropeptide Y from rat hypothalamus during the estradiol-induced luteinizing hormone surge: Estimation by push-pull perfusion. Neuroendocrinology, 1999; 69: 245-53.

Kottegoda S, Shaik I, Shippy SA. Demonstration of low flow push-pull perfusion. Journal of Neuroscience Methods, 2002; 121: 93-101.

LaPlaca MC, Lee VMY, Thibault LE. An in vitro model of traumatic neuronal injury: loading rate-dependent changes in acute cytosolic calcium and lactate dehydrogenase release. Journal of neurotrauma, 1997; 14: 355-68.

Macdonald AG. The Effects of Pressure on the Molecular Structure and Physiological Functions of Cell Membranes. Philosophical Transactions of the Royal Society of London. Series B, Biological Sciences, 1984; 304: 47-68.

Mace E, Cohen I, Martin A, Montaldo G, Fink M, Tavitian B, Tanter M. *In vivo* brain elasticity mapping in small animals using ultrasound and its application to cerebral ischemia. Biomedical Imaging: From Nano to Macro, 2010 IEEE International Symposium on, 2010: 245-8.

Milan JL, Planell JA, Lacroix D. Computational modelling of the mechanical environment of osteogenesis within a polylactic acid-calcium phosphate glass scaffold. Biomaterials, 2009; 30: 4219-26.

Myers RD, Gurleyorkin L. New micro push-pull catheter system for localized perfusion of diminutive structures in brain. Brain Research Bulletin, 1985; 14: 477-83.

Niven GW, Miles CA, Mackey BM. The effects of hydrostatic pressure on ribosome conformation in Escherichia coli: an *in vivo* study using differential scanning calorimetry. Microbiology (Society for General Microbiology), 1999; 145: 419-25.

Patrachari AR, Podichetty JT, Madihally SV. Application of computational fluid dynamics in tissue engineering. Journal of Bioscience and Bioengineering, 2012; 114: 123-32.

Peña A, Pickard JD, Stiller D, Harris NG, Schuhmann MU. Brain tissue biomechanics in cortical contusion injury: a finite element analysis. In Poon W, Chan MV, Goh KC, Lam JK, Ng SP, Marmarou A, Avezaat CJ, Pickard J, Czosnyka M, Hutchinson PA, Katayama Y, editors. Intracranial Pressure and Brain Monitoring XII. Springer Vienna, 2005: 333-6.

Redgrave P. A modified push-pull system for the localised perfusion of brain tissue. Pharmacology Biochemistry and Behavior, 1977; 6: 471-4.

Robinson DL, Hermans A, Seipel AT, Wightman RM. Monitoring Rapid Chemical Communication in the Brain. Chemical Reviews, 2008; 108: 2554-84.

Shain W, Spataro L, Dilgen J, Haverstick K, Retterer S, Isaacson M, Saltzman M, Turner JN. Controlling cellular reactive responses around neural prosthetic devices using peripheral and local intervention strategies. Neural Systems and Rehabilitation Engineering, IEEE Transactions on, 2003; 11: 186-8.

Shigehisa T, Ohmori T, Saito A, Taji S, Hayashi R. Effects of high hydrostatic pressure on characteristics of pork slurries and inactivation of microorganisms associated with meat and meat products. International Journal of Food Microbiology, 1991; 12: 207-15.

Smelt JPPM, Rijke AGF, Hayhurst A. Possible mechanism of high pressure inactivation of microorganisms. High pressure research, 1994; 12: 199-203.

Szarowski DH, Andersen MD, Retterer S, Spence AJ, Isaacson M, Craighead HG, Turner JN, Shain W. Brain responses to micro-machined silicon devices. Brain Research, 2003; 983: 23-35.

Turner JN, Shain W, Szarowski DH, Andersen M, Martins S, Isaacson M, Craighead H. Cerebral astrocyte response to micromachined silicon implants. Experimental Neurology, 1999; 156: 33-49.

Vickroy B, Lorenz K, Kelly W. Modeling Shear Damage to Suspended CHO Cells during Cross-Flow Filtration. Biotechnology Progress, 2007; 23: 194-9.

Watson CJ, Venton BJ, Kennedy RT. *In vivo* measurements of neurotransmitters by microdialysis sampling. Analytical Chemistry, 2006; 78: 1391-9.

Wouters PC, Glaasker E, Smelt JP. Effects of High Pressure on Inactivation Kinetics and Events Related to Proton Efflux in Lactobacillus plantarum. Appl Environ Microbiol, 1998; 64: 509-14.

CHAPTER 5

CONCLUSIONS AND FUTURE WORK

Conclusions

Motivated by the necessity to elucidate the chemistry of biological mechanisms, the sampling and analysis of extracellular fluid in brain tissue has provided an invaluable picture of the processes of neural activity in the brain. Methods like push-pull perfusion (PPP) and microdialysis (MD) have been developed to sample and manipulate the extracellular environment *in vivo*. Along with significant improvements in the field of neurochemical sensing, these methods have been substantially enhanced since their creation. Connecting PPP and MD to analytical techniques, like mass spectrometry and capillary electrophoresis with laser-induced fluorescence, have enabled analysis of low-volume, low-concentration samples.

A major benefit of methods such as PPP and MD is the prospect and flexibility for drug delivery into the brain through the probe inlets. The effect of stimuli on the brain's metabolism and chemistry can be observed as the microenvironment of the sampling area is altered. For example, recent clinical advances in MD include monitoring conditions of severe brain injury, detection and prevention of secondary brain damage, investigating neurometabolic derangements in epilepsy patients, and exploring the role of cytokines in inflammation following acute brain injury (Matzneller and Brunner, 2011).

With the advent of microfluidics and the development of analytical techniques (e.g. segmented flow) to counter the decrease in temporal resolution, PPP was modified

for adaptability with lower flow rates (10-50 nL/min), thereby minimizing tissue response caused by infusion of larger fluid volume and higher flow rates. Partly because this brain tissue damage was a major deterrent to the widespread use of PPP, MD flourished as the prominent method of neurochemical sampling. There was a clear need to characterize the tissue response in low-flow PPP and compare it to MD.

The studies conducted herein revealed a difference in tissue response between low-flow PPP and MD. Through cell viability stains, we calculated dead/total cell ratio in the sampling area and concluded that both needle-sheathed PPP and mini PPP caused at least ~10% less cell death ($p<0.05$). By labeling specific neural cell types with immunohistochemical (IHC) stains, changes in cytoarchitecture due to flow were quantified. We concluded that cell spatial distribution was unaffected, but microglial branch length and degree of activation was significantly increased in needle-sheathed PPP, and more so in MD ($p<0.05$). Finally, we graphed force fields (velocity, pressure, shear stress) in the sampling area via computational modeling for mini PPP and MD. Force gradients, namely shear stress, were found to be greater in MD versus PPP, yet less extensive than in experimental data for both cases.

In Chapter 2, we characterized the cell viability in needle-sheathed PPP, mini PPP, and MD. As measured by dead/total cell ratio, both PPP designs caused less overall damage than MD in flow conditions ($p<0.05$). Mini PPP flow caused greater, though not significant, damage than needle-sheathed PPP. This may be due to the geometry of a tapered needle versus a blunt capillary tip, and the corresponding displacement and compression of cells (Li et al., 2011). In particular, tissue experiences a more graded, as opposed to abrupt, shear force in tapered needles, decreasing the chance of cell rupture.

Thus for PPP sampling, there is a trade off between higher spatial resolution in mini PPP, and less clogging and damage in needle-sheathed PPP. Overall, the majority of cells (at least 60%) in the sampling area remained intact in all probe designs, confirming the value of MD and low-flow PPP for monitoring neurochemicals in the brain.

In Chapter 3, we characterized the cytoarchitecture in needle-sheathed PPP and MD. By labeling neural cells and structures (cell nuclei, neurons, microglia and vasculature) with IHC stains, we examined the changes in cellular distribution and morphology following acute PPP and MD. Visually, disturbances in cytoarchitecture were proportional to sampling effects (no insertion < insertion without flow < insertion with flow). Compared to no insertion controls, probe insertion and flow did not cause a significant change in density for cell nuclei, neurons, or microglia ($p>0.05$).

Although more precise cell density analysis (e.g. counting cells within smaller concentric rings) may reveal differently, current findings suggest that PPP and MD have the potential to extract information from all cells in the sampling area uniformly, damaged or not. Parallel to results in Chapter 2, PPP flow caused significantly less change in microglial average branch length and degree of activation than MD flow ($p<0.05$).

In Chapter 4, we computed the forces due to flow in mini PPP, MD and microfabricated PPP. We created models of velocity, pressure, and shear stress during sampling in preparatory mini PPP (500 nL/min for 10 s), experimental mini PPP (50 nL/min for 200 min), and MD (1 μL/min for 200 min) to determine the effect of flow on tissue damage. We also calculated the flow rate in MD at the membrane/tissue interface and the sampling area in all methods. All force distribution values and sampling area

were greater in MD than experimental mini PPP, consistent with findings in Chapters 2 and 3. Microfabricated probes induced critical shear stress on surrounding brain tissue at 50 nL/min, but the reduced size of the probe may limit the area of damage.

Although both preparatory mini PPP and MD force distribution levels exceeded the shear stress threshold value, the former unlikely occurred long enough to cause significant tissue damage (LaPlaca et al., 1997). Specifically, flow rates at the membrane/tissue interface in MD reached approximately 166 nL/min. While the sampling area, or flow field, was much greater in MD than mini PPP, the area of pressure and shear stress fields in both methods was much smaller than that observed in experiments. This indicates that most of the tissue damage from neurochemical sampling may be due to penetration injury. All in all, COMSOL models can guide future experiments by predicting the amount of damage due to different physical properties and parameters, such as membrane material, flow rate, and probe geometry.

Overall, data presented herein and elsewhere supports low-flow push-pull perfusion as a suitable method for neurochemical sampling. Using microdialysis as a reference point for successful *in vivo* monitoring, low-flow PPP caused no more, mostly less, damage in terms of cell viability, cytoarchitecture, and computational fluid flow. Although preparatory PPP tissue response metrics approached those of MD, they were in effect for an infinitesimal fraction of total sampling time, rendering their influence insignificant. Complementary to these promising tissue response findings, PPP has already proven effective in several chemical monitoring studies. Multiple amino acids were detected with high separation efficiencies in excess of 250,000 plates in 30 s, and measurement of concentration changes with ~75 s response time (Cellar and Kennedy,

2006). Further, glutamate was measured with multiphase segmented flow at an improved temporal resolution of 7 s, with potential to apply to other neurochemicals (Slaney et al., 2011). The neurotoxic effects of salsolinol on the central nervous system have been elucidated with PPP (Misztal et al., 2011). Even the ability of MD to collect large bioactive molecules has been enhanced with a PPP system in freely moving animals (Takeda et al., 2011).

Future Work

Minimizing tissue response to invasive sampling methods is critical to optimizing neurochemical signal, thereby facilitating the interpretation of data. This information helps to decipher neuronal communication and provides a basis for pharmacological and behavioral intervention. Many strategies have been employed to control the foreign body immune response including improving material biocompatibility and infusion of bioactive molecules. Furthermore, refinement of tissue damage experiments, enhancement of spatial/temporal resolution, and integration of electrophysiology all contribute to the advancement of neurochemical sensing technology.

Material Science

In addition to reducing cross sectional area and overall probe size, biological techniques have been applied to neural probes in order to minimize the foreign body response. Biocompatible materials and coatings reduce immune responses, degradation, and fouling of surfaces. For example, titanium is a widely used material for implants due to its corrosion resistant and bioinert properties (Ignatov and Petrovskaya, 2003; Yoon et al., 2010). Silicon is another biocompatible material that is often used to make

microfabricated electrodes and sensors (Hansford et al., 1998). More applicable to the needle-sheathed PPP probe, plasma polymerized hexamethyldisiloxane (HMDSO) films deposited by plasma enhanced chemical vapor deposition (PECVD) on stainless steel have improved cell activity at the implant-tissue interface (Prasad et al., 2005). For MD probes, different membrane materials, such as polyacrylonitrile and polycarbonate-polyether, could be tested for biocompatibility (Hsiao et al., 2006).

Drug Delivery

Anti-inflammatory reagents can be delivered via the probes or microinjectors to mitigate reactive responses and improve neurochemical signal strength. Dexamethasone treatment of rats significantly reduced the astroglial response to implanted neuroprosthetic devices (Spataro et al., 2005). Potential candidates for immuno-suppressive therapeutics include pseudoephedrine, cannabinoid-based drugs, and luteolin (Fiebich et al., 2010a; Fiebich et al., 2010b; Klein, 2005; Seelinger et al., 2008).

Experimental Design

Studies conducted herein can be expanded upon by applying experimental methods to improved probe designs, and using more sophisticated tools to measure tissue damage markers with higher resolution. For cell viability experiments, live-dead cell stains can be infused through microelectrodes and electrochemical sensors, via microfluidic channels, to quantify dead/total cell ratio. In IHC experiments, mini PPP could also be investigated, although, like needle-sheathed PPP, it would probably cause less damage than MD. Future work can build upon this study by characterizing other intrinsic measurements like spatial locations, branching patterns, vessel width variation,

and membranous area surfaces. Moreover, associative measurements quantifying the relationships between two or more structures would provide further insight on the cellular dynamics of brain injury (Bjornsson et al., 2008). For computational modeling, needle-sheathed PPP can also be modeled, although the geometry of the needle is more complex. 3D models will provide more accurate information on velocity, pressure and shear stress gradients. Moreover, the solid mechanics of probe insertion can be computed with more advanced calculations.

Overall, current experiments could be modified to get a more comprehensive and precise idea of brain tissue response from neurochemical sampling. Probes could be left in the brain during fixation to better quantify dimensions. Of particular interest, chemical sampling and analysis experiments could be modified to determine how acute tissue damage affects neurochemical levels and signal accuracy. For instance, the quantification of lactate dehydrogenase, a biomarker for neuronal damage, could be coupled to cell viability dye infusion and IHC labeling (LaPlaca et al., 1997). Furthermore, these measurements could be performed in awake, freely moving animals for a more dynamic view of neural activity during brain injury. The chronic immune response could also be explored to develop a timeline of tissue response in neurochemical monitoring. Finally, studying the interplay between neuro-inflammation and physiological conditions like alcohol intake will enable treatments for neurological disorders (Crews et al., 2012).

Spatial and Temporal Resolution

Interrelated with tissue damage, spatial and temporal resolution are parameters in neurochemical monitoring that need continuous optimization. Cross-sectional area, size, shape, texture, and tip geometry all need to be taken into account when designing probes.

Although MD membrane active lengths have been reduced to as short as 0.5 mm (Mabrouk, in preparation), PPP probes still offer superior spatial resolution because they directly contact the extracellular environment. Specifically, microfabricated silicon probes are in development with tip widths of approximately 80 μm and inlet diameters of approximately 15 μm (Lee, in preparation). Temporal resolution has been dramatically improved by coupling sampling to analytical techniques like HPLC, CE-LIF, and MS. By applying multiphase segmented flow *in vivo* in MD, temporal resolution as good as 2s has been achieved off-line (Wang et al., 2010). By using the same methods in PPP, temporal resolutions of 7s and sub-seconds have been accomplished *in vivo* and in vitro, respectively (Slaney et al., 2011).

Dual Neurochemical and Electrophysiological Sensing

Still, the spatial and temporal resolution of neurochemical sampling methods remain inferior to electrophysiological recording devices. Microelectrode arrays (MEA) have been instrumental for measuring neuroelectrical signals *in vivo* (Polikov et al., 2005). These signals, caused by a catalytic or binding event, are proportional to analyte concentrations that can be detected by electrochemical biosensors (Ronkainen et al., 2010). However, only one analyte can be measured at a time. MEAs with incorporated electrochemical biosensors have demonstrated simultaneous measurements of electrophysiological and single neurochemical signals *in vivo* and *in vitro* (Johnson et al., 2008; Song et al., 2012). PPP, particularly the microfabricated design previously mentioned, offers considerable potential for incorporation into MEAs to create dual neuro- electrical/chemical sensors with multi-analyte capability.

PPP has evolved into a promising tool for precise and comprehensive neurochemical monitoring. Undoubtedly, incorporation of low-flow PPP has dramatically reduced the tissue damage caused by the higher flow rates in earlier iterations. Because of the relative factors characterized with cell viability stains, IHC, and COMSOL, it follows that PPP causes no more brain tissue damage than MD. In fact, these findings validate PPP as a preferred choice over MD in terms of tissue response. Since MD is an established tool for neurochemical monitoring, the results herein support the more widespread use and development of low-flow push-pull perfusion for engineering and neuroscience applications. Furthermore, cell viability, cytoarchitecture, and computational fluid dynamics data establish a reference point of tissue damage measurements. Improved probe designs and procedures can be developed to minimize tissue response, ultimately optimizing neurochemical sensing and facilitating the understanding and treatment of brain-related disorders.

References

Bjornsson CS, Lin G, Al-Kofahi Y, Narayanaswamy A, Smith KL, Shain W, Roysam B. Associative image analysis: A method for automated quantification of 3D multi-parameter images of brain tissue. Journal of Neuroscience Methods, 2008; 170: 165-78.

Cellar NA, Kennedy RT. A capillary-PDMS hybrid chip for separations-based sensing of neurotransmitters in vivo. Lab on a Chip, 2006; 6: 1205-12.

Crews F, Qin LY, Vetreno R, Zou J. Overview of neuroinflammatory changes produced by alcohol. Alcoholism, clinical and experimental research, 2012; 36: 78A-A.

Fiebich L, Caballero FJ, Collado JA, Rose T, Munoz E, Bellido ML. Anti-inflammatory activity of pseudoephedrine. Brain, Behavior, and Immunity, 2010b; 24, Supplement 1: S62.

Hansford D, Desai TA, Tu JK, Ferrari M. Biocompatible silicon wafer bonding for biomedical microdevices. Proc. SPIE 3258, Micro- and Nanofabricated Structures and Devices for Biomedical Environmental Applications, 1998: 164-8.

Hsiao JK, Ball BA, Morrison PF, Mefford IN, Bungay PM. Effects of different semipermeable membranes on in vitro and in vivo performance of microdialysis probes. Journal of Neurochemistry, 2006; 54: 1449-52.

Ignatov VP, Petrovskaya TS. Biocompatible coatings on titanium implants. Science and Technology, 2003. Proceedings KORUS 2003. The 7th Korea-Russia International Symposium on, 2003: 197-201 vol.1.

Johnson MD, Franklin RK, Gibson MD, Brown RB, Kipke DR. Implantable microelectrode arrays for simultaneous electrophysiological and neurochemical recordings. Journal of Neuroscience Methods, 2008; 174: 62-70.

Klein TW. Cannabinoid-based drugs as anti-inflammatory therapeutics. Nat Rev Immunol, 2005; 5: 400-11.

LaPlaca MC, Lee VMY, Thibault LE. An in vitro model of traumatic neuronal injury: loading rate-dependent changes in acute cytosolic calcium and lactate dehydrogenase release. Journal of neurotrauma, 1997; 14: 355-68.

Li M, Tian X, Schreyer DJ, Chen X. Effect of needle geometry on flow rate and cell damage in the dispensing-based biofabrication process. Biotechnology Progress, 2011; 27: 1777-84.

Matzneller P, Brunner M. Recent advances in clinical microdialysis. TrAC Trends in Analytical Chemistry, 2011; 30: 1497-504.

Misztal T, Hasiec M, Tomaszewska-Zaremba D, Dobek E, F√ºl√∂p F, Romanowicz K. The influence of salsolinol on dopaminergic system activity within the mediobasal hypothalamus of anestrous sheep: A model for studies on the salsolinol‚Äìdopamine relationship. Acta neurobiologiae experimentalis, 2011; 71: 305.

Polikov VS, Tresco PA, Reichert WM. Response of brain tissue to chronically implanted neural electrodes. Journal of Neuroscience Methods, 2005; 148: 1-18.

Prasad GR, Daniels S, Cameron DC, McNamara BP, Tully E, O'Kennedy R. PECVD of biocompatible coatings on 316L stainless steel. Surface and Coatings Technology, 2005; 200: 1031-5.

Ronkainen NJ, Halsall HB, Heineman WR. Electrochemical biosensors. Chemical Society Reviews, 2010; 39: 1747-63.

Seelinger G, Merfort I, Schempp CM. Anti-Oxidant, Anti-Inflammatory and Anti-Allergic Activities of Luteolin. Planta Med, 2008; 74: 1667-77.

Slaney TR, Nie J, Hershey ND, Thwar PK, Linderman J, Burns MA, Kennedy RT. Push-Pull Perfusion Sampling with Segmented Flow for High Temporal and Spatial Resolution in Vivo Chemical Monitoring. Analytical Chemistry, 2011; 83: 5207-13.

Song Y, Lin N, Liu C, Jiang H, Xing G, Cai X. A novel dual mode microelectrode array for neuroelectrical and neurochemical recording in vitro. Biosensors and Bioelectronics, 2012; 38: 416-20.

Spataro L, Dilgen J, Retterer S, Spence AJ, Isaacson M, Turner JN, Shain W. Dexamethasone treatment reduces astroglia responses to inserted neuroprosthetic devices in rat neocortex. Experimental Neurology, 2005; 194: 289-300.

Takeda S, Sato N, Ikimura K, Nishino H, Rakugi H, Morishita R. Novel microdialysis method to assess neuropeptides and large molecules in free-moving mouse. Neuroscience, 2011; 186: 110-9.

Wang M, Slaney T, Mabrouk O, Kennedy RT. Collection of nanoliter microdialysate fractions in plugs for off-line in vivo chemical monitoring with up to 2 s temporal resolution. Journal of Neuroscience Methods, 2010; 190: 39-48.

Yoon H, Deshpande DC, Kim TH, Jeong E-K. Development of Titanium Needle Probes for Neural Recording and Evaluation of Magnetic Resonance Imaging Artifacts. Journal of nanotechnology in engineering and medicine, 2010; 1: 11004.